

Fatigue Crack Initiation Behaviour of Additive Manufactured
Ti-6Al-4V
Delft University of Technology
Faculty of Aerospace engineering
VDL ETG

Thomas Cheylus

June 28, 2017

Acknowledgements

This piece of work was the fruitful collaboration of two leading organisations: The Delft University of Technology (faculty of Aerospace engineering) and VDL Enabling Technologies Group. As such there are many people whom I need to thank. Let's start with TUDelft:

Most of all, I would like to thank Professors Calvin Rans and Santiago Garcia from the Materials and Structures track who helped me at each step of the way. Their combined knowledge of fatigue and additive manufacturing, and chemical treatment was very insightful. Furthermore, I would like to thank Professor Johan Blijvelt for so graciously helping me in the faculty's chemical laboratory. Last but far from least, I would like to thank Frans Oostrum for agreeing to help with the confocal microscope.

From VDL ETG, I would like to extend my profound thanks towards Gerrit Oosterhuis and Koen Schoenart. This project would not have been possible without Gerrit's investment nor would the fatigue test tool be work if not for Koen's engineering skills. In addition, I would like to thank Eric ten Brick for helping me organise the project.

Abstract

This master thesis investigates the effect of surface morphology of Selectively Laser Melted Ti-6Al-4V on fatigue performance. The literature study performed here identifies roughness as one of three major causes for the decreased performance of the additive manufactured alloys (along side porosity and residual stresses). In order to eliminate the two other causes for poor fatigue, and isolate the surface roughness, a hot isostatic pressing (HIP) treatment was performed on every sample. Luckily, a first set of tests proved that chemical treatments, specifically electropolishing and plasma-polishing, greatly improve the surface quality. A second series tests (rotating bending fatigue tests) concluded that, although specific roughness parameter such as R_a reach lows of 0.2μ there was no statistically sound relation between fatigue performance and an improved surface roughness. Upon further investigation of the specimens, it was discovered through CT scans, that their porosity was in fact much closer to that of non HIP treated specimens. This master thesis illustrates once more that the effect of surface roughness on SLM Ti-6AL-4V alloys cannot be properly identified if the bulk material shows internal defects.

Contents

I	Introduction	6
1	Additive manufacturing	6
2	Motivation for the research	7
II	Literature review	8
1	Selective laser melting	8
1.1	Process parameters and part defects	8
1.2	The surface morphology of AM parts	10
2	Surface morphology	11
2.1	Surface morphology characterisation	11
2.2	Surface morphology terminology	12
3	Fatigue testing and Fatigue of titanium	13
3.1	Fatigue testing	13
3.2	Fatigue of Ti-6Al-4V	14
3.3	Fatigue performance of SLM Ti-6AL-4V	14
3.4	Effect of the built direction	14
3.5	The critical role of surface roughness	15
4	Post-treatments to improve fatigue	16
4.1	Heat treatments	16
4.2	HIP treatments	17
4.3	Surface treatments	17
5	Knowledge gaps	18
III	Experimental methods	19
1	Witness Specimen and fatigue specimen design and fabrication	21
2	Surface treatments and measurements	21
2.1	Post treatment selection	21
2.2	Surface treatment	22
2.3	Surface measurements	23
3	Fatigue testing	23
3.1	Manufacturing and assembly	23
3.2	Fatigue tests	24
4	Post fatigue analysis	24
4.1	SEM analysis	24
4.2	CT scan	25
IV	Experimental results	29
1	As-built + HIP specimens	29
2	Post processing	29
2.1	Chemical etching	29
2.2	Electropolishing	30
2.3	Plasmapolishing	31
3	3D surface renderings	31
4	Fatigue tests	31
5	Results of the post fatigue analysis	32

V	Discussion	42
1	Influence of the surface treatment on roughness	42
1.1	Chemical etching	42
1.2	Electropolishing	42
1.3	Plasmapolishing	44
1.4	Surface treatment perspectives	44
2	Fatigue tests	44
2.1	General observations	44
2.2	Untreated specimens	47
2.3	Fatigue of treated specimens	47
VI	Conclusion	49
1	Conclusion	49
2	Recommendations and perspective for future research	49
A	A step-by-step guide for chemical treatments	53
1	Chemical etching	53
2	Electropolishing	54
B	Roughness data	56
C	Fatigue data	67
D	Fatigue data	78
1	As-built + HIP	78
2	Electropolished	78
3	Plasmapolishing	78

Chapter I

Introduction

Fatigue failure is a mechanical failure that is responsible for nearly 90% of mechanical failures world wide [1]. In layman's terms, the fatigue phenomena is the accumulation of microscopic damage at the surface of a part that propagates through the bulk material. Once this damage reaches a critical amount, the products fails at load levels that are often much lower than the maximum load the part is design to handle. Fatigue has been extensively researched since the 1842 Versailles train accident, during which the train derailed due to an axle breaking in a front locomotive, was identified as a fatigue failure. This accident lead to the death of at least 50 passengers. The behaviour of metal parts under dynamic loading is now well understood, making it possible to predict the fatigue life. This is very important in the aerospace industry since the aluminium that constitutes the skeleton of aircraft is constantly subject to dynamic loads.

However, given the constant drive for lighter parts, the aerospace industry is now shifting to composite structures, who's fatigue behaviour is not yet well understood. It is actively being research all around the world, especially at TU Delft. Composite products are not the answer to every heavy part in the aerospace industry, since certain parts can be subject to extremely high temperature or their complexity makes their cost too high. For these parts, a new manufacturing technique, namely, additive manufacturing, holds significant promise. It is able to create complex 3D shapes in wide variety of metal alloys. Unfortunately, this manufacturing process is still at its debut and more research is necessary before it can be applied in critical location in air- and spacecraft.

1 Additive manufacturing

Additive Manufacturing (AM) is a novel manufacturing technique that enables the creation of freeform structures. Additive Manufacturing is defined by ASTM as "a process of joining materials to make objects from 3D model data, usually layer upon layer, as opposed to subtractive manufacturing methodologies" [2] [3]. This general description is applicable to all AM process variants and material variants. There exist many process variations that are adapted to all kinds of materials such as polymers, ceramics, and metals. Of interest for industrial applications, the metal additive manufacturing techniques are the prime candidates. Techniques such as powder bed fusion (PBF), where metal powder is selectively melted with a laser, can build complex parts with a good accuracy.

In order to obtain quality parts, an intrinsic knowledge and control of the processing parameters is required. The built orientation, the built angle, and the laser power are but a few examples of a long list. Another issue with PBF parts is their relative poor surface quality compared to machined ones. As the laser races over the powder and melts it into shape, a heat zone occurs around the melt pool. This heat zone leads to the unwanted sintering of surrounding powder particles to the part's surface, thereby generating a rough surface.

Unfortunately, this inferior surface quality affects the mechanical fatigue performance of printed parts by promoting crack initiation sites. This fatigue problem hinders the adoption of PBF parts, even though their high added value could lead to significant costs savings, performance increases, and lead time reductions , especially in the aerospace and high precision industries. According to literature reviews [4], improving the surface quality of PBF parts leads to increased fatigue performance. Since the formation of the surface roughness is intrinsic to the process itself, it is

necessary to develop post processing treatments that are able to improve the surface of parts with complex geometries.

This research project aims at investigating different post processing techniques and testing their effect on the fatigue performance of Selective laser melted parts. The metal of choice is the titanium alloy Ti-6Al-4V due to its naturally high mechanical properties and widespread usage in high-tech industries.

2 Motivation for the research

Additive manufacturing is capable of creating nearly 100% dense metallic materials with the application of HIP treatments [6] [7]. Furthermore, their mechanical properties are comparable to traditionally manufactured materials [2]. This opens the door to new possibilities in manufacturing and in product design. However, the parts still suffer from poor surface quality [8]. This heterogeneous surface is a major disadvantage of AM parts and it is suggested as one of the main reasons for their poor fatigue performance [4]. Since it is so much lower than that of TM counterparts [4], applications of 3D printed Ti-6Al-4V products is limited to static or non critical applications, drastically limiting their use in the aerospace or high precision industry.

The key requirements for the aerospace industry are low weight, possibility for certification, and long fatigue life. AM parts thus have a great potential for application in the aerospace sector [6]. Indeed, the functional integration possibilities and the complete design freedom can lead to the production of high strength and low weight parts. Unfortunately, the de Havilland Comet incidents of the 1950's¹, have taught us that fatigue is a major issue in aircraft design. The fractured skin of one of these aircraft can be observed in figure I.1. Therefore, improvement of the fatigue performance of AM parts can lead to reliable and certifiable parts that can be mounted as structural components in military and civilian aircraft alike.

The high precision industry needs products that guarantee a high level of accuracy and reliability. This is especially the case for mechanical flexures that can deliver a bending motion with a high precision without the need for lubrication. AM can be used to design complex flexures with several degrees of motion and large displacements. As for the aerospace industry, the major problem is fatigue. Since changing a flexure can be quite labor intensive (if it is located in the center of a complex machine, e.g.: a wafer-handler), a large amount of cycles before failure is often sought out.

As it has been shown, there is a major industrial need for reliable and durable AM parts. In both cases, the use of the Ti-6Al-4V alloy makes sense due to its high specific strength [2]. Furthermore, the large price gap between wrought aluminium and titanium (the latter being much more expensive than the former) is significantly reduced in the case of AM powders since these need expensive production methods. The higher performance of titanium, and the low cost increase associated to its use make it a suitable candidate for AM systems [9].



Figure I.1: Fatigue failure at the forward escape window of the De Havilland Comet [5]

¹During 1953 and 1954, three De Havilland comets suffered catastrophic failure while in flight. It was later discovered that fatigue cracks were generated at the square corner of the forward escape hatch window [5]

Chapter II

Literature review

This chapter is a review of the state-of-the-art knowledge on selective laser melting, the fatigue of titanium alloy Ti-6Al-4V, and surface morphology characterisation. The information developed here is critical to the understanding of this thesis project. Indeed, the fatigue of materials is dependent on both the surface of the material and its bulk properties [10]. The bulk properties of a metal alloy depend on its microstructure which is controlled through thermal treatments [11]. On the other hand, surface conditions arise during to the manufacturing of the part. The large amount of process variants in selective laser melting affect the surface morphology of the pieces it produces. The surface roughness of selectively laser melted parts is generally inferior in quality to parts produced using traditional techniques such as casting or milling [12]. This is a main contributor the poor fatigue performance of SLM parts and post treatments that can improve the fatigue life by smoothing the part are actively sought out.

1 Selective laser melting

Additive manufacturing is a general term that encompasses a large variety of different manufacturing techniques [12]. Of interest for this master thesis, the fundamental working principles of laser powder based metal systems is presented. This manufacturing technique is named Selective Laser Melting (SLM).

In SLM, a thin layer of metal powder (typically 30 μm for Ti-6Al-4V) is deposited on a substrate [13]. A high energy laser is then used to melt the powder in predetermined locations. Once all the locations of the first layer have been melted, a second layer of powder is placed on top of it. This second layer is also melted in specific locations. New layers are thus applied one after the other until the final part is obtained. A solid part is obtained since each new layer of powder is melted onto the previous one [12] [14] [2].

SLM is widely used for industrial applications since strong metals, such as titanium or tantalum, can be used [2]. Furthermore, SLM enables the creation of unique shapes which can lead to weight saving, performance increases, and decreased lead times [3]. To understand this process in details, it is necessary to know what are the main parameters that affect the quality of the final product and what defects should be expected.

1.1 Process parameters and part defects

1.1.1 Process parameters

Similarly to any manufacturing method, there are many process parameters that affect the quality of the final part, and research is continuously carried out to identify the best combination of these parameters [7]. These process variation stems from the complexity of PBF and the many different sources of the variables (e.g.: the laser source, the powder, the heat of the built chamber). The main families of process parameters are discussed here as well as their effect on part quality.

Powder parameters These parameters relate to the quality of the powder used to produce the part. These include the sphericity of the powder particles, the homogeneity of the size distribution, and the density of the powder. Additionally, other factors such as the humidity

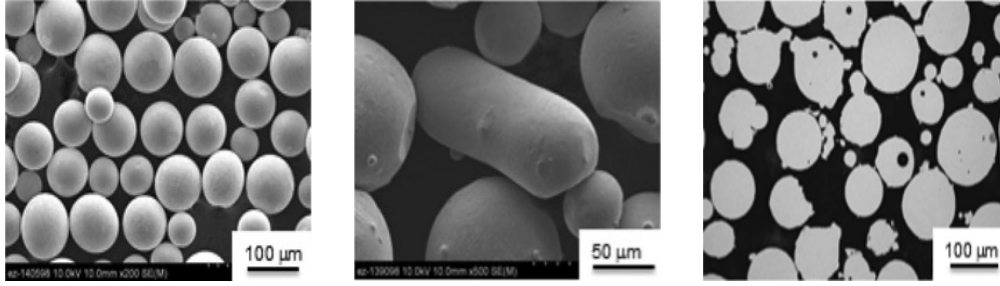


Figure II.1: Highly spherical powder obtained with plasma rotating electrode process [15] Figure II.2: Elongated particles using the rotary atomisation process [15] Figure II.3: Powder obtained using the gas atomisation technique [15]

of the powder, and the density of the powder particles themselves (as it can be seen in figure II.3) can also affect the final quality of the part. Small ($15\mu m < d < 50\mu m$) [13] and homogenous powders are strived for, just like the ones obtained with the plasma rotating electrode process illustrated in figure II.1. An inhomogeneous size distribution (that can be seen in figure II.2 combined with a large particle size) can lead to poor surface quality [15].

Laser parameters Laser parameters include the speed at which the laser races over the metal powder, the diameter of the beam on the powder (spot size), its frequency (the laser beam is not applied continuously), and of course its power. The laser parameters affect the way the particles sinter/melt together: too little power and the bond between the metal particles is not strong enough, too much power melts too many particles and results in poor dimensional accuracy [12] [13].

Built chamber parameters These parameters concern mostly the atmospheric conditions of the built chamber. When a laser is used to melt the powder, an inert atmosphere is necessary. Gases such as argon or nitrogen are used [15]. Furthermore, the absence of oxygen prevents oxide layers from forming (especially for titanium alloys) or explosive reactions from occurring (with aluminium). On the other hand, when an electron beam is used, the built chamber must be in a vacuum to prevent the electrons from scattering [15]. Controlling the atmosphere also prevents gas molecules from getting entrapped in the final product, which would increase its porosity.

Built orientation The layer-by-layer nature of the process means that grain growth occurs in the vertical direction. This anisotropy of the microstructure leads to different mechanical properties of the built part depending on the direction of the applied force. The tensile strength tends to be lower when the force is parallel to the built direction [16]

1.1.2 Part defects

The aforementioned parameters affect the quality of the final part. If a single one of them is not set correctly, the quality of the final part can be seriously affected. Here are the principal defects that occur in PBF parts.

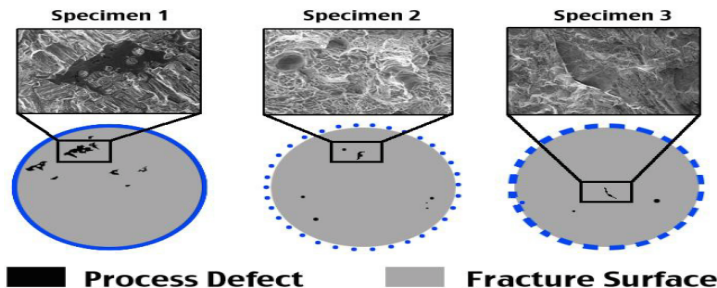


Figure II.4: Specimen 1: lack of fusion, Specimen 2 and 3: voids [17]

Surface morphology The surface morphology of PBF parts is inhomogeneous [8] [12]. This leads to shorter crack initiation times and thus a lower fatigue performance [10]. Surface roughness is a leading defect of PBF parts [4]. It is generated by several processing parameters, including the built orientation, the laser spot size, and the powder quality [18] [12]. Poor surface roughness yields poor fatigue properties by creating stress raisers at the free surface of the part [10].

Lacks of fusion Lacks of fusion occur when particles in close proximity are not totally melted together and form an agglomerate of loose particles. This is a particularly dangerous defect as it is hard to detect since it is analogous to a void that is filled with material (the use of CT scanners is necessary to detect them). Furthermore, there is no way to fix this defect once the part is completed. Lacks of fusion arise when the energy density of the heat source is not high enough to melt the powder particles together. These lacks of fusion negatively affect the mechanical properties of the part even when they represent but 1vol% of the total part volume [19].

Voids Voids are the result of a gas bubble that are entrapped in the part when the energy density of the heat source is too high. Its effect on mechanical properties is similar to lacks of fusion although it starts being dangerous when the volume percent of voids approaches 5 vol% [19]. Luckily, since there is no material filling the void, it can be easily detected by density testing. Furthermore, a HIP treatment is capable of reducing the size of the voids and thus limiting their negative impact. Although they are the result of different processing parameters, and need different techniques to be identified, they both lead to internal fatigue crack initiation [4].

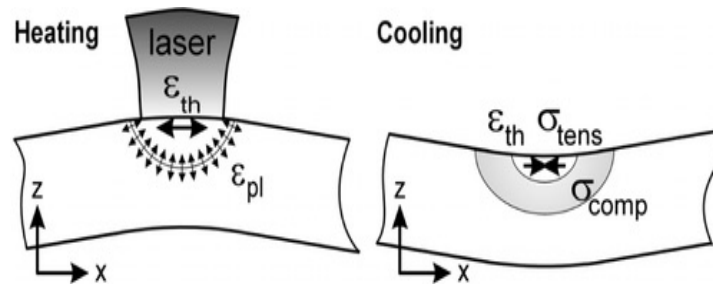


Figure II.5: The origin of residual stresses [20]

Residual stresses Such stresses are present in PBF parts due to the heat that dissipates through the part while it is being built. This phenomenon happens at each passage of the laser, as it is presented in figure II.5 [20]. These thermal stresses make fatigue crack initiation much easier since the final stress state of the part is tension [10]. In certain instances, residual stresses are so important that they lead to the formation of cracks in the part. This is an extreme case, and the part is likely to be disposed of, but it illustrates how critical residual stresses are.

1.2 The surface morphology of AM parts

The surface morphology is relatively poor compared to that of parts obtained from TM techniques. Their surface exhibits spherical features, reminiscent of the powder it was created out of. Furthermore, the layer-by-layer deposition technique leads to poor surface quality [8]. The different mechanisms leading to a PBF part's surface roughness are henceforth explained in detail.

Staircase effect The so-called staircase effect occurs when a part is printed at an angle to the substrate. Since AM parts encourage the use of novel design, inclined surfaces are likely to be present. When such a feature is printed each new layer is melted slightly to the side [18]. Even though the displacement is small and a layer relatively thin, the effect over a large flat distance creates a structure resembling a staircase (hence the name). The phenomena can be very well seen in figure II.6.

Heat dissipation When a part is printed, the heat generated by the laser point is dissipated through the part and into the substrate. As the heat dissipates through the part, it is reheated. This can lead to the aggregation of powder particles to the surface of the part [18]. This is particularly true when a feature is parallel to the substrate: the heat is directly dissipated into the powder bed. Once more, figure II.6 illustrates how the heat flows through the part as it is being built.

Dual surface roughness The unique manufacturing mechanisms of SLM leads to the formation a coat of sintered power particles on its surface. This has lead Greitemeier et al. in [8] to name it secondary roughness, as it is not the actual roughness of the part, rather the morphology of the sintered particles. However, this secondary roughness seems to affect the fatigue performance similarly to surface roughness in the traditional sense of the term [2].

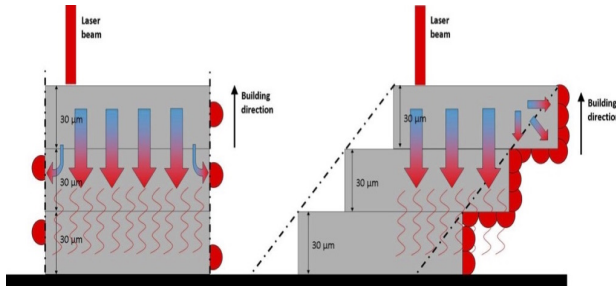


Figure II.6: Effect of heat dissipation and staircase effect [18]

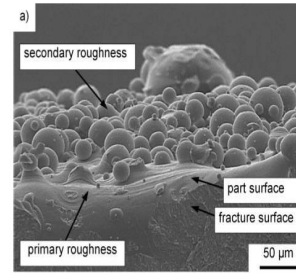


Figure II.7: The sintered particles and the actual surface roughness [8]

This section explained how SLM is able to manufacture fully dense part. Furthermore, the different processing parameters that affect the process, and how their control is crucial to obtain fully dense parts was also detailed. The next section focuses on surface morphology, more specifically, on how it is measured and how it is quantified.

2 Surface morphology

Surface morphology is a term used to describe the different aspects that the surface of a material can have. A surface can be wavy with smooth peaks (similar to a sinusoidal wave) or be much more jagged similarly to a mountain range on Earth's surface. Surface morphology is the interface between the bulk material and the environment. It has thus a large effect on the mechanical behaviour of the part. In certain instances, a controlled and organised surface morphology, like the ones observable on lotus leaves or butterfly wings, can lead to stunning self-cleaning or colour creating properties [21]. On the other hand, an inhomogeneous surface morphology, with deep pits can negatively affect mechanical properties, such as tensile strength, corrosion resistance, or fatigue, by promoting crack formation.

2.1 Surface morphology characterisation

Surface morphology can be characterised using different techniques that allow the user to quantify it. There are two main categories, optical techniques and mechanical techniques. The former rely on optical systems to give a 3D image of a parts surface while the latter use precision instruments to measure changes on the part's surface.

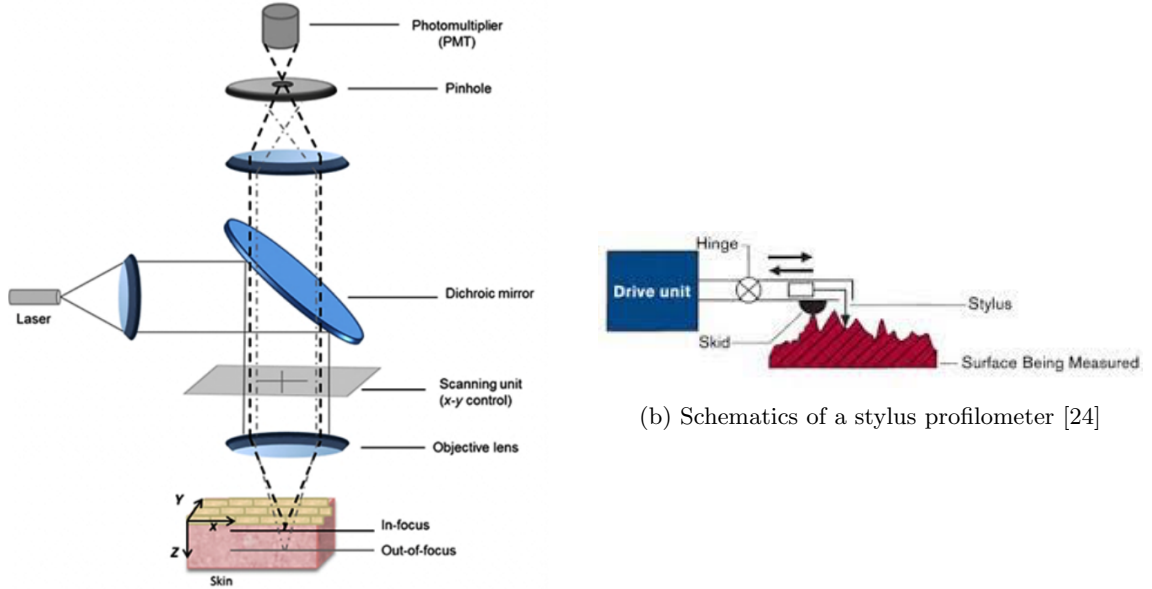
2.1.1 Optical Techniques

A confocal microscope is a tool used to observe the surface of material on a micro scale. The specificity of this microscope is its ability to take multiple scans of a surface and identify the contrast between the images. By superimposing the images, it is thus possible to obtain a 3D

image of the surface. This 3D image is analysed by a computer program which can then compute values of specific roughness parameters [22] [23]. A schematic view of the confocal microscope can be seen in figure II.8a.

2.1.2 Mechanical techniques

Mechanical techniques involve the use of a probe containing a small diamond stylus that moves over the surface of a material. The motion of the stylus is recorded and it is then possible to obtain a 2D profile. This technique can be seen in figure II.8b.



(a) A schematic representation of a confocal microscope [23]

(b) Schematics of a stylus profilometer [24]

Figure II.8: Optical and mechanical techniques

2.2 Surface morphology terminology

Surface roughness can be defined as a measure of how jagged or smooth a surface is. It can be quantified using different parameters that take different aspects into account. Another important aspect of a part's surface is the waviness. This is, in layman's terms, the roughness measured at a greater scale (i.e. the sampling distance is much bigger than for the roughness). This means that the waviness might be perceivable with a naked eye but its effect on mechanical properties is probably quite small. Of the different roughness parameters that can be observed, the following ones are explained in more details:

P_c Peak count or the number of peaks included in the analysis. A peak is defined as a point whose height is above a software selected bandwidth. [25]

R_p Highest peak. The maximum distance between the mean line and the highest point within the sample. It is the maximum data point height above the mean line through the entire data set. [25]

R_v Lowest valley. The maximum distance between the mean line and the lowest point within the sample. It is the maximum data point height below the mean line through the entire data set. [25]

R_t Maximum peak-to-valley height. The absolute value between the highest and lowest peaks. [25]

$$R_t = R_p + R_v \quad (\text{II.1})$$

R_a Arithmetical mean deviation. The arithmetic average of the absolute values of the roughness profile. [25]

$$R_a = \frac{1}{L} \int_0^L |z(x)| dx \quad (\text{II.2})$$

R_{sk} Skewness. A measure of symmetry of the profile about the mean line. Negative skew indicates a predominance of valleys, while positive skew indicates a "peaky" surface. [25]

$$R_{sk} = \frac{1}{n(R_q)^3} \sum_{i=1}^{i=n} (Y_i)^3 \quad (\text{II.3})$$

R_{ku} Kurtosis is a measure of the randomness of heights, and of the sharpness of a surface. A perfectly random surface has a value of 3; the farther the result is from 3, the less random and more repetitive the surface is. Surfaces with spikes have higher values; bumpy surfaces lower ones. [25]

$$R_{ku} = \frac{1}{n(R_q)^4} \sum_{i=1}^{i=n} (Y_i)^4 \quad (\text{II.4})$$

This sections presented the different parameters that are behind the general term "surface roughness". In addition, it showed that the surface of a material affects its overall mechanical properties in a positive or negative manner. The next section focuses of mechanical fatigue.

3 Fatigue testing and Fatigue of titanium

As it was explained in the introduction, fatigue is the leading cause of mechanical failure in the world. The extensive research on this topic has lead to a strong base of theoretical and practical knowledge about fatigue and how it leads to mechanical failure. A fundament aspect of fatigue are the different phases that occur to a part when it is subject to dynamic loading. These phases are well illustrated in image II.9 bellow: As it can be seen in figure II.9, fatigue is divided into

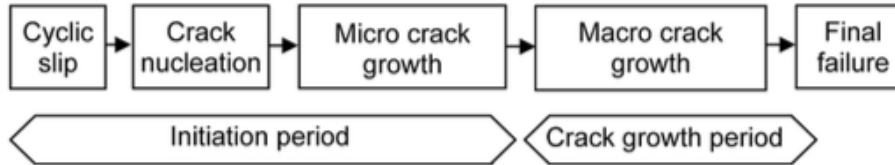


Figure II.9: Different phases of the fatigue life

two main life periods: the crack initiation period and the crack growth period. During the crack initiation period, fatigue is viewed as a surface phenomena while it is considered a bulk material phenomena during the crack growth period [10]. Crack initiation therefore depends on the state of the part at its free surface, and roughness thus has a large impact on how it will behave. Lastly, it should be noted that the crack initiation period usually accounts for 90% of the entire fatigue life. in other words, doubling the crack initiation life nearly doubles the total fatigue life.

3.1 Fatigue testing

Fatigue tests are a way to estimate the behaviour of a material under a dynamic load. The results of such tests can be extrapolated and used to design components that are subject to cyclic loads over their life time and will not fail under a known amount of cycles. This is called fail-safe design and is widely used in the aerospace industry. Fatigue test are carried out using standardised test specimens (either ISO or ASTM). This ensures that each fatigue test can be put in relation with previously performed ones. The nature of the test specimens depends on the type of load applied to it and what aspect of fatigue should be tested. Tension, bending, and torsion are common fatigue tests. Furthermore, some fatigue tests evaluate the tendency of a material to resist crack growth, while other try to see how cracks initiate [10].

The fatigue performance of a part depends on the material of the part, the design of the part, and

the type of load. There are several parameters that can affect the results of the fatigue test. They are the following:

- The test specimen size: In general, the smaller the test specimen, the longer the fatigue life. Indeed, larger test samples have a larger volume and thus a larger free surface. Since fatigue cracks initiate at the surface of a material, larger specimens are more likely to have shorter crack initiation times [26].
- The mean stress of the test: it limits the stress amplitude that a test can have. As it gets closer to the maximum allowable stress the specimen can handle, the closer the stress amplitude reaches zero [26].
- The stress concentration: stress concentration can be desired to force a sample to break in a specific location. Stress concentrations locally increase the stress and lead to earlier failures [26]. Unwanted stress concentrations (i.e.: from surface roughness) can also lead to early failure of a fatigue sample.
- Surface effects: fatigue life is very sensitive to the surface condition of a part. A rough surface creates local stress raisers and facilitates the occurrence of corrosion [26].

3.2 Fatigue of Ti-6Al-4V

The fatigue properties of TM titanium alloy Ti-6Al-4V are better than those of steel and aluminium or even CP (commercially pure) titanium. This alloy belongs to the $\alpha + \beta$ category as it contains Aluminium and vanadium which are α and β stabilisers respectively. The superior fatigue performance is mainly due to its microstructure that can be obtained with such alloys. It is composed of α and β grain types. These grain types correspond to hexagonal (hex) and cubic (bcc) unit cells types. The cyclic slip occurs in the α grains, thus making fatigue crack initiation strongly dependent on the length of the α slip, thus very fine equiaxed microstructures perform best under fatigue loading. However, the arrangement and morphology of the microstructure, with respect to the α and β phases, also has a strong influence on fatigue performance [27]. Figure II.10 presents an S-N curve of Ti-6Al-4V for different traditional production techniques. These S-N curves make the effect of the microstructure quite clear: lamellar or martensitic microstructures, due to their elongated grain sizes, perform less well than bimodal ones.

3.3 Fatigue performance of SLM Ti-6AL-4V

When compared to traditionally manufactured alloys, the fatigue performance of as-built AM titanium alloys is disappointing. As it can be seen in the S-N curves of Li et al., shown in figures II.11, the fatigue performance can vary significantly depending on the heat or HIP treatment as well as eventual post-machining. The main defects of as-built Ti-6Al-4V are its porosity (defects as big as 200 μm have been reported), the poor surface roughness, and the residual stress due to high thermal gradients during part production [4]. Moreover, when the loading of the specimen is aligned with the built direction, the performance is considerably decreased compared to perpendicular load cases [4]. This is linked to the built direction and is explained in detail in the next section. Although as-built specimens perform quite poorly for the aforementioned reasons, figures II.11, also informs us that significant improvements can be obtained through heat treatments, HIP treatments, and surface polishing. In fact, a fatigue performance comparable to that of TM parts can be reached with heat treatments and post-machining.

3.4 Effect of the built direction

The layer-by-layer nature of the SLM process is responsible for the formation of a unique microstructure. It is a result of the fast cooling rates the powder is subjected to, as well as the remelting of the metal (the heat source is applied on top during the melting of a new layer) and the size of the metal powder. Since the powder is added vertically, the grain growth occurs in this direction resulting in columnar β grains. This anisotropy in the bulk material's microstructure leads to components with inhomogeneous mechanical properties. Forces applied parallel to the built direction lead to mechanical failures at lower stress levels than forces applied perpendicular

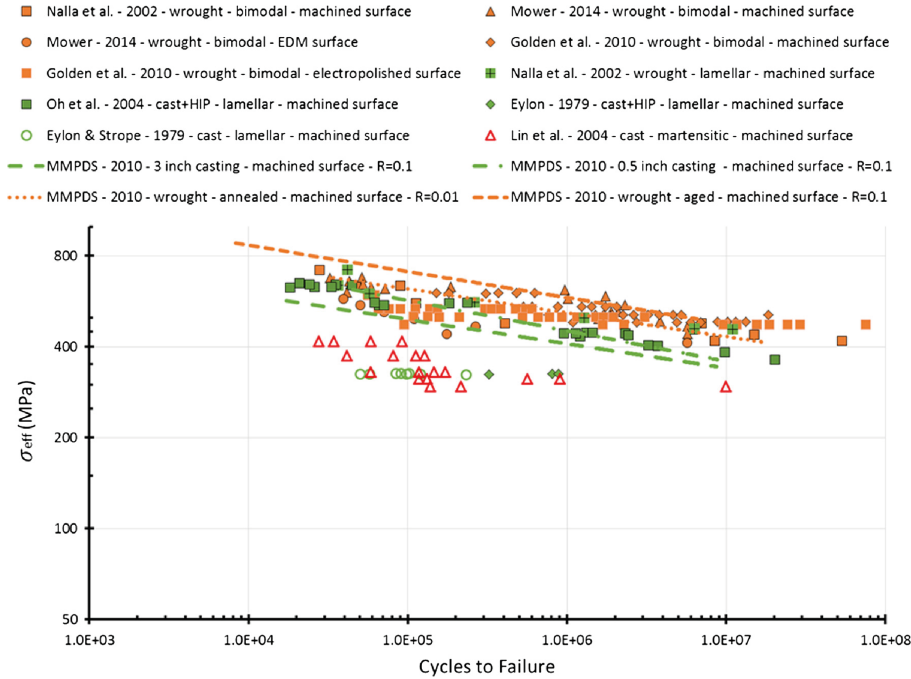


Figure II.10: S-N diagrams of wrought Ti-6Al-4V

to the built orientation. Moreover, this built direction dependency is also observable for fatigue performance. This can be observed in the the S-N curves obtained by Edwards and Ramulu [28] in figure II.12. These fatigue test results for as-built surface show a decrease of the fatigue limit of about 50 MPa at 200 00 cycles compared to samples built in the X or Y direction. This fatigue limit is even worse when looking at LCF since it is as high as 150 MPa. Furthermore, it is interesting to notice that the difference in fatigue performance between vertical and horizontal sample is more noticeable when the surface of the test samples has been machined. In this case, for a given number of cycles the fatigue limit is about 150 MPa lower for the vertically printed specimens. This corresponds to reduction of 250%. Hence, knowledge of the forces that will be applied to the part is critical before producing it with SLM.

3.5 The critical role of surface roughness

In the paper of Li et al., that reviews the current state of fatigue performance of AM parts, it appears clear that as-built parts should in no way be considered for dynamically loaded situations. However, when PBF Ti-6Al-4V has been HIPed and it's surface machined, the fatigue performance is in some cases, better than tradition TM parts. Since HIP can be performed on complex parts, the real defect that PBF parts have is their surface roughness. Although it can be improved by machining, this technique is not very practical. The often complex shapes of PBF parts, or the presence of internal channels, make surface machining very complex. In light of the S-N curves present in [4], new surface treatment should be developed such that they can be applied to any AM part.

Since surface roughness is a surface parameters, it only influences the crack initiation life of materials. Indeed, during crack growth life, the bulk properties of the material have a dominant effect on fatigue life [10] [29]. Furthermore, the effect of surface roughness is dominant at HCF life [8]. Although surface roughness is random, it is still possible to generate Estimated Initial Flaw Size

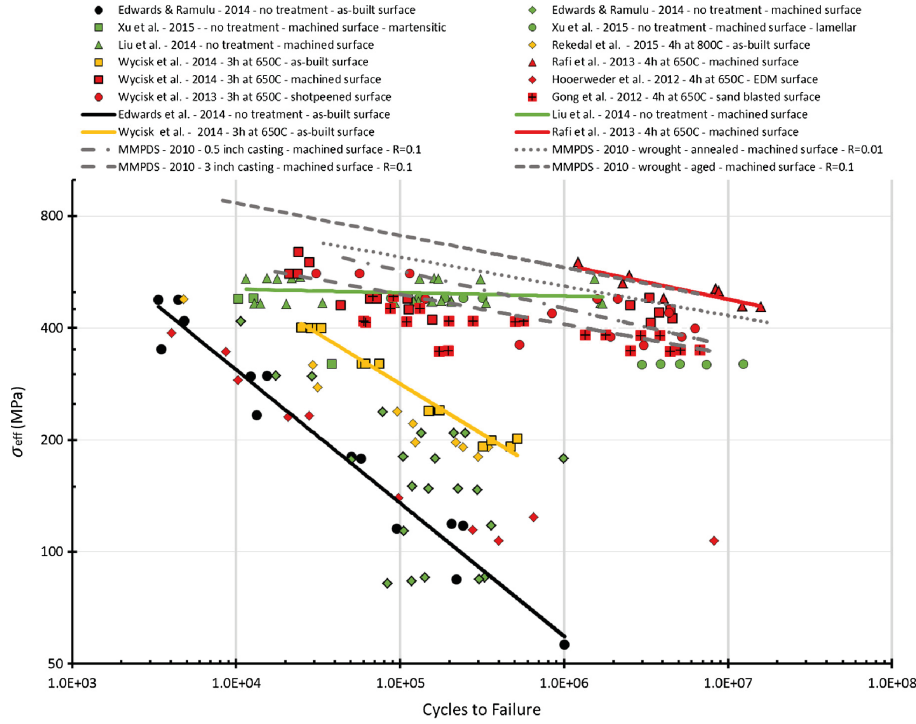


Figure II.11: S-N diagrams of AM Ti-6Al-4V, R=0.1

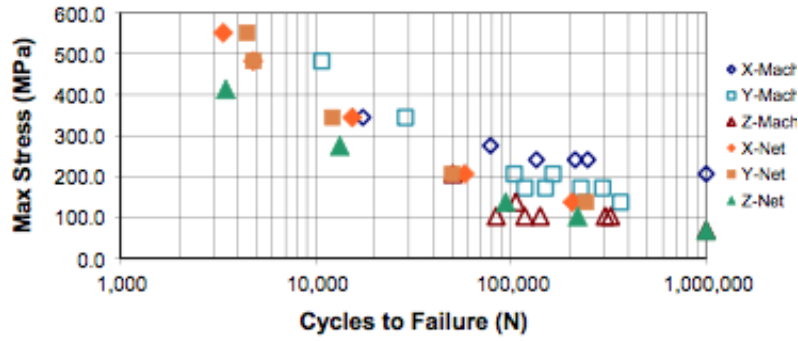
(EIFS) models that can accurately predict the HCF life of test specimens. This can be seen in the research performed by Greitemeier et al [8], where fatigue tests of tension-compression specimens at $R = -1$, $K_t = 1$, and 720°C heat treatment for 2 hours were performed.

4 Post-treatments to improve fatigue

Although the aforementioned as-built defects of section 1.1.2 and 1.2, and the poor fatigue performance illustrated in section 3.3 seem discouraging, there exist several post-treatments that can improve the properties of PBF parts, such that they can be used as dynamically loaded parts. These treatments act on different parts of the part. Of greatest importance, the heat treatments that remove the residual stresses are applied. In addition, it is often possible to use surface treatments to smoothen the naturally rough surface of SLM parts.

4.1 Heat treatments

These treatments are common place in metal processing. In general, they are applied to change the microstructure of the alloy being processed. In the case of PBF, heat treatments act as a stress relieving mechanism that reduces, if not removes entirely, the internal stresses due to manufacturing induced head dissipation. Heat treatments of SLM metal parts is much different than that of TM metal parts. This is a consequence of the unique microstructure that is obtained from the rapid cooling rate and the large thermal gradients that occur during production [30]. These thermal effects, that the workpiece is subject too, create stress concentration that affect the fatigue, strength, and dimensional accuracy of the final product [31]. On top of acting as a stress relieving mechanism, heat treatments can be used to homogenise the microstructure and

Figure II.12: Fatigue of SLM Ti-6Al-4V at $R = -0.2$

form stable $\alpha + \beta$ regions [32]. Vranckens et al. performed a series of heat treatments on SLM Ti-6Al-4V and has identified the following parameters as affecting the quality of the final part:

- The temperature of the heat treatment
- The duration of the heat treatment
- The cooling rate of the heat treatment

The most important aspect of the heat treatment is the temperature. Indeed, as long as it remains below the β transus temperature of the alloy, the fine α microstructure, that results from the high cooling rates of the printing process, is preserved [30].

4.2 HIP treatments

Hot Isostatic Pressing treatments serve two functions: they are able to alleviate internal stresses due to heat dissipation, and reduce the size of the voids present in the part. Indeed, since the part is subject to an isostatic pressure, often between 50 to 100 Mpa, local dislocations occur in the part that promote void closure. Parts produced by additive manufacturing techniques, be it SLM or EBM, have a higher amount of voids as it was explained earlier. By subjecting SLM parts to HIP treatments, the size of the pores is reduced and since the process is applied at a high temperature, a fully coarse $\alpha + \beta$ microstructure can form [33] [34].

4.3 Surface treatments

As it has been explained in the previous chapters, the surface morphology of SLM parts needs to be homogenised if the parts are to be used for functional applications. There already exists many post treatments that can be used to make a part smoother. These are divided in two categories: mechanical treatments and chemical treatments.

mechanical treatments Mechanical treatments use an abrasive to remove material from the product's surface. This abrasive is composed of hard particles, usually silicone carbide. The workpiece can be placed in an agitating bath containing abrasive powder (this process is tumbling) or simply polished with sand paper with either mechanical or manual motion. However, these processes are not easily applicable to complex 3D shapes, thereby limiting the use of these post treatments for post SLM applications [35]. Some abrasive treatments that involve mixing the abrasive with magnetic particles and moving this mixture with powerful electric fields could be used in the future since 3D shapes would be less of a challenge [36]. However, internal channels would still remain troublesome.

chemical treatments Chemical treatments include a large range of different variations but the underlying principle is the same: expose a work piece to an extremely corrosive environment in a controlled manner to remove some of its surface. Chemical treatments vary based on the acid used, the concentration of acid, the exposure time, and the temperature. Furthermore, an electrical current can be applied through the work piece to force the ionic transfer. This is called electropolishing. Chemical treatments are currently under investigation since they

are able to homogeneously treat complex 3D shapes. Many different acids and acid solution are investigated, especially HF, HCl, HNO₃, H₂SO₄, HCl₄. Since titanium is the material of choice for SLM, most research focuses on chemical treatments that can effectively etch this material. Titanium is extremely corrosion resistant which makes it very hard to etch with conventional solutions. Currently, the most effective solution contain HF (hydrofluoric acid) in high concentration. Although this acid is able to significantly reduce a part's surface, it is extremely dangerous and harmful to the environment [37] [38] [39] [40] [41] [42], [18].

A novel surface treatment technique, namely plasma polishing, show promise for future application to AM parts. Indeed, this treatment is able to smoothen the surface of a workpiece to a nano scale while using little amounts of dangerous chemicals. In this process, the workpiece is submerged in a salt bath and a high electrical current is applied. The surface can then be smoothed to a nanoscale [43].

5 Knowledge gaps

This literature review presents the key mechanism of part production via SLM as well as the major defects such parts can have. Moreover, a clear link between the surface roughness and the fatigue performance of SLM part is identified. It seems possible to improve the fatigue performance of SLM parts using post-treatments. In these cases, the fatigue life can be as good as that of wrought Ti-6Al-4V parts. None-the-less, these large improvements are observed on machined fatigue test specimens. Machining cannot be applied on complex 3D shapes and thus much research focuses on using chemical treatments to smoothen the surface of SLM Ti-6Al-4V parts. In these papers, the principal acid used is hydrofluoric acid, which is extremely toxic and corrosive substance. Hence, to obtain SLM parts that perform well under dynamic loading, it is necessary understand how crack initiation occurs at their surface and develop surface treatments that can smoothen the surface of complex 3D shapes in a safe manner. Thus, this thesis answers the following questions:

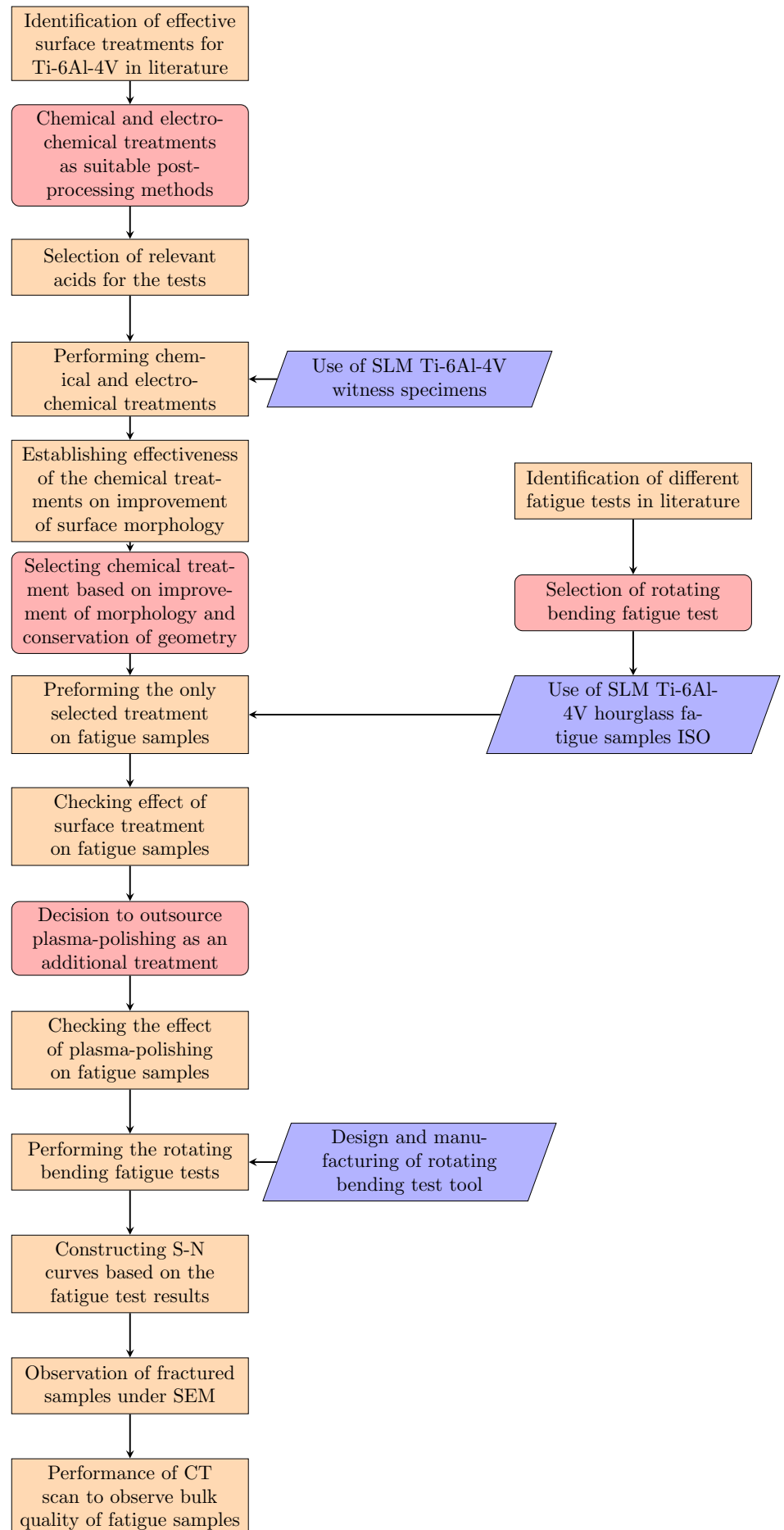
- What are the fatigue crack initiation mechanisms in SLM Ti-6Al-4V
- Are there key differences between crack initiation of SLM and wrought Ti-6Al-4V?
- What post treatments can be applied to SLM Ti-6Al-4V parts to improve the surface quality in a safe manner?
- Do surface morphology improvements lead to fatigue improvements?
- Can a model be developed to accurately predict the failure of SLM Ti-6Al-4V?

The experiments conducted during this master thesis aim at answering these questions.

Chapter III

Experimental methods

This chapter gives detailed information on the experimental methods that were carried out during this thesis. It indicates how the parts were manufactured, what treatments were selected and why, and the conditions in which the tests were carried out. The test specimens were manufactured by a leading additive manufacturing firm. The chemical surface treatments were carried out at TU Delft and the plasma polishing at a specialised company. The fatigue test tool was designed and assembled at VDL ETG and the fatigue tests were performed in their clean room. Lastly, SEM images were generated using the SEM at the DSML group in the faculty of aerospace engineering of TU Delft. A complete, step-by-step flowchart of the thesis is visible below. Subsequently, each step of



the process is described.

1 Witness Specimen and fatigue specimen design and fabrication

The purpose of this thesis is to understand how the surface morphology of AM titanium affects its failure mechanism under dynamic loading. Thus, it is necessary to identify what chemical treatments can effectively modify the surface of the Ti6Al4V alloy before treating the fatigue test samples. Hence, two different samples were designed and manufactured, namely witness specimens and fatigue test specimens. Both specimens were designed using a CAD software: Siemens Unigraphics (NX). Once the designs were completed they were verified by a senior mechanical engineer and then sent (as step files) to a leading additive manufacturing supplier and manufactured according to their parameters. The parts were all printed in one batch. Subsequently, they were subjected to a HIP treatment, carried out by the same company that was in charge of manufacturing them. The parts were located in the centre of the chamber so as to avoid large heat differences. The fatigue test specimens are hourglass fatigue test samples whose design is in accordance with ISO standard 42 for rotating bending fatigue tests. It was chosen to print the samples in the vertical orientation. As this is the weakest printing direction, the results obtained should be the most conservative ones. The witness specimens were simple rectangular plates. Their design was aimed at reducing costs as much as possible while allowing an evaluation of the effect of different chemical treatments on their surface. In total, 60 fatigue test specimens and 40 witness treatment specimens were manufactured. The detailed drawings of these parts can be found in the appendix.

2 Surface treatments and measurements

The literature review made clear that treating the surface of SLM Ti-6Al-4V parts cannot be done with any post treatment technique. This alloy is highly corrosion resistant and complex 3D shapes cannot be treated with standard 5-axis CNC machines. Hence a trade-off is required to identify applicable treatments. Once the treatments have been done, it is also necessary to quantify the eventual improvement on the surface morphology by means of surface analysis.

2.1 Post treatment selection

As it was explained in section 4, there exists a large amount of different treatments that can smoothen a part's surface. An in-depth post-treatment analysis was conducted to assess the potential of different treatments. A first level trade-off was conducted based on three high level criteria:

- Possibility to treat complex 3D shapes
- Proven effect on titanium
- Implementable in the context of a Master thesis

These three criteria are set as go/no go criteria, implying that if even one is not valid, it should not be considered further.

Once the high-level trade-off was conducted, a selection of the most promising treatments was possible. More attention was given to the specifics of each treatments and assessed precisely. This trade-off determined the suitable acids to use for the chemical etching and electropolishing.

Following the high level trade-off, It was determined that acids treatments seemed to be the most promising post processing methods. However, the oxide layer formed at the surface of titanium alloys means that not any acid can be used for the chemical etching and the electropolishing treatment. For instance, although HF (Hydrofluoric acid) is regarded as being, by far, the most effective way to smoothen Ti-6Al-4V, it is also extremely dangerous to manipulate. The acids that would be used are HCl (Hydrochloric acid), HClO₄ (perchloric acid), and H₂SO₄ (Sulphuric acid). These acids are often used in literature to treat the surface of AM Ti-6Al-4V.

In addition to chemical treatments, plasma polishing treatment appeared to be an interesting option since it is not often used in literature but has the potential to smoothen complex 3D shapes. Since plasma polishing requires specific equipment to be performed this post treatment was subcontracted in a specialist company. According to the company's website, this process immerses the parts in salt bath containing a small amount of acids (about 2-3 wt %). Just like for the

electropolishing process, the work piece plays the role of the anode but is subjected to about 200 V. This high voltage is required to create a stable plasma at the surface of the work piece. Lastly, since this process uses non toxic components, it can be regraded as a sustainable and environmentally friendly process [44].

2.2 Surface treatment

Both chemical treatment, chemical etching (CHE) and electropolishing (EP), were performed using equipment from the chemical laboratory at the aerospace engineering faculty of Delft University of Technology. The acid solutions were selected based on effective treatments found in literature. Each treatment was performed in a small beaker (100ml), thereby limiting the amount of acid used. For each treatment, a new witness sample was used. After each treatment, the samples were rinsed in water, dried, and placed in an individual sealed bag. On each bag, the sample number, the acid solution used, the time, and the temperature were indicated. The time was recorded using a stop watch. The details of each treatment can be seen in table III.1.

Regarding the handling of the samples, usual lab wear was used. This enable easy positioning of the samples and of the electrical wires during electropolishing. Furthermore, the beakers were placed on top of a heating plate that indicated the temperature value of the solution. Lastly, the electrical source for the electropolishing was a delta power supply with output current ranging going up to 30 V. For the entire duration of the treatments, a lab coat, gloves, and protective glasses were used. All treatments were conducted under a fume hood.

The chemical treatments can be reproduced by following the step-by-step guidelines presented in appendix A.

Process family	Sample number	Acid(s) used	Concentration	Time	Temperature	Votage	Mixing speed
Chemical etching	Sample 13	Hydrochloric acid	37 wt%	10 mins	25 C	N/A	none
	Sample 17	Perchloric and acetic acid	5 wt% and 95 wt%	20 mins	25 C	N/A	none
	Sample 23	Hydrochloric and sulphuric acid	3,5 ml @ 37wt% + 1,2ml @ 95wt%	5 mins	25 C	N/A	none
	sample 27	Perchloric and acetic acid	5 wt% and 95 wt%	5 mins	25 C	N/A	none
	Sample 28	Hydrochloric acid	37wt%	5 mins	25 C	N/A	none
	Sample 31	Perchloric and acetic acid	5 wt% and 95 wt%	10 mins	25 C	N/A	none
	Sample 37	Hydrochloric and sulphuric acid	3,5 ml @ 37wt% + 1,2ml @ 95wt%	10 mins	25 C	N/A	none
Electro-polishing	Sample 11	Perchloric and acetic acid	5 wt% and 95 wt%	5 mins	50 C	30,90 V	500 rpm
	Sample 14	Perchloric and acetic acid	5 wt% and 95 wt%	15 mins	25 C	30 V	500 rpm
	Sample 15	Hydrochloric acid	37 wt%	5 mins	25 C	6,5V 5A	500 rpm
	Sample 35	Hydrochloric acid	37wt%	2 mins	25 C	6,5V 5A	500 rpm
	Sample 36	Perchloric and acetic acid	5 wt% and 95 wt%	15 mins	50 C	30,9V	500 rpm

Table III.1: Chemical treatments

The setup of the chemical treatment can be seen in figure:

Lastly, a set of 12 fatigue samples was also plasma-polished. This treatment was conducted by a specialised company.

2.3 Surface measurements

The surface measurements for the treatment specimens were performed using a confocal microscope. One measurement gave an extensive amount of roughness parameters. The parameters selected were R_a , R_z , R_t , R_k , R_p , and R_V . For each treatment specimen, six measurements of the different parameters were performed at different locations. Then, the average value of each roughness parameter of the specimen (the average of the six measurements) was calculated using Microsoft excel. This procedure was also used to compute the roughness of the electropolished fatigue samples. Moreover, since there are 12 electropolished fatigue specimens, it was possible to compute a batch average for each of the roughness parameters.

The surface measurements of the as-built and the plasma-polished samples were obtained using the mechanical stylus technique. This was performed with a Mytutoyo instrument. The reason this instrument was used instead of the confocal microscope is due to a software malfunction of the confocal microscope: it was no longer possible to obtain roughness values. None-the-less, six measurements on each samples were also performed leading to the calculation of a sample average roughness and subsequently of a batch average roughness. These values are presented in the result section.

3 Fatigue testing

There exists a large amount of different fatigue tests that can be applied to standardised test specimens. These include tension-tension, torsion, fracture toughness, and bending. Performing a rotating bending fatigue test was preferred over the other fatigue tests possible. There are several reason for this, specifically:

- The size of the test specimens can be quite small.
- A test tool for such an experiment is relatively straight-forward: a motor, some bearings, and timing belts are the principal components.
- The test specimens are subjected to pure bending, at R-ratio equal to -1 . This stress ratio is suggested by Li et al in [4] as a preferred choice for further research in fatigue of PBF titanium.
- These tests have high speeds, ranging from 50 to 100 Hz [26].

It is for all of the reasons above that the rotating bending test is selected. A schematic view of this type of fatigue test can be seen in figure III.2: As it can be seen in figure III.2, the specimen is attached to a rotating shaft and held by a set of bearings. The load applied at the end creates a permanent bending moment in the hourglass specimen and since it rotates, the load at each point is fully reversed. The shaft that rotates the samples can be connected via a timing belt to the motor, and the simple nature of the motion as well as the small size of the specimens makes it possible to rotate more than one specimen in parallel at the same time.

3.1 Manufacturing and assembly

The test tool is composed of off-the-shelf-components as well as specific components that were designed and manufactured for this purpose. The off-the-self-components are listed in table C.1 that can be found in the appendix B.

The specific components where designed using Siemens Unigraphics (NX). These components where designed to allow four samples to rotate at the same time. they consisted of a housing for the motor, housings for the bearings, and a shaft for the drill heads. The engineering drawing for these parts can be found in the appendix. The parts where manufactured by the ASME department of the Aerospace faculty of the TUDelft. The raw material was purchased by VDL ETG. Furthermore, pulleys and centering units for the timing belts were also taken from standard VDL ETG products.

The weights were obtained by cutting a steel rod with a rectangular cross section in small cuboids of 2 and 3 cm thick. They weighed approximately 200 and 300 grams respectively.

The individual components of the fatigue tool were assembled at VDL ETG under the supervision of a senior mechanical engineer, Koen Schoneart. All the components were mechanically fastened or press fitted. Loctite 601 was applied to the bearings and housing that held the weights to ensure that no motion would occur between these bearings and the housing.

The fatigue test tool can be seen in the following images:

3.2 Fatigue tests

The fatigue tests were carried out in the clean room of VDL ETG. The computer software used was standard issue Maxpos software. This enabled the run the motor continuously at 3000 rpm. It was observed that the shaft closest to the motor exhibited vibration visible to the naked eye while the others did not. It was thus not used for fatigue testing. Since it was thus not possible to test 4 samples at a time, the furthest shaft from the motor was also disconnected to lower the torque required by the motor. This enabled faster acceleration to 3000 rpm. The time to failure was recorded using a stop watch connected to the sample that recorded the time to failure.

Three sets of fatigue tests were performed:

- a 12 sample set in the "as-received" condition (HIP treatment but no surface modification)
- a 12 sample set that was subjected to an electropolishing treatment (HIP and surface modification)
- a 12 sample set that was subjected to a plasma polishing treatment (HIP and surface modification)

Each set was tested at three different stress levels with four repetitions at each stress level. The stress levels were around 200 MPa, 100 MPa, and 50 MPa. These stress levels corresponded to approximately 1,13kg, 600grams and 300 grams respectively. Since the stress level is very sensitive to the diameter of the specimen (this is because the stress is proportional to the cube of the diameter), the diameter of each sample was measured with the confocal microscope to ensure the most accurate calculation of the stress level.

4 Post fatigue analysis

4.1 SEM analysis

Post fatigue analysis can be performed using a Scanning Electron Microscope (SEM). This type of microscope uses a beam of electrons that interact with the surface of the workpiece on an atomic level. It is thus possible to obtain very high magnifications and thereby observe micro- and nanoscopic phenomena. More images obtained with this system have a large depth of field and it is thus possible to see 3D objects accurately.

The SEM imaging was performed at the faculty of aerospace engineer of TU Delft under the supervision of Frans Oostrum. Two samples were observed: an as-built + HIP and a plasma polished. These samples were both subject to low stresses. Images were first taken at a low magnification to identify zone to zoom into. There were several specific features that were sought out:

- Dimples, characteristic of a brittle failure
- Striations, characteristic of fatigue crack propagation
- Fatigue crack initiation point
- Production defects (e.g. : voids or lacks of fusion)

4.2 CT scan

In order to assess the quality of the bulk material, a CT scan (Computer Tomography) was performed on 3 fatigue specimens simultaneously. Two of the selected fatigue specimens were as-built specimens and one was a plasma-polished specimen that did not fail after 8 million cycles. This quality inspection test was outsourced at a specialised metrology company. The minimal resolution level of test is $7\text{ }\mu\text{m}$ meaning that defects smaller than that cannot be identified.



Figure III.1: EP setup, with base heating plate, counter anodes, electrical wires and beaker

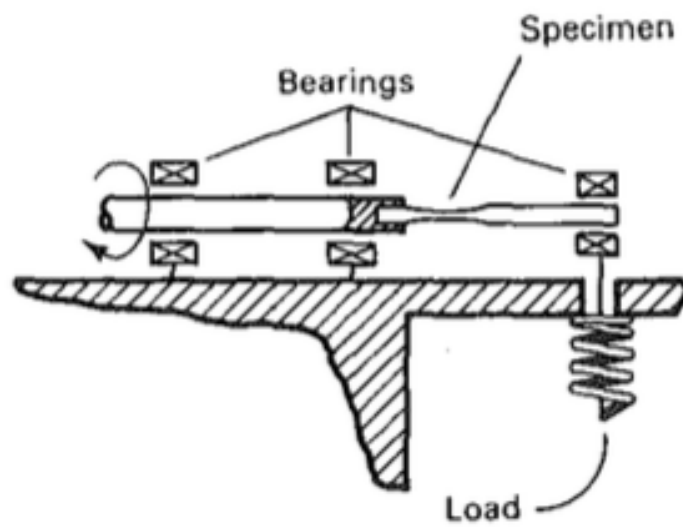


Figure III.2: A schematic view of the rotating bending fatigue test

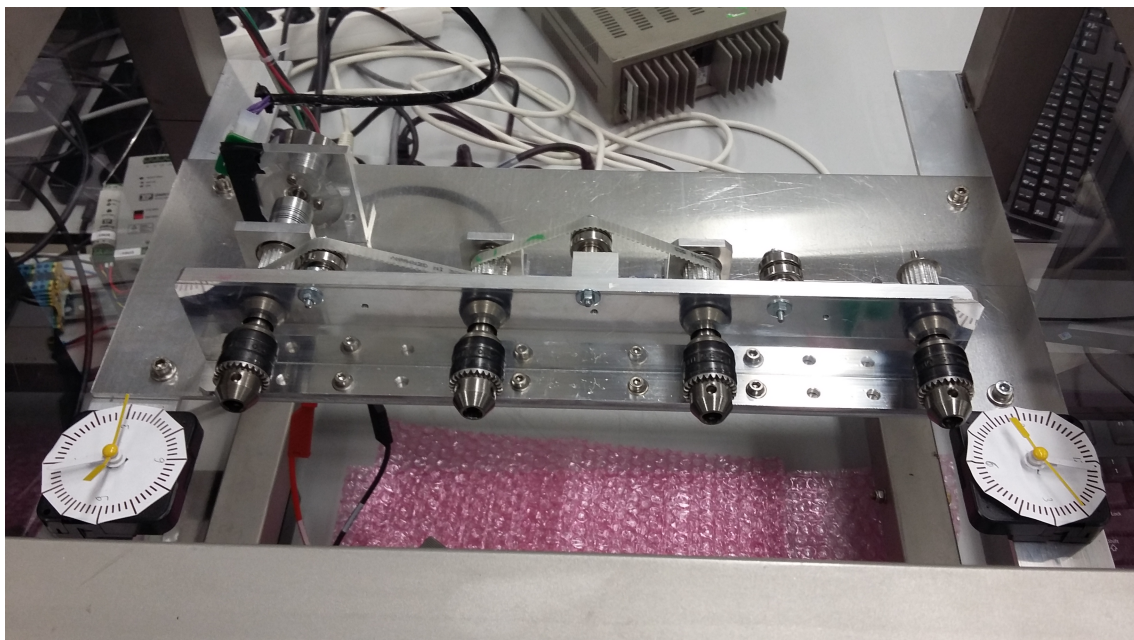


Figure III.3: Top view of the test tool, with the chucks, the housing units, the timing belts, and the motor

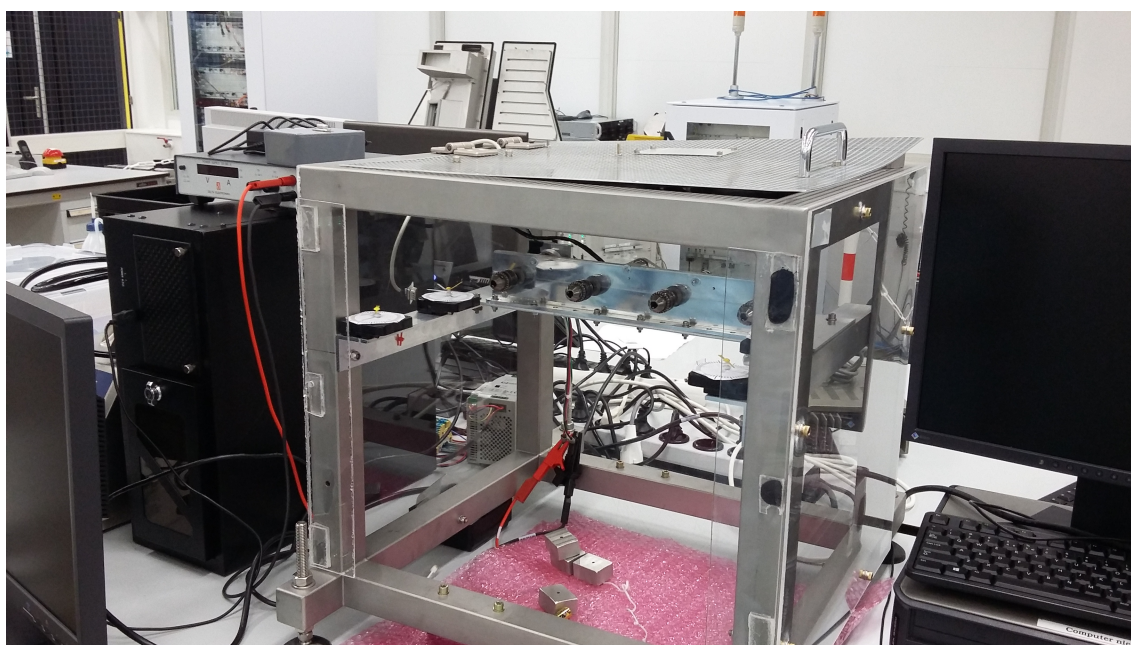


Figure III.4: Side view of the test tool, with the frame and the connectors to the computer and the power supply

Chapter IV

Experimental results

This chapter presents the results of the experiments. The effect of the chemical etching, electropolishing, and plasma polishing on surface morphology is detailed along side three fatigue curves resulting from different surface conditions (i.e.: as built + HIP, electropolished with HCl, and plasma polished). The results of the chemical treatments show a clear reduction in surface roughness compared to the as-built case. The plasma polishing lead to the smoothest, shiniest surface. The as-built +HIP samples failed with relatively low scatter but a low stress and low cycles compared to wrought Ti-6AL-4V. An improvement of fatigue life is only visible at low stresses when post treatments are applied but it does not seem statistically significant.

1 As-built + HIP specimens

The specimens were obtained from the manufacturer and their dimensions were measured. With the naked their surface quality appears to be quite good. The exact values can be seen in table IV.1

Surface parameter [μm]	R_p	R_v	R_t	R_a
As-built + HIP	8.46	8.94	25.9	1.7
Standard deviation	5.95	6.93	12.43	0.94

Table IV.1: Roughness values of As-built + HIP treatment specimens

2 Post processing

The measurable effect of the chemical treatments can be plotted as a function of acid used, time, and temperature of the process. Furthermore, it is possible to compare the effect of different acids when looking at the plots. It appears that the surface of Ti-6Al-4V gets smoother as the time of the process increase. Furthermore, electropolishing is much more effective at generating smooth surfaces within a short time but a too long exposure leads to large dimensional deformations.

2.1 Chemical etching

The following graphs present the effect of the different chemical treatments on the surface of 3D printed Ti-6Al-4V. Figure IV.1 shows the effect of treatment time when using HCL. In this case the concentration and the temperature were held at the same level, 37wt% and 25 deg C respectively. This acid concentration corresponds to the purest level of Hydrochloric acid available. It is clear that the surface quality improves with increasing treatment time. This observation can also be done with perchloric acid (figure IV.2), as well as Sulphuric acid (figure IV.3). In every case, the acid were used at their highest commercial concentration. It is also possible to observe the effect of the acid on the surface of the titanium alloy. This is visible in figure IV.4. The comparison is done at time = 10 mins. The most noticeable difference between the acids is their effect on the

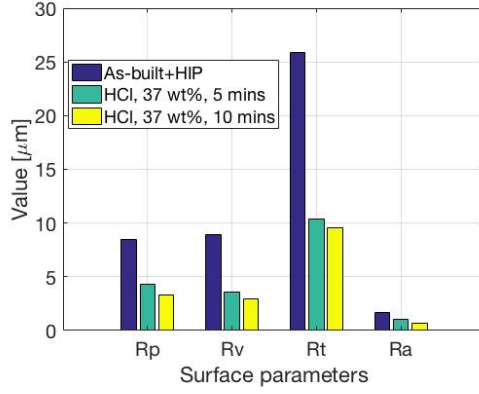


Figure IV.1: Surface roughness as a function of treatment time with hydrochloric acid

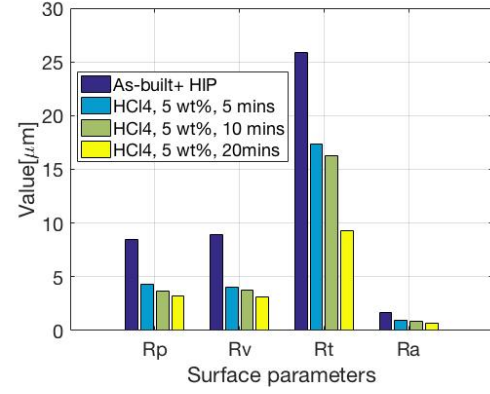


Figure IV.2: Surface roughness as a function of treatment time with Perchloric acid

peak count (P_c) and the R_t .

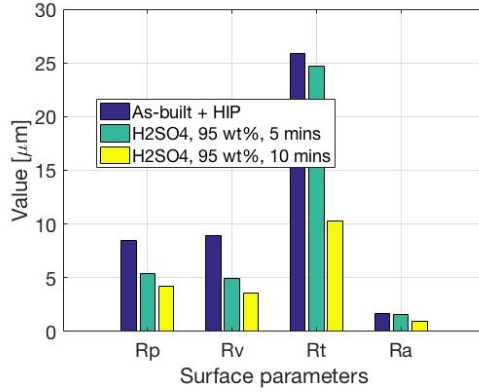


Figure IV.3: Surface roughness as a function of treatment time with Sulphuric acid

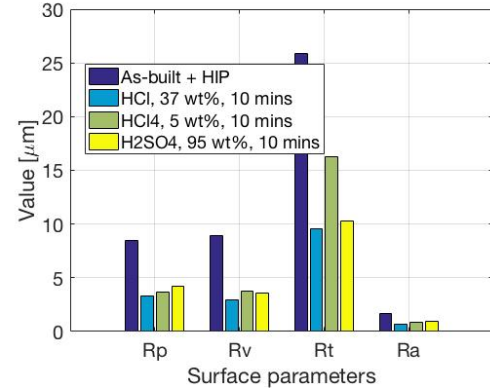


Figure IV.4: effect of acid

Surface parameter [μm]	R_p	R_v	R_t	R_a
HCl, 37 wt%, 5 mins	4.33	3.61	10.4	1.043
HCl, 37 wt%, 10 mins	3.34	2.91	9.53	0.69
HCl4, 5 wt%, 5 mins	4.29	4.07	17.34	0.99
HCl4, 5 wt%, 10 mins	3.63	3.77	16.27	0.82
HCl4, 5 wt%, 20 mins	3.21	3.11	9.3	0.64
H2SO4, 95 wt%, 5 mins	5.44	4.90	24.66	1.54
H2SO4, 95 wt%, 10 mins	4.2	3.60	10.3	0.96

Table IV.2: Exact values of the bar plots chemical etching

2.2 Electropolishing

The electropolishing process adds complexity with the introduction of an electrical current that forces the reaction to occur at the surface. As it can be seen in figure IV.5, the temperature increase does not lead to a smoother surface roughness than a treatment conducted at room temperature. When conducting an electropolishing treatment using HCl, the 5 mins treatment significantly reduces the roughness. However, this treatment also caused a severe decrease in dimensional tolerance. Therefore, a 2mins treatment was also conducted. The two aforementioned treatments

can be see in figure IV.6.

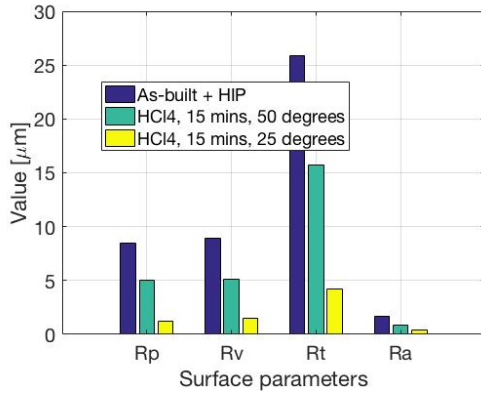


Figure IV.5: Effect of temperature on electropolishing with perchloric acid

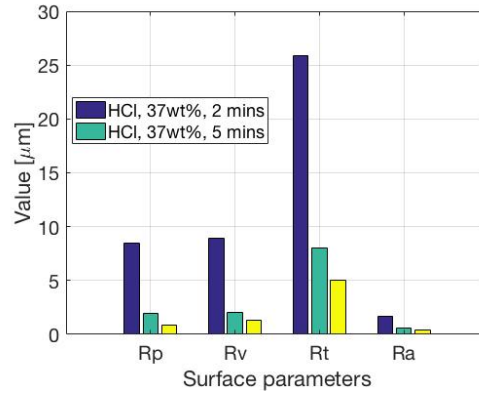


Figure IV.6: Effect of time on electropolishing with HCL

Surface parameter [μm]	R_p	R_v	R_t	R_a
HCl, 37 wt%, 2 mins	1.90	2.05	7.99	0.58
HCl, 37 wt%, 5 mins	0.90	1.33	5.0	0.42
HCl4, 5 wt%, 15 mins, 50 degrees	5.05	5.16	15.74	0.83
HCl4, 5 wt%, 15 mins, 25 degrees	1.23	1.52	4.2	0.42

Table IV.3: Exact values of the bar plots electropolishing

2.3 Plasmapolishing

The measured values of the surface parameters for the plasma polished samples can be seen in table IV.4. When looking at the different values of the parameters, it can be seen that the R_v is almost 1.5 time larger than the R_a . This indicates a pronounced presence of pits at the surface of the material.

Surface parameter [μm]	R_p	R_v	R_t	R_a
Plasma polishing	0.44	0.520	3.54	0.31

Table IV.4: Plasma polishing

3 3D surface renderings

On top of the numerical data obtained through the surface measurements, it was also possible to collect visual data thanks to the versatility of the confocal microscope. These images of the surface topology of witness specimens after chemical treatments can be seen at the end of this chapter in figure IV.22 and IV.23.

4 Fatigue tests

The fatigue tests were performed on three sets of fatigue samples. After performing the fatigue tests, it was possible to obtain an S-N curve and compare it with the roughness of the fatigue samples. The S-N curve can be observed in figure IV.7. As it can be observed in figure IV.7 the as built samples all fail within a close cycle range at a given stress level (high, medium, and low). This is also the case for the high and medium stress level of the electropolished and plasma polished samples. The consequence of the change in roughness can be observed a low stress levels:

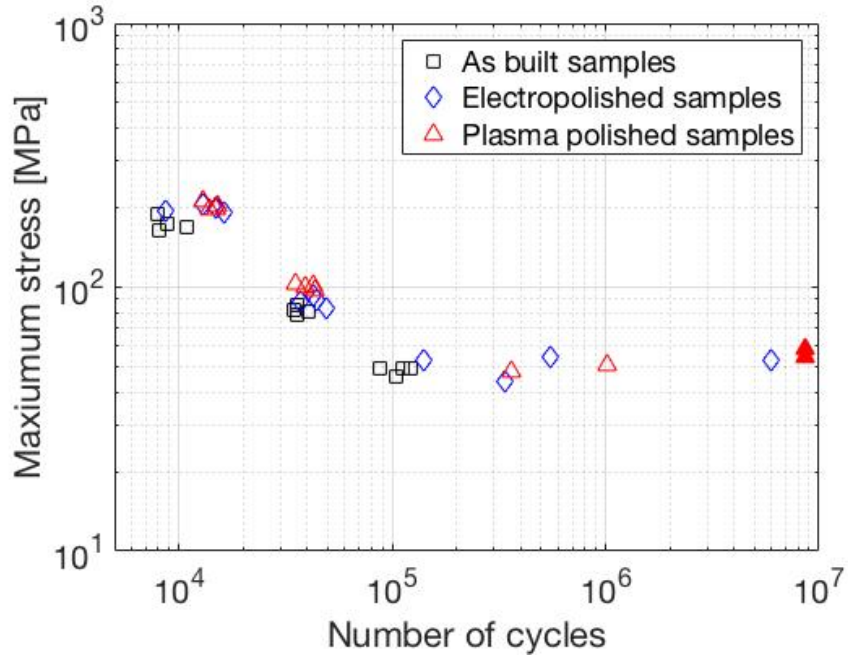


Figure IV.7: S-N curve with R=-1, SLM ti6Al4V

two samples did not fail after 8×10^6 cycles.

When looking at the roughness values of the samples, it is clear that the treatments significantly reduce the roughness, both within the same ball park.

5 Results of the post fatigue analysis

The important fatigue features such as dimples and striations were identified on both the as-built + HIP sample and the plasma-polished sample. Moreover, some voids were also present in the part. These different features can be seen for the as-built specimens in figures IV.8, IV.9, IV.10, and revoidab and for the plasma polished specimens in figures IV.12, IV.13, IV.14, IV.15, and IV.16. A detailed description of what can be observed on each image is presented in the legend.

In addition to SEM imaging, three fatigue specimens that were not subjected to a fatigue test were analysed with a CT scanner. The purpose of this test is to analyse the internal features of a material and detect porosities. The CT scan was conducted after the fatigue tests since their results were not as good as expected. The results of the CT scan revealed that the average real density of a sample is 99.74% with pore sizes as big as 0.00055 mm^3 . The plot of pore size versus number of pores can be observed in figure IV.17.

As it can be seen in figure IV.18, IV.19, IV.20, and IV.21, all samples exhibit pores within the bulk material. Furthermore, some pores are located in the subsurface region, a zone that is highly stressed during rotating-bending fatigue tests.

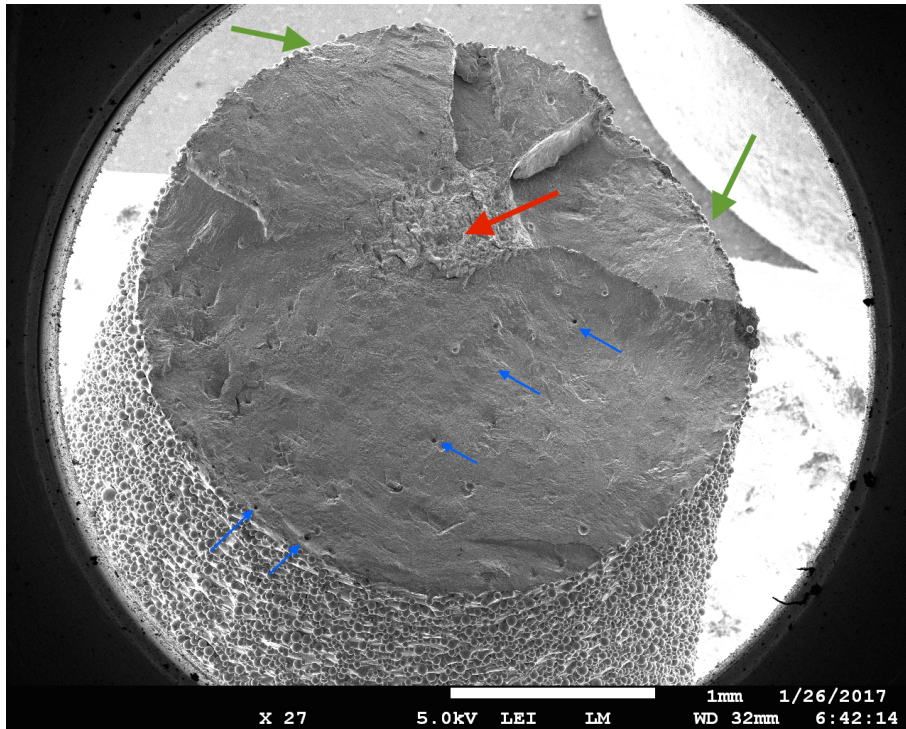


Figure IV.8: 27x magnification, As-built sample. The red arrow points to the central region featuring dimples: this is the final brittle failure location. The green arrows point at possible crack initiation sites. The blue arrows point at pores within the cross-section of the sample. One can notice that some pores are located in the subsurface region.

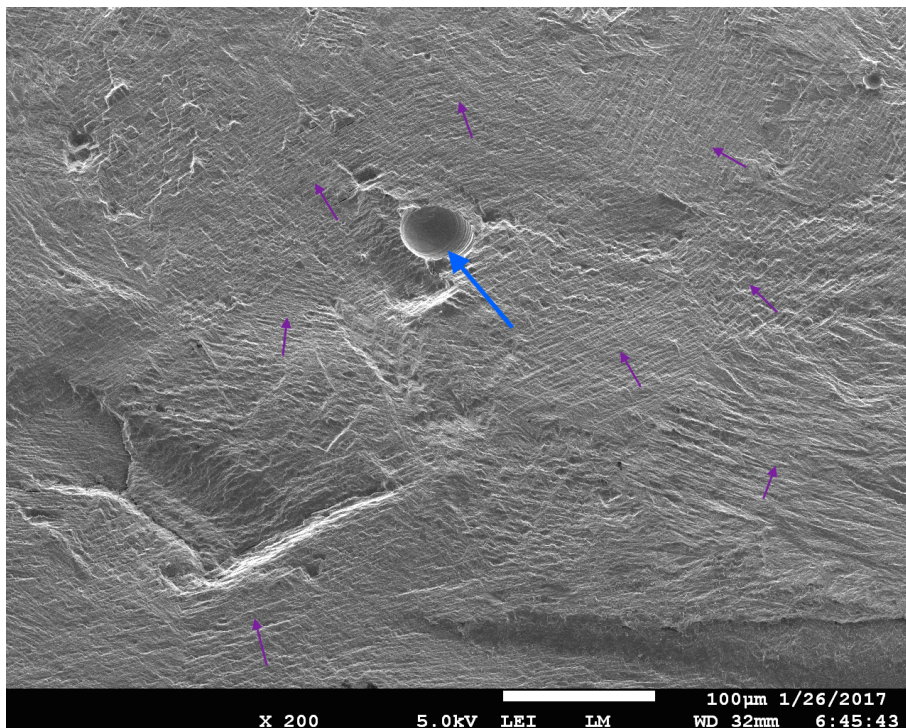


Figure IV.9: 200x magnification, as-built sample. The blue arrow points to an irregularity of the bulk material, the sphericity of the defect would tend to signify that it is an unmelted particle. The purple arrows show the directions of the fatigue growth marks, the many different directions indicates multiple initiation sites.

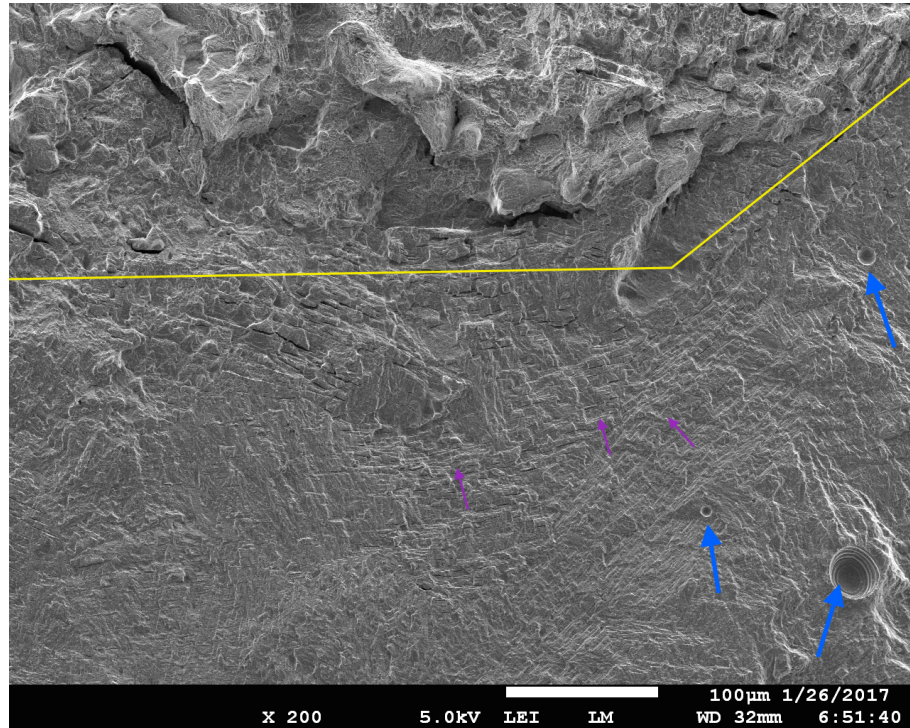


Figure IV.10: 200x magnification, as-built sample. The Blue arrows point to spherical defects: unmelted particles. This image is that of the interface between the fatigue fracture surface and the brittle failure surface: the brittle failure is located above the yellow line.

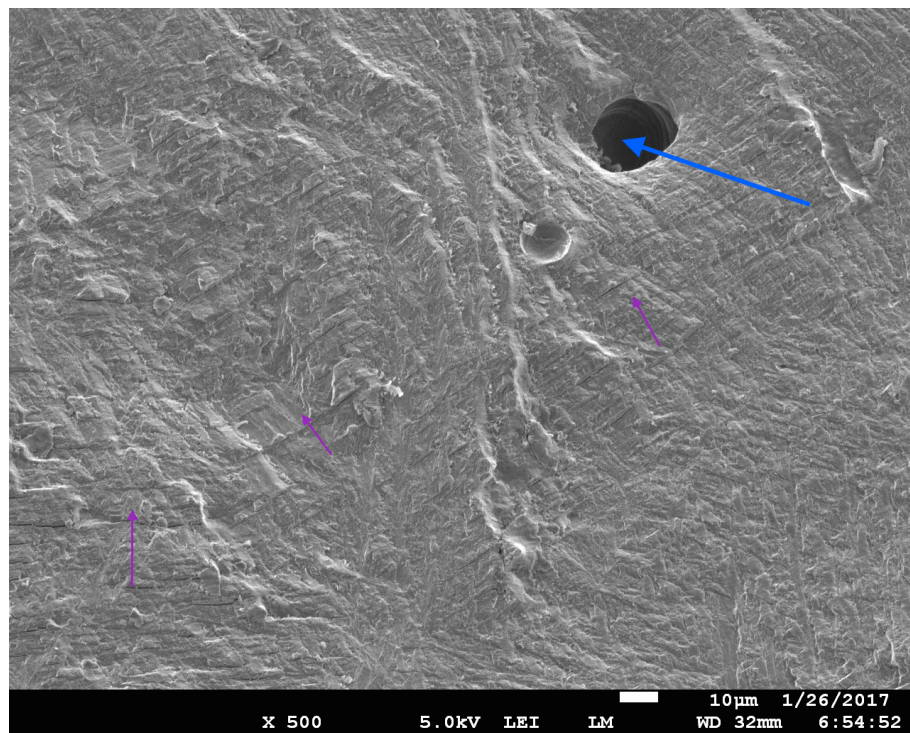


Figure IV.11: 500x magnification, as-built sample. The Blue arrow indicates the presence of a void, while the purple ones point in the direction of crack growth bands.

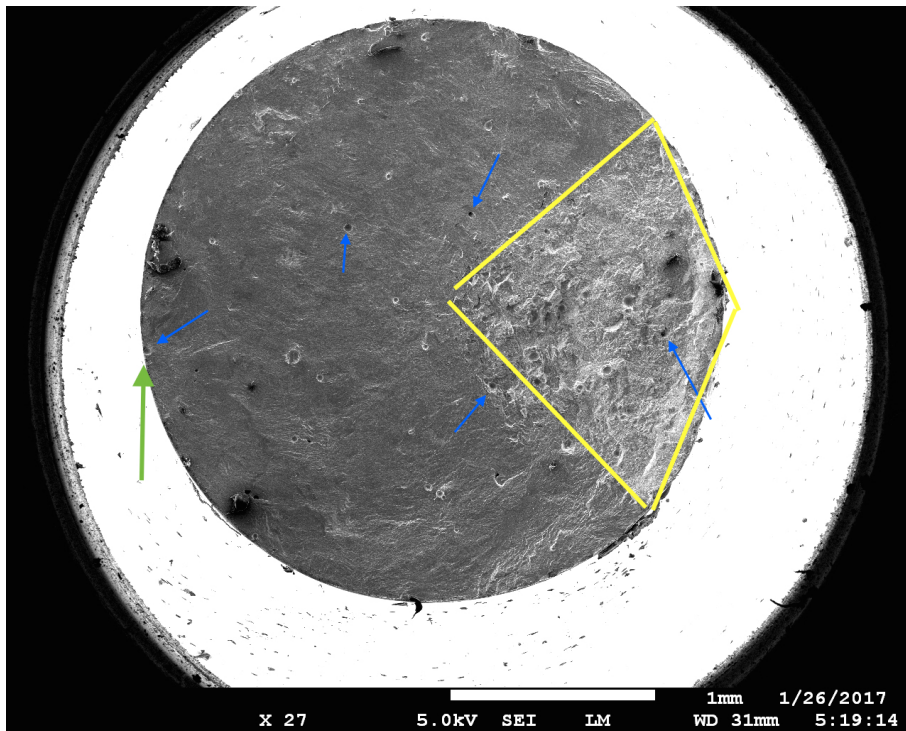


Figure IV.12: 27x magnification, plasma-polished sample. The region marked by the yellow lines is the brittle failure zone, opposite of which the green arrow presents the probable crack initiation site. The blue arrows point to pores.

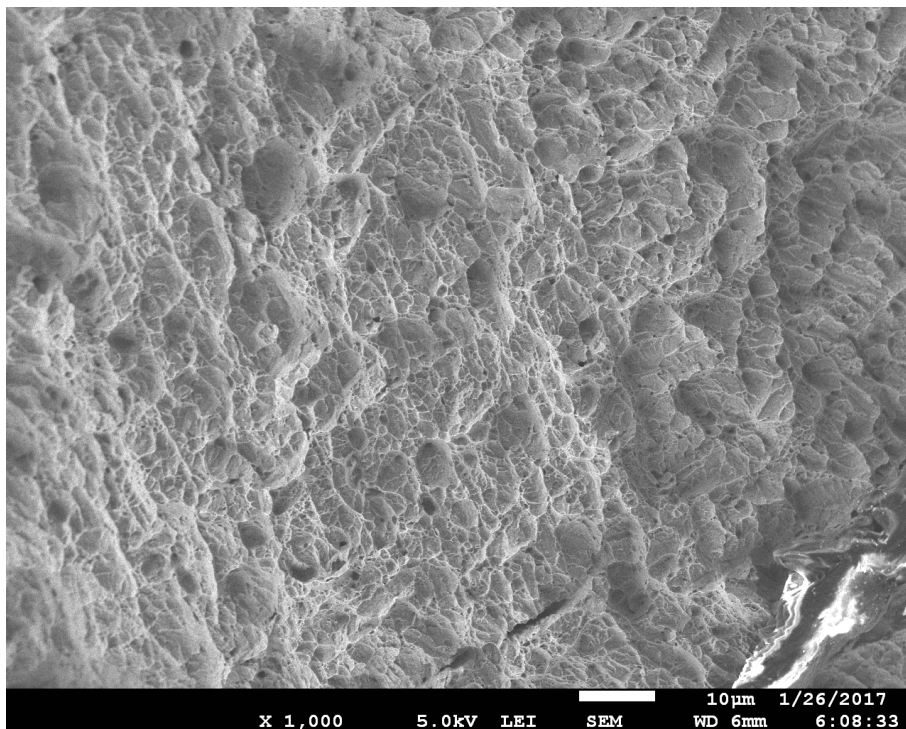


Figure IV.13: 1000x magnification, plasma-polished sample. This image consists entirely of dimples, corresponding to the brittle failure region.

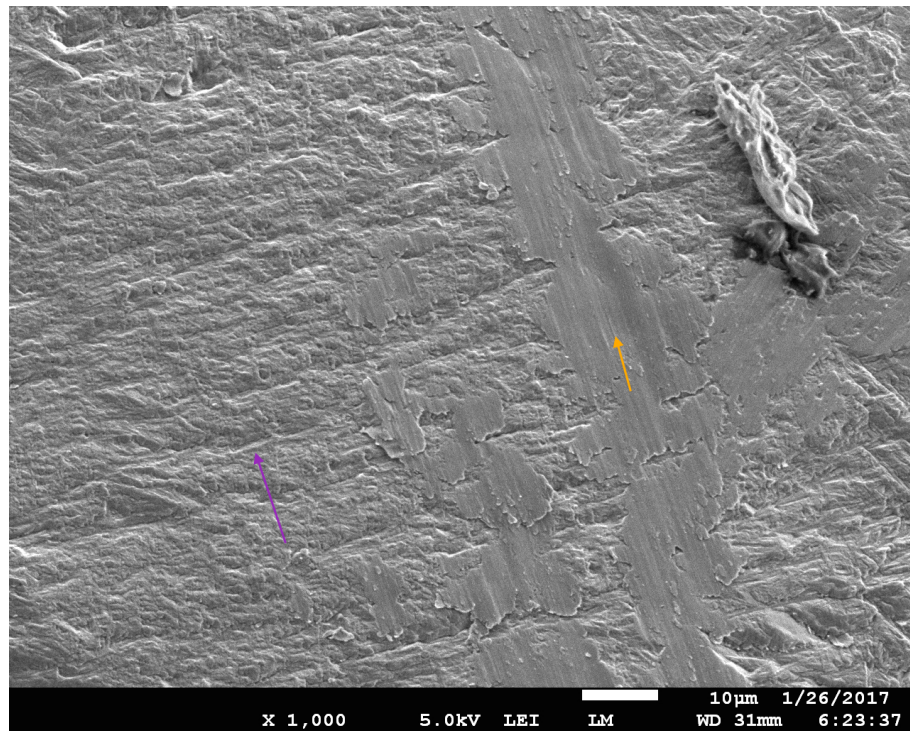


Figure IV.14: 1000x magnification, plasma-polished sample. The purple arrow shows the direction of the fatigue crack growth while the orange one presents a zone that has been smoothed due to the compression that occurred at each cycle.

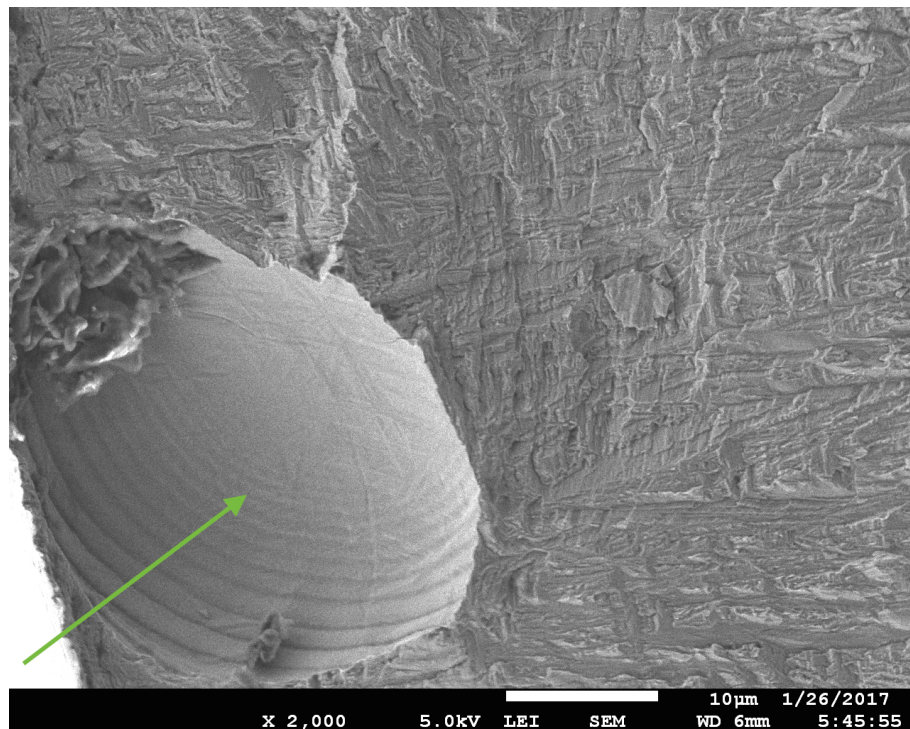


Figure IV.15: 2000x magnification, Plasma polished sample. The green arrow points to a surface defect that is very similar to internal pores observed in previous images. It is likely that this pore was present at the sub surface of the specimen and that the plasma polishing process allowed it to be brought to the surface. This is probably the crack initiation site that lead to the final failure.

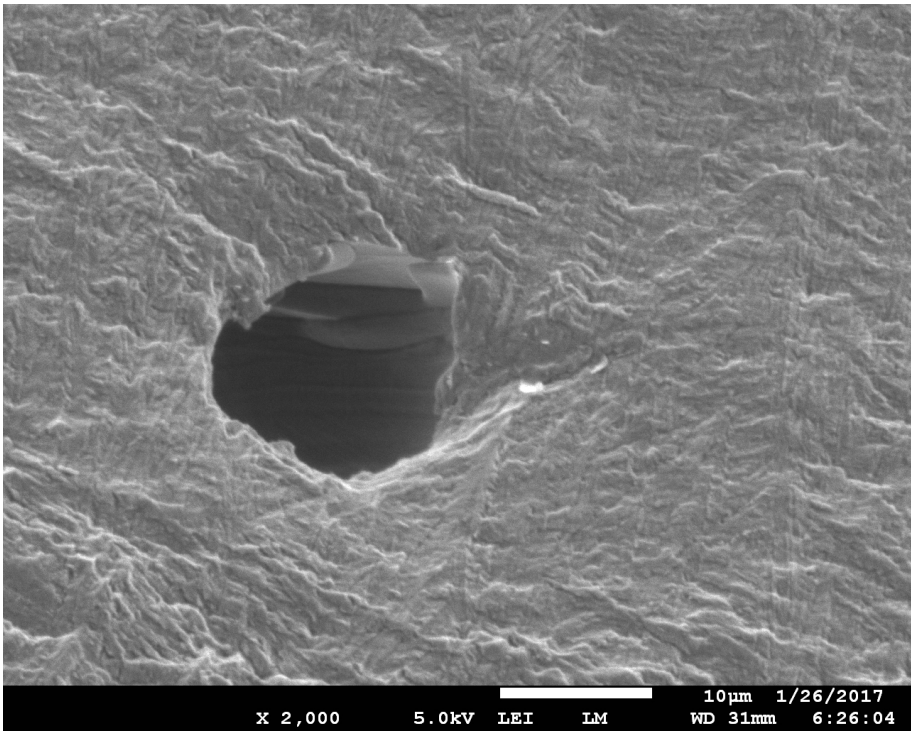


Figure IV.16: 2000x magnification, plasma polished sample. A void in the bulk material, of about 15 μm

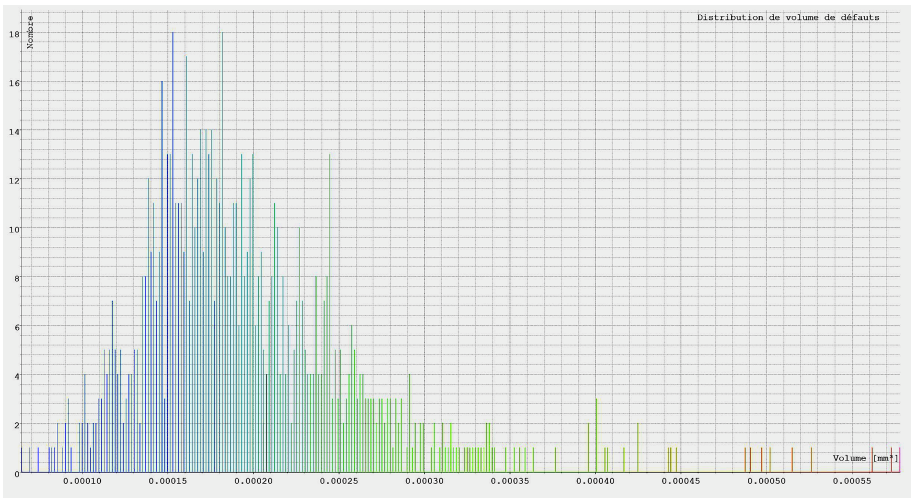


Figure IV.17: Pore size vs amount of pores for the three samples analysed

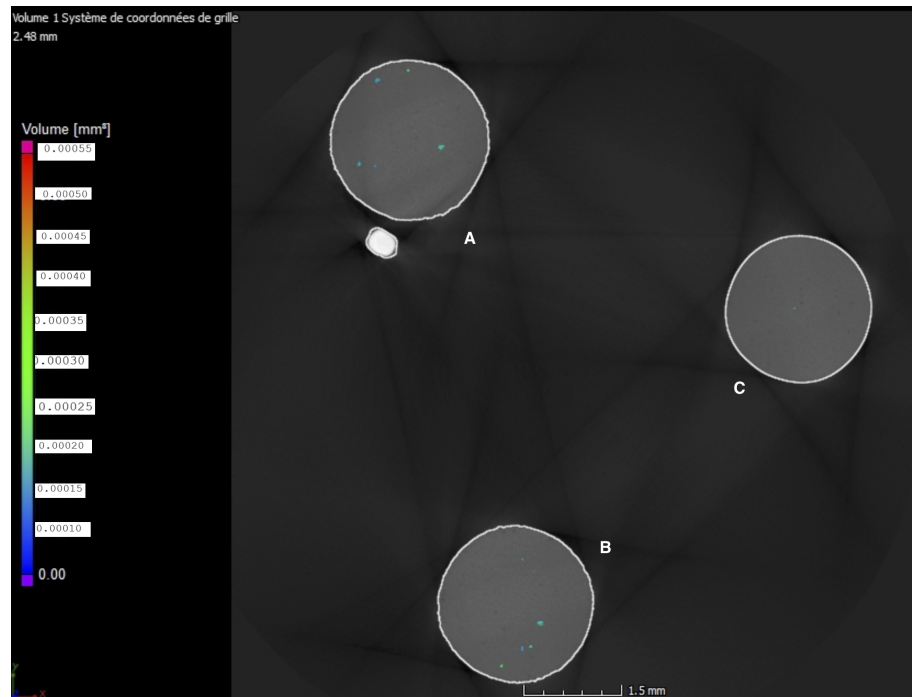


Figure IV.18: Top view of the samples, cut at the minimum cross section. Samples A and B are in the as-built condition while Sample C one is the plasma-polished one (observation done by analysing the circumference of the specimens). The white circle under sample A is an artefact created by the diffraction of X-rays during the CT scan.

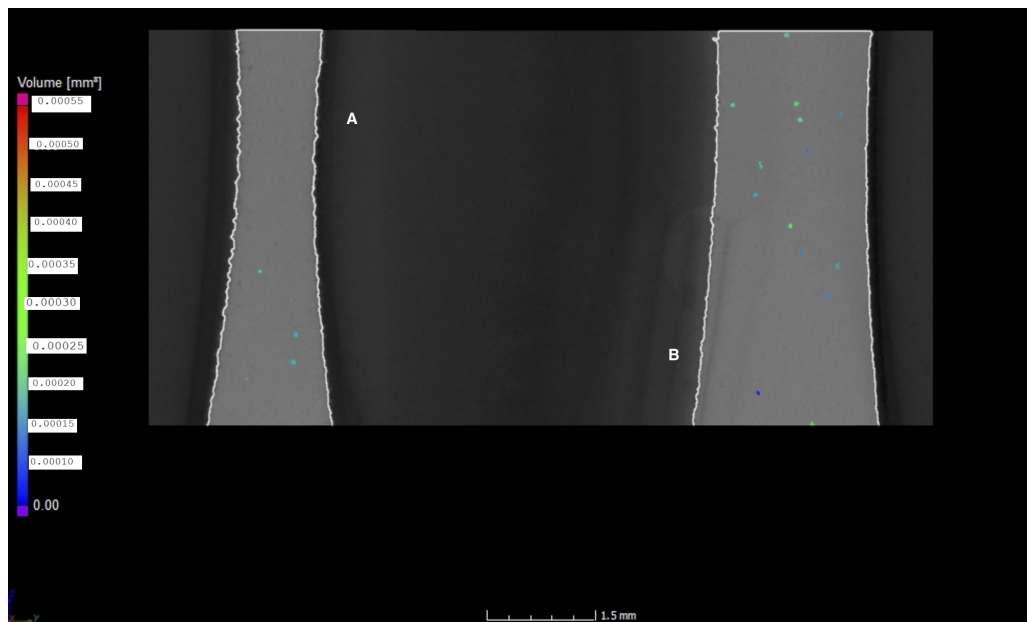


Figure IV.19: Samples A and B at different location of the (vertical) cross section.

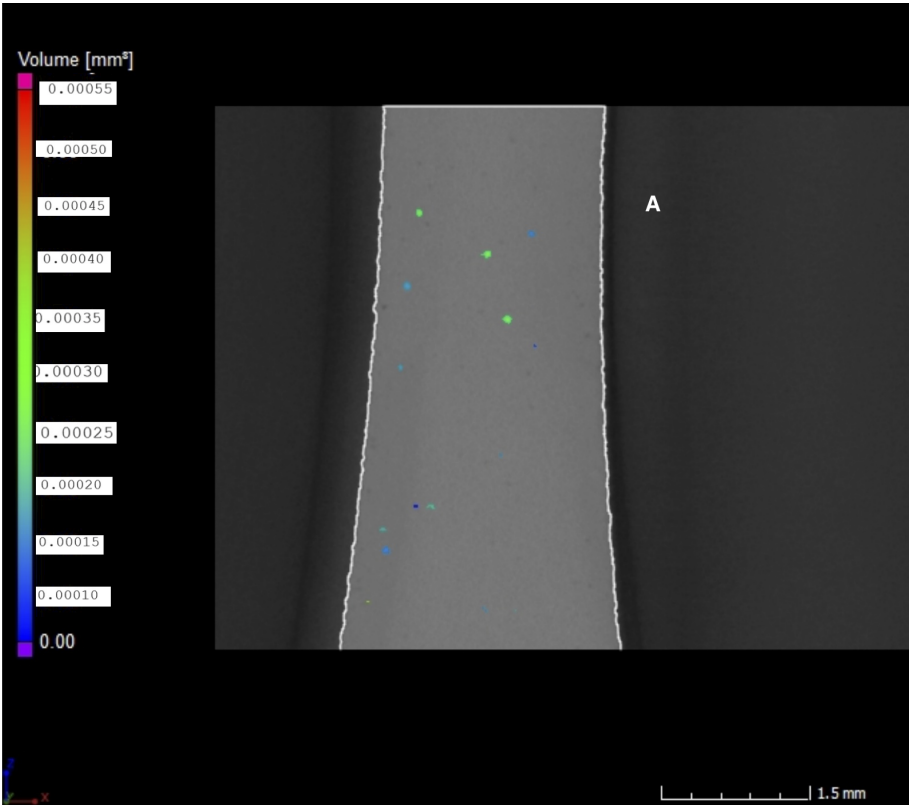


Figure IV.20: Sample A in central vertical cross section. Several defects can be observed in the subsurface region.

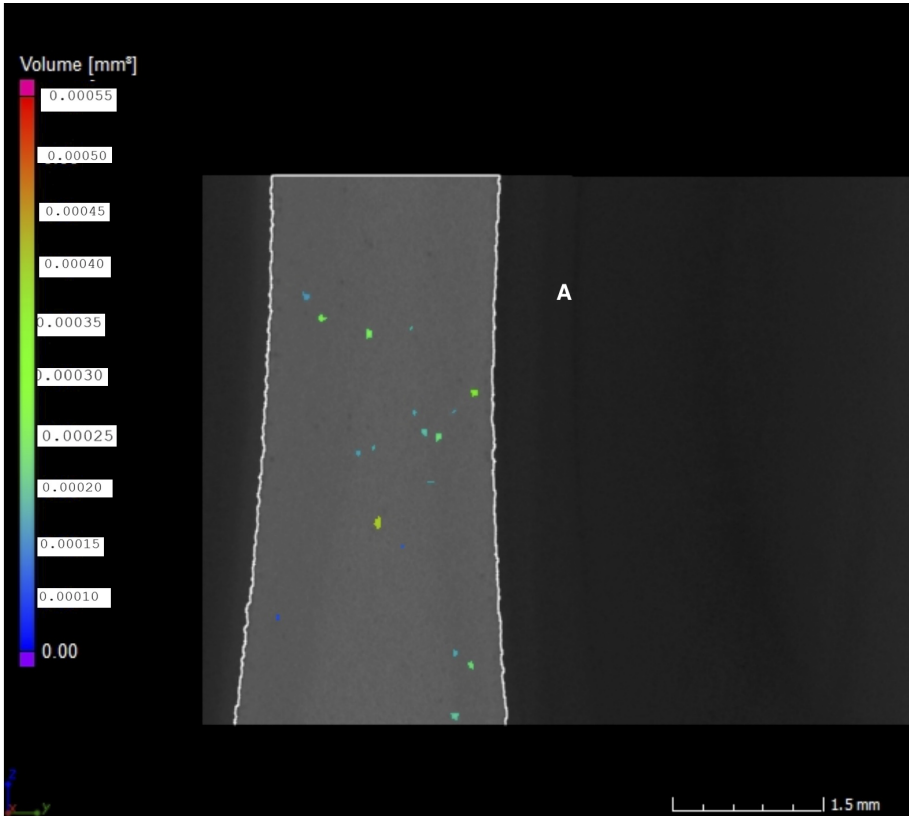
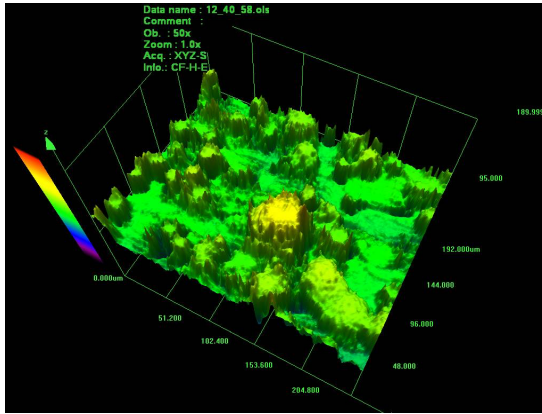
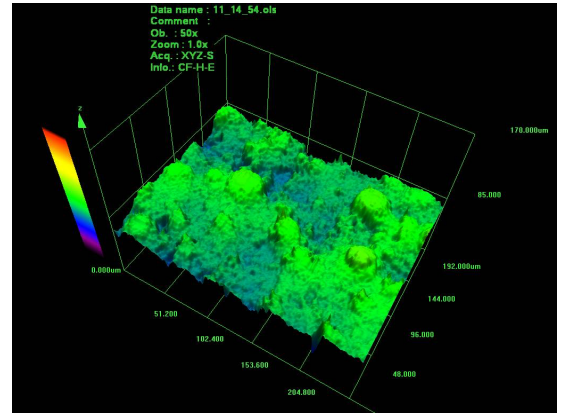


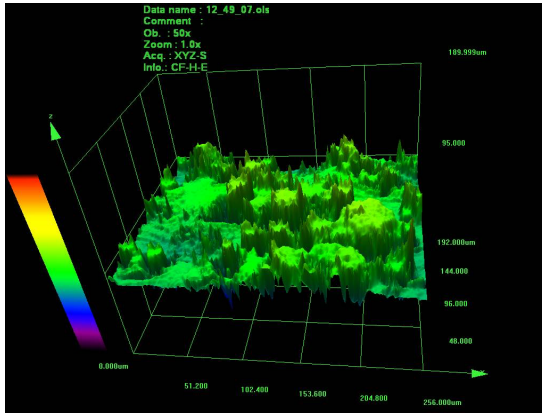
Figure IV.21: Sample A at a different cross section. Once more, multiple defects can be observed in the region



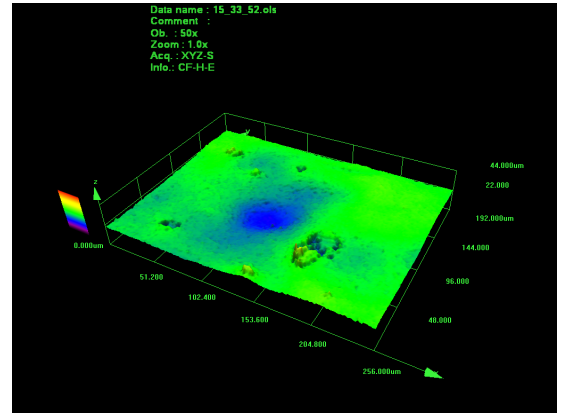
(a) 3D map of the surface of sample 11 after 5 mins of electropolishing with the perchloric and acetic acid solution at room temperature. Image obtained with a confocal microscope, mag x50.



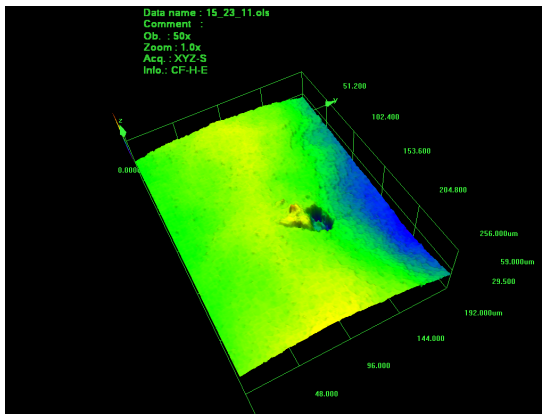
(b) 3D map of the surface of sample 14 after 15 mins of electropolishing with the perchloric and acetic acid solution at room temperature. Image obtained with a confocal microscope, mag x50.



(c) 3D map of the surface of sample 36 after 15 mins of electropolishing with the perchloric and acetic acid solution at 50 degrees. Image obtained with a confocal microscope, mag x50.

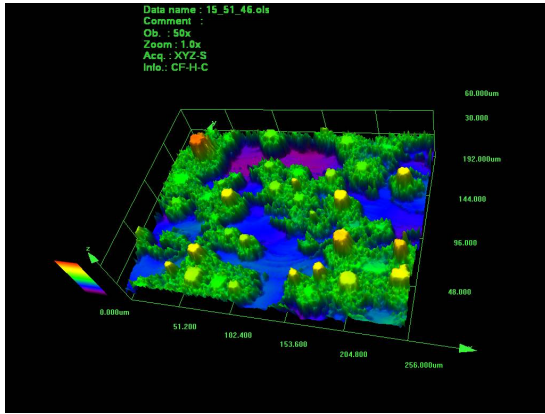


(d) 3D map of the surface of sample 35 after 2 mins of electropolishing with the hydrochloric acid solution at room temperature. Image obtained with a confocal microscope, mag x50.

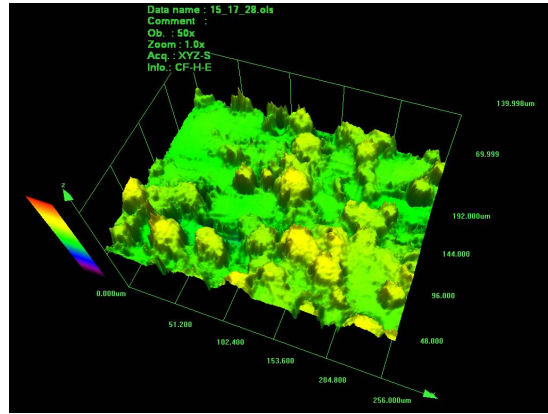


(e) 3D map of the surface of sample 15 after 5 mins of electropolishing with the hydrochloric acid solution at room temperature. Image obtained with a confocal microscope, mag x50.

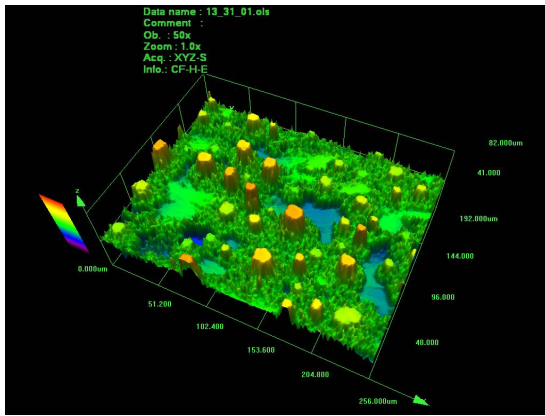
Figure IV.22: 3D surface renderings of chemically etched witness specimens



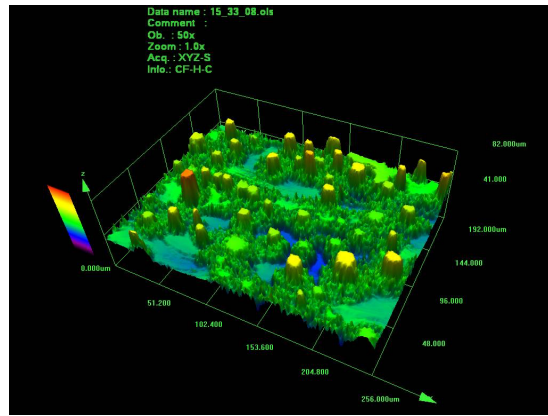
(a) 3D map of the surface of sample 13 after 10 mins of chemical etching with hydrochloric acid at room temperature. Image obtained with a confocal microscope, mag x50.



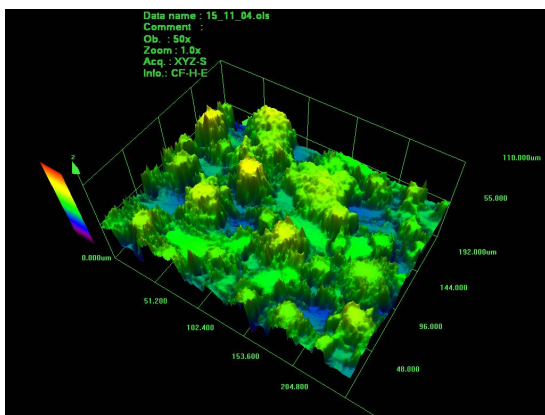
(b) 3D map of the surface of sample 17 after 20 mins of chemical etching with the perchloric and acetic acid solution at room temperature. Image obtained with a confocal microscope, mag x50.



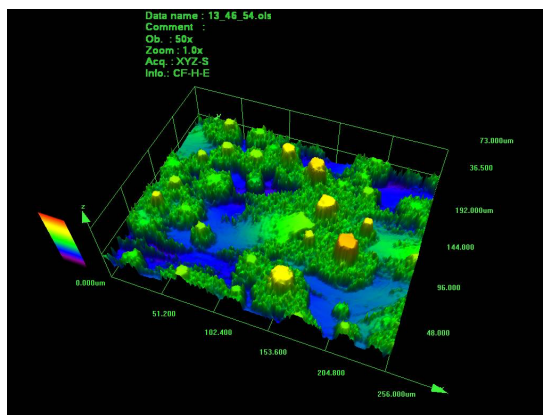
(c) 3D map of the surface of sample 23 after 5 mins of chemical etching with the hydrochloric and sulphuric acid solution at room temperature. Image obtained with a confocal microscope, mag x50.



(d) 3D map of the surface of sample 28 after 5 mins of chemical etching with the hydrochloric acid solution at room temperature. Image obtained with a confocal microscope, mag x50.



(e) 3D map of the surface of sample 31 after 10 mins of chemical etching with the perchloric and acetic acid solution at room temperature. Image obtained with a confocal microscope, mag x50.



(f) 3D map of the surface of sample 37 after 10 mins of chemical etching with the hydrochloric and sulphuric acid solution at room temperature. Image obtained with a confocal microscope, mag x50.

Figure IV.23: 3D surface renderings of electropolished etched witness specimens

Chapter V

Discussion

The purpose of this thesis is to investigate the effect of surface morphology on the fatigue performance of SLM Ti-6Al-4V. However, testing of the samples has revealed that the internal structure of the fatigue samples has a high amount of pores. The presence of these internal defects explain, in part, the poor results of the fatigue tests.

1 Influence of the surface treatment on roughness

Over the series of the experiments, surface treatments always reduce the roughness of the Ti-6Al-4V specimens. This reduction in roughness is observable over the entire range of treatments and there is no specific roughness parameter that is affected more than another. Moreover, the selection of the acid treatments was based on the results of the tests performed on the witness specimens. Since only one test was performed per acid solution (one set of acid concentration, temperature, and time), it cannot be said that the selected treatment is actually the best one.

1.1 Chemical etching

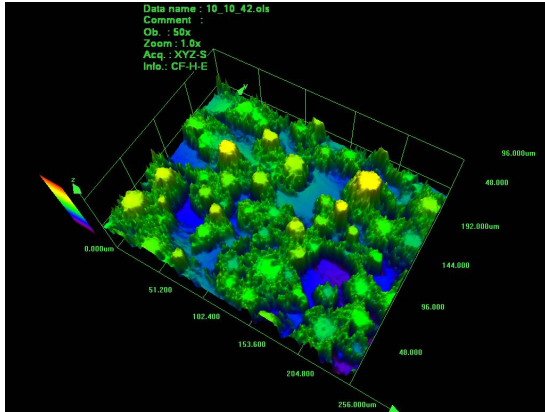
Although most literature suggest that HF is the only acid that can effectively polish the surface of Ti-6Al-4V [37] [40], HCl appears to be an interesting alternative when it is applied with an electrical current. Even though every acid treatment lead to material being removed from the surface, the material removal rate varied, making some treatments more effective than others. This is especially true for the HCl treatment. Furthermore, there is a clear time dependence of the treatments, with lower R_p , R_v , R_a , and R_t as the treatment time increase. Since the longest treatment time was 20 minutes it can't be said with absolute certainty that increasing the time of the treatment further leads to a smoother surface, nor if after a certain time, the acid attacks and damages the surface.

One important point to mention regarding the chemical etching and electropolishing treatment of the witness specimens is the complete absence of repetition of the experiments. It was purposely chosen to proceed this way as it would allow to test a larger array of chemical treatments. Moreover, the purpose of the chemical tests is to identify the most effective ones at smoothening the surface of Ti-6Al-4V. Thus, establishing exactly within what bounds a specific chemical treatment can smoothen the surface of the titanium alloy is not of paramount importance for the scope of this master thesis.

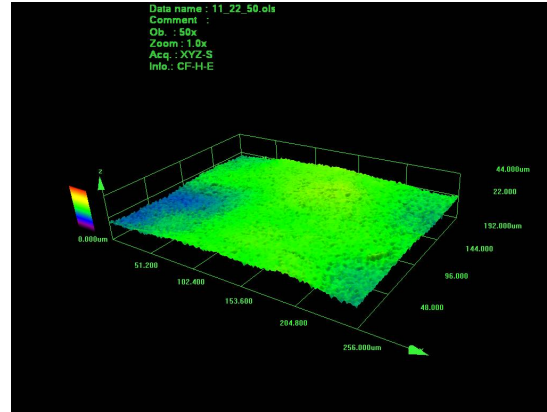
1.2 Electropolishing

The electropolishing treatment is more effective than the chemical etching. The addition of the electrical current between the workpiece (the anode) and the cathode forces the ionic exchange at the surface of the material. Similarly to the chemical etching process a time dependency was observed. The smoothest surfaces were obtained after a 5 minutes treatment with hydrochloric acid. However, this treatment also lead to severe damage to the geometrical accuracy of the part. Effectively, electropolishing is limited in time by its effect on geometrical tolerances. Another interesting observation that can be seen in figure IV.5 is the decreased effect of the treatment as

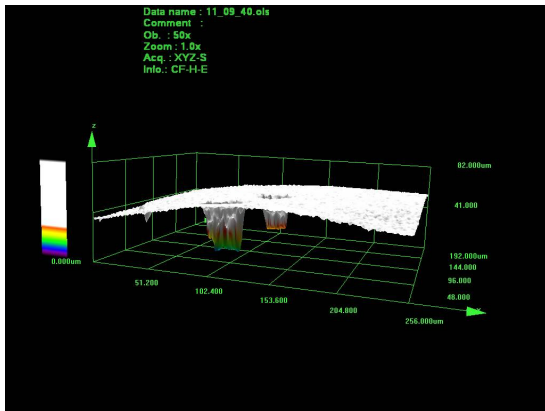
the temperature is increased. This could be due to increased evaporation of the acid species or the kinetics of the reaction could be increased so much that the treatment has a negative effect on the surface.



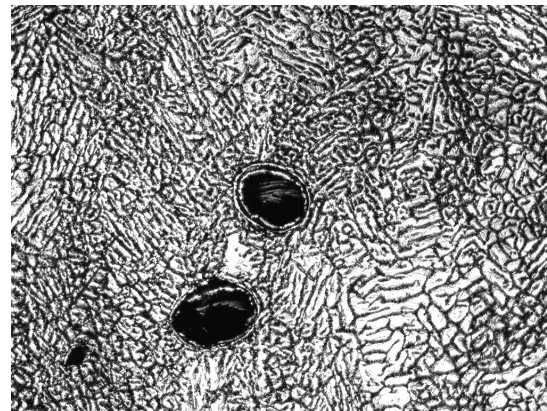
(a) A 3D rendering of the surface of a fatigue specimen in the as-built condition obtained with a confocal microscope in the cross section of a specimen (mag x 50).



(b) A 3D rendering of the surface of a fatigue specimen after electropolishing with HCl for 2mins obtained with a confocal microscope in the cross section of a specimen (mag x 50).



(c) A 3D rendering of the surface of a fatigue specimen after electropolishing with HCl for 2mins obtained with a confocal microscope in the cross section of a specimen (mag x 50). This images shows two pits that go deep under the surface.



(d) A 2D view of the surface of a fatigue specimen after electropolishing with HCl for 2 mins obtained with a confocal microscope in the cross section of a specimen (mag x 50). The two pits have a very spherical shape.

Figure V.1: 3D rendering of the surface of electropolished fatigue specimens

Figure V.1a gives a good overview of the surface morphology of an untreated specimen. It is very uneven, with large peaks and some deep valleys. These valleys create local stress raiser and lead to the initiation of fatigue cracks in the untreated specimens. Now, when looking at figure V.1b it is possible to observe a completely different surface morphology. It is not as jagged as the as built one. There are no specific locations for large peak stresses. However this image was only conducted over a small portion of the surface. Indeed, looking at figures V.1c and V.1d one can clearly observe two deep pits that start at the surface. these pits could be due to the chemical treatment or could be sub-surface pores that are now open due to surface removal during the treatment. Observing solely figure V.1c one could only speculate as to the cause of these deep pits, but figure V.1d does show that these pits have a very circular cross section. This last point, combined with the results of the CT scan suggests that these pits were once pores that are now located at the surface.

1.3 Plasmapolishing

Of all the post-treatments, plasma-polishing leads to the smoothest surfaces. The Ra values are as low as $0.2\mu m$. However, it is still possible to conclude that there are many pits at the surface of the part since the R_v is greater than R_a . These pits are not very deep but they still act as stress raisers on a processed part's surface.

1.4 Surface treatment perspectives

The majority of chemical treatments performed in this study show consistence with those performed in literature [38] [8] [37]: the effect on surface roughness depends primarily on treatment time and acid concentration. In addition, chemical etching of Ti-6Al-4V seems too have little effect if HF is not used. This is not true in the case of electropolishing. The treatment performed with high concentrations of HCl greatly improves the surface on all 12 treated fatigue samples making it a repeatable and statistically sound process. This process was conducted using a combination of high voltage and high acid concentration that is not often tested in literature. This treatment is promising as it could be an interesting (and safer) alternative to HF. One drawback of this treatment is its sensitivity to time: the geometry of the sample is completely lost after a 5 min treatment time while stays relatively close to the original one after 2 mins of treatment. This treatment can thus be effectively applied for a limited amount of time before it irreversibly damages the workpiece. More control over the time sensitivity of this electrochemical process could be achieved by increasing the control over the kinetics of the reaction. This can be achieved by reducing the concentration of acid or the applied current but a more original approach would be to lower the temperature of solution. A solution of 37 wt% HCl remains liquid until $-27^\circ C$. Lowering the temperature has the advantage of keeping the initial amount of reactants the same and maintaining the same current density during the process.

Another promising treatment performed in this thesis is plasma-polishing. This process has many advantages over chemical treatments since it does not use toxic acids to smoothen the surface. What's more, the obtained surface is extremely smooth. The major limiting factor for this treatment is the required voltage (200V) to obtain the plasma [44]. None-the-less, this treatment is by far the most effective one for polishing SLM Ti-6Al-4V.

2 Fatigue tests

2.1 General observations

As a general observation, it can be seen from the S-N curves that the results indicate a poor fatigue performance of all the samples and no clear effect of the surface roughness can be identified. In fact, the observed fatigue performance is lower than similar tests conducted in literature. None-the-less, There is a tight grouping of failures, especially in the as built conditions. This observation is consistent with the work done in [45]. To understand the poor fatigue behaviour of these samples there are several elements to take into account.

The S-N curve of figure V.2 indicates the number of cycles until failure at a given stress level for the as-built + HIP samples as black squares. These results can be compared to the as-built and as-built + heat treatment plots in the paper by Li et al. [4]. Furthermore, after applying the correction factor for the stress at R ratios other than -1, it is also possible to compare the results of this study with the one performed by Edwards in [28] on as-built samples. The first observation is that the printing direction decreases the fatigue performance of the part. Moreover, the as-built + HIP samples of this study perform worse than the simply as-built samples from Li and Edwards [4] [28]. However, the HIP treatment should have eliminated the residual stresses and the size of possible voids entrapped in the part [34] [33] meaning that the fatigue performance of HIP processed sample should be superior to that of non HIP processed samples [4]. Differences between the fatigue test in this study and the ones done in literature are the load case (fully reversed bending in this study and tension-tension in the others) as well as the vertical printing direction, and the size of the samples. However, it is clear that these differences alone do not account for the lower fatigue performance and that high porosity measured with the CT scan seems to be another contributing factor to poor fatigue.

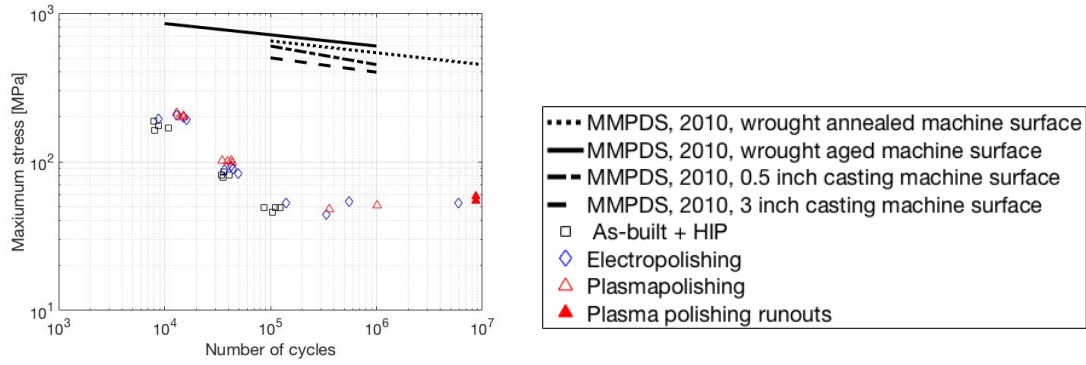


Figure V.2: SLM versus traditional manufactured methods

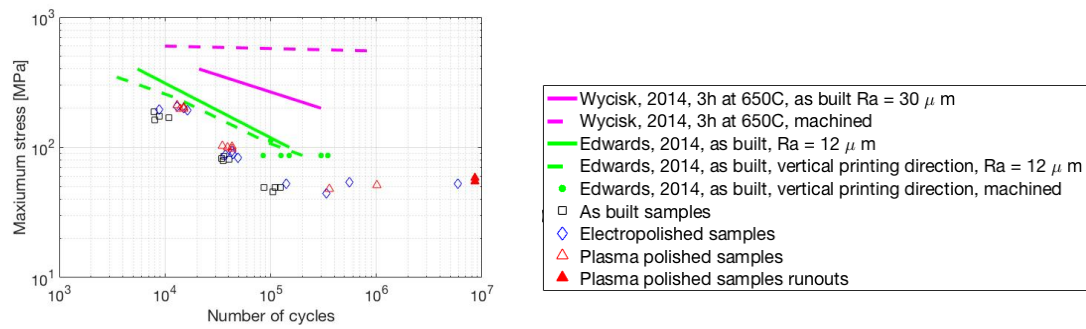


Figure V.3: SLM versus literature

Size of the fatigue specimens

Firstly, the size of the cross section of the specimens in this study is quite small. Although it is 300mm^2 for the specimens in Edwards and 78.5mm^2 for the specimens in Li, it is only 4.15mm^2 in this study. Generally, the fatigue life decreases with increasing cross section area [26] [46]. This is simply because a larger cross section area means that the surface of the part is bigger leading to a higher probability of surface defects and crack initiation sites at the free surface of the part [10]. However, the surface of as built SLM parts (regardless of HIP or heat treatment) contain a high level of inhomogeneity, as it can be observed by the high Ra, Rv, Rp and Rt values. This signifies that there is a large density of stress raisers over the entire surface of as-built SLM parts. Hence, when SLM parts are subject to fatigue loading, crack nucleation happens almost instantaneously. The crack initiation period is not the dominant phase of the the fatigue life anymore, the crack propagation is. This would explain why the SLM parts of the other studies performed better under fatigue than small parts used here. In order to verify this hypothesis, namely, that the crack growth life is longer for larger specimens, a crack growth model was generated using the crack growth tool available at efatigue.com. It was possible to model a circular bar with with circumferential crack subjected to a bending load. The loading and a sketch of the model are presented in figure V.4. Using a model on efatigue.com, an estimation of the crack growth can be generated. The crack growth material constants for standard titanium are used, namely $C = 4e - 14\text{m/cycle}$ and $\Delta K_{TH} = 9\text{MPa}$. The initial crack size was set at $85\mu\text{m}$ and the value of $2b$ ranged from 2.3mm (like the samples in this study) to 50mm . Such a model represents the poor surface roughness of SLM parts quite accurately since it considers a homogenous crack all along the bar. The software of efatigue.com is able to estimate the crack growth life of each bar based on their diameter. The results are presented in graph V.5.

The analysis from efatigue.com clearly shows that in the case of an initial flaw, the fatigue life increases as the diameter increases. However, this increase in diameter is not linear. Between, a diameter of 2.3mm (the samples from this study) and one of 10mm (the samples from Wycisk),

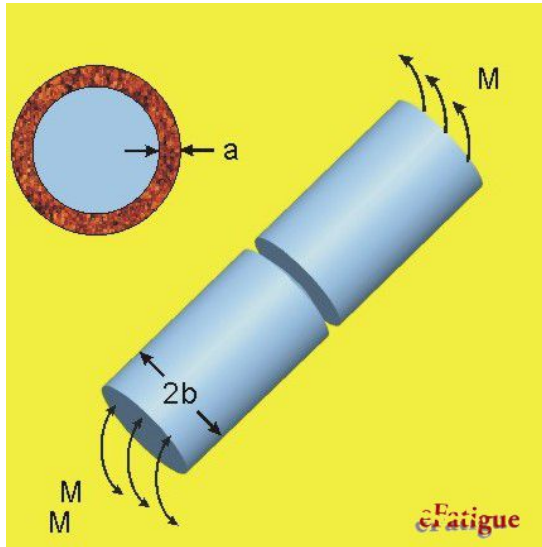


Figure V.4: Loading type for the simulation

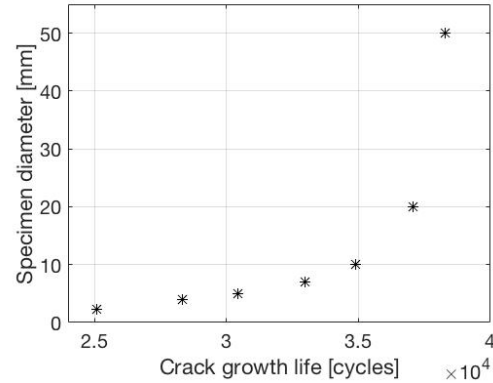


Figure V.5: Effect of specimen diameter on crack growth life

there is a 28% increase in crack growth life. However, the increase in crack growth life between a 10mm diameter and a 50mm diameter is only 9%. This indicates that the size effect of the test samples is particularly visible when their diameter is below 10mm and explains why there is such a difference in the fatigue performance of the samples in this study compared to those of other studies.

Porosity of the fatigue specimens

Secondly, the results from the tomography analysis indicate that the amount of internal porosities is higher than expected. This is especially true when one considers that the specimens have been subjected to a HIP treatment which should considerably reduce the amount of internal pores. The density of the samples, as calculated with the tomography analysis, reveals a porosity as high as 0.26%. Moreover, such high porosity does not correlate with porosity levels reached in literature. This suggests that the HIP treatment was either not performed correctly, or was simply not performed at all. Hence, the bulk properties of the material, are not well suited to investigate the effect of the surface roughness of the fatigue life of AM titanium. Indeed, although the surface treatments are able to smoothen the surface by removing material, this also means that internal defects, that used to be in the subsurface, are now present at the surface. These pores can thus act a prime locations for fatigue crack initiation. The images in V.6 are obtained from [47]. This this

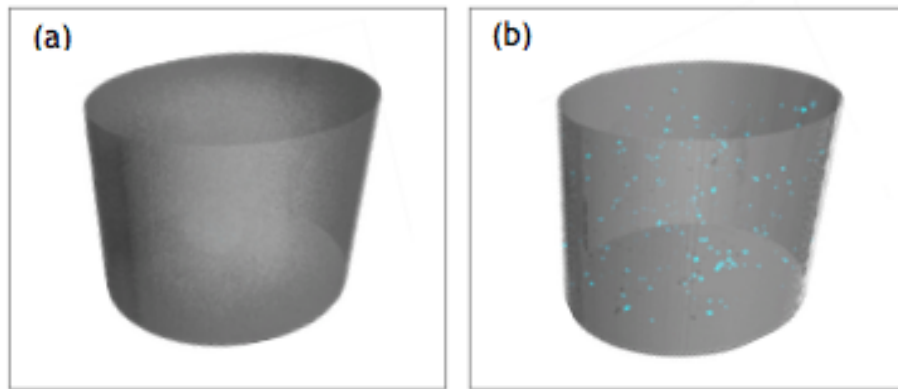


Figure V.6: CT scan of a 3 mm diameter cylinder showing porosity (blue coloured) and distribution, where a) HIP, b) as-built. After the HIP process the porosity was below the resolution limit of 3 μm [47]

paper, Becker et al. investigate the effect of different heat treatments as well as HIP on the (static)

mechanical properties selectively melted Ti-6Al-4V. In their work, the HIP treatment lead to the suppression of any pores greater that $3\mu m$. Unfortunately, this cannot be said about the fatigue specimens used for this thesis. Indeed, as it was presented in the results section, the samples used still have many pores, ranging from 0.00010 to $0.00055mm^3$. The CT scan of the specimens used in this thesis, that can be observed in figures IV.18, IV.19, IV.20, and IV.21, as well as the results obtained in [47], support the hypothesis that the HIP treatment was omitted for the the samples of this thesis.

Another observation that supports the sub-surface porosity's responsibly for early fatigue failure can be seen when looking at IV.18 , sample C. This is the CT scan of a plasma-polished sample that did not fail after 8 million cycles. What is striking is the absence of pores near the sample's surface, suggesting that an improved surface roughness can lead to higher fatigue performance.

2.2 Untreated specimens

As explained previously, the untreated specimens performs worse than specimens tested in literature, especially compared to other HIPed samples. Their performance is much closer to that of as built samples. This would suggest that the samples have not been subjected to an HIP treatment. This claim is supported when the high porosity is observed and compared to non HIP AM titanium in literature [47]. In spite of their poor mechanical performance, these samples to exhibit a similar, low scatter failure mechanism. This observation is also made by Hooreweder " the failure mechanism is consistently leading to low statistical scatter in the fatigue data" [45]. The short spread of the fatigue life at a given stress level is believed to be a consequence of the rough surface: fatigue crack initiation happens within the first hundred cycles in a homogenous fashion along the surface line. Hence, the crack growth life is the lead part of the fatigue life.

When observing the fracture surfaces of the as built + HIP samples, it is always possible to observe a brittle failure zone, as well as, crack growth zone near the surface. This suggest that crack initiate at the surface, merge, and lead final failure. The brittle surface failure, is comparable to that of TM titanium failures under rotating fatigue loading. In fact it can be compared to the images C and F of figure V.7.

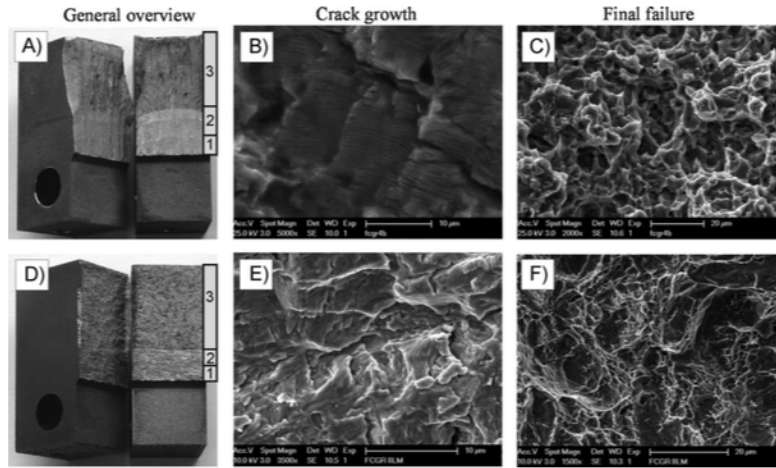


Figure V.7: General overview, crack growth, and final failure microscopy of fractured CT specimens from titanium (A,B and C) and SLM titanium (D, E and F)

The dimples observed in the samples of this study correlate with the SLM ones of the study of Hooreweder. As explained in the paper, these dimples are consistent with a more brittle failure and a fine martensitic phase obtained through fast cooling rates.

2.3 Fatigue of treated specimens

The failure of the surface treated specimens differs with that of the untreated specimens. At low and medium cycle fatigue, failure occurs at slightly longer life periods, but the same grouping of the fatigue lives can be observed as in the case of the untreated samples. However, the mechanics

of failure change with lower stresses, at high cycle fatigue. Indeed, the fatigue life seems to increase significantly at lower loads. Non the less, the increase in fatigue life is not constant and there is a large spread in the results. Looking at the fracture surfaces, it can be seen that the crack pattern is much different than that of the as built samples. The brittle fracture zone is located in one of the cross section, starting at an arc of the surface and going inwards towards the center. In fact the brittle failure zone mimics the shape a single slice of pizza. This fracture type is inconsistent with regular rotating bending fatigue failures where a central brittle zone is observed. This new failure mode can be explained when taking into account the bad internal characteristics of the parts. The following steps lead to part failure and the "pizza slice" brittle zone:

- Surface treatment smoothens the surface and removes material.
- Internal pores are now present at the surface.
- During the first cycles of the fatigue test, surface pores act as crack initiation sites.
- As the crack progresses at the surface of the sample, the peak stress in that location increases.
- When the crack is in compression, the opposite zone does not experience higher peak stresses.
- As the crack increases in size, so does the peak stress, which speeds up the crack growth
- Final failure occurs, the crack initiated in a zone opposite to the "pizza slice"

The surface treatment has two consequences on the surface of the part: firstly, it remove the rough layer of material. Secondly, and because the bulk material is ridden with pores, subsurface defects are brought to the surface and can then become prime crack initiation sites. This theory is further supported when looking at a surface defect of the SEM image of the plasma polished sample: at spherical void is located near the surface and it's smooth interior shape suggest it was a defect that occurred during the manufacturing process [48].

Chapter VI

Conclusion

1 Conclusion

The initial objective of this study was to investigate the effects of surface treatments on the fatigue performance of SLM Ti-6Al-4V. However, the important amount of pores in the test samples lead to early failure of the test samples and it was thus not able to obtain any conclusive evidence. None-the-less, several chemical treatments, as well as plasma polishing, are capable of significantly reducing the surface roughness of SLM Ti6-Al-4V. These results are encouraging since they suggest that alternatives to HF are readily available for surface treatment of Ti-6Al-4V. In addition, the fatigue tests in this study are consistent with other tests performed on specimens non subjected to HIP treatments: low scatter in the fatigue life and no real fatigue limit is observed. The fatigue properties of SLM Ti-6Al-4V are still inferior to the traditionally manufactured alloy due to the surface roughness in the as built conditions and due to residual sub surface pores that come to the surface if post treatments are applied.

2 Recommendations and perspective for future research

The following set of recommendations is set for future researchers:

- Electropolishing with HCl should be further investigated, specifically, more control over the process kinetics needs to be achieved.
- Obtaining fully dense metallic alloys is paramount for the application of SLM alloys in fatigue sensitive application, research should primarily focus on this point.
- The bulk properties of SLM Ti-6Al-4V should always be checked. This should be performed using a CT scan in order to obtain the maximum amount of information regarding the bulk properties. In fact, it seems that performing a CT scan should be performed for any metal alloy produced by SLM.
- This research should be carried out again using SLM Ti-6Al-4V with a higher density in order to establish a link between surface roughness and fatigue performance. Moreover, the cross section of the specimens should be closer to those encountered in literature.
- The existence of a fatigue limit for as-built + HIP samples should be investigated.
- Given the low scatter of the as built + HIP samples, it would be interesting to determine the fatigue crack growth rate within the bulk material. This could potentially lead to an accurate estimation of the fatigue life and limit the need of surface treatments.

Bibliography

- [1] ASM international. Fatigue, Chapter 14 2008.
- [2] William E Frazier. Metal additive manufacturing: A review. *Journal of Materials Engineering and Performance*, 23(6):1917–1928, February 2014.
- [3] Y Huang, M C Leu, J Mazumder, and A Donmez. Additive manufacturing: current state, futur potenital, gaps and needs, and recommendations. *Journal of manufacturing science and engineering*, 137, 2015.
- [4] P. Li, D.H. Warner, A. Fatemi, and N. Phan. Critical assessment of the fatigue performance of additively manufactured ti-6al-4v and perspective for futur research. *International Journal of Fatigue*, 2015.
- [5] 2017.
- [6] Eckart Uhlmann, Robert Kersting, Tiago Borsoi Klein, Marcio Fernando Cruz, and Anderson Vicente Borille. Additive manufacturing of titanium alloy for aircraft components. *Procedia {CIRP}*, 35:55 – 60, 2015. {MIC2015} – 15th Machining Innovations Conference for Aerospace Industry.
- [7] Galina Kasperovich and Joachim Hausmann. Improvment of fatigue resistance and ductility of tial6v4 processed by selective laser melting. *Journal of Materials Processing Technology*, 2014.
- [8] D. Greitemeier, C. Dalle Donne, F. Syassen, J. Eufinger, and T. Melz. Effect of surface roughness on fatigue performance of additive manufactured ti-6al-4v. *Special issue article Minerals and Mining*, 2015.
- [9] D Dutta and F H Froes. *Titanium powder metallurgy*. Elsevier Inc, 2015.
- [10] Jaap Schijve. *Fatigue of structures and materials*. Springer, 2nd edition, 2001.
- [11] *Material Science*. Elsevier Inc, 2009.
- [12] Ian Gibson, David Rosen, and Brent Stucker. *Additive Manufacturing Technologies*. Springer, second edition edition, 2015.
- [13] H Gong, H Gu, K Zeng, and J J Lewandowski. Melt pool characterization for selective laser melting of ti-6al-4v pre-alloyed powder. In *25th annual international solid freeform fabrication symposium*, 2014.
- [14] Amanda J. Sterling, Brian Torries, Nima Shamsaeil, Scott M. Thompson, and Denver W. Seely. Fatigue behavior and failure mechanisms of direct laser deposited ti-6al-4v. *Materials Science and Engineering A*, 2015.
- [15] W. J. Sames, F. A. List, S. Pannala, R. R. Dehoff, and S. S. Babu. The metallurgy and processing science of metal additive manufacturing. *International Materials Reviews*, 2016.
- [16] Erhard Brandl, Christoph Leyens, and Frank Palm. Mechanical properties of additive manufactured ti-6al-4v using wire and powder based processes. *Materials Science and Engineering*, 2011.

- [17] Amanda Sterling, Nima Shamsaei, Brian Torries, and Scott M. Thompson. Fatigue behaviour of additively manufactured ti-6al-4v. *Procedia Engineering*, 2015.
- [18] Grzegorz Pyka, Greet Kerckhofs, Ioannis Papantoniou, Mathew Speirs, Jan Schrooten, and Martine Wevers. Surface roughness and morphology customization of additive manufactured open porous ti6al4v structures. *Materials*, 6(10):4737, 2013.
- [19] Haijun Gong, Khalid Rafi, Hengfeng Gu, G.D. Janaki Ram, Thomas Starr, and Brent Stucker. Influence of defects on mechanical properties of ti-6al-4v components produced by selective laser melting and electron beam melting. *Materials and Design*, 2015.
- [20] Peter Mercelis and Jean-Pierre Kruth. Residual stresses in selective laser sintering and selective laser melting. *Rapid prototyping journal*, 12(5):254 – 265, 2006.
- [21] S Garcia. Lecture 3 functional coatings. Lecture slides, 2015.
- [22] S. W. Paddock. Confocal laser scanning microscopy. *BioTechniques*, 27:992–1004, November 1999.
- [23] Fabia Cristina Rossetti, Livia Vieira Depieri, and Maria Vitoria Lopes Badra Bentley. Investigation of skin drug delivery systems and diagnosis of skin disorders. *Confocal laser microscopy - principles and applications in medicine, biology, and the food sciences*, 2013.
- [24] 2017.
- [25] Zygo. Surface texture parameters.
- [26] H. E. Boyer. Fatigue testing. Technical report, ASM International, 1986.
- [27] Christoph Leyens and Manfred Peters. *titanium and titanium alloys*. Wiley-VCH, 2003.
- [28] P. Edwards and M. Ramulu. Fatigue performance evaluation of selective laser melted ti-6al-4v. *Materials Science and Engineering A*, 2013.
- [29] G. Deng, K. Nagamoto, Y. Nakano, and T. Nakanishi. Evaluation of the effect of surface roughness on crack initiation life. Master’s thesis, University of Miyazaki, 2008.
- [30] Bey Vrancken, Lore Thijs, Jean-Pierre Kruth, and Jan Van Humbeeck. Heat treatment of ti6al4v produced by selective laser melting: Microstructure and mechanical properties. *Journal of Alloys and Compounds*, 541:177 – 185, 2012.
- [31] M. Shiomi, K. Osakada, K. Nakamura, T. Yamashita, and F. Abe. Residual stress within metallic model made by selective laser melting process. *{CIRP} Annals - Manufacturing Technology*, 53(1):195 – 198, 2004.
- [32] T. Vilaro, C. Colin, and J. D. Bartout. As-fabricated and heat-treated microstructures of the ti-6al-4v alloy processed by selective laser melting. *Metallurgical and Materials Transactions A*, 42(10):3190–3199, 2011.
- [33] Chunlei Qiu, Nicholas J.E. Adkins, and Moataz M. Attallah. Microstructure and tensile properties of selectively laser-melted and of {HIPed} laser-melted ti–6al–4v. *Materials Science and Engineering: A*, 578:230 – 239, 2013.
- [34] Xiaoli Zhao, Shujun Li, Man Zhang, Yandong Liu, Timothy B. Sercombe, Shaogang Wang, Yulin Hao, Rui Yang, and Lawrence E. Murr. Comparison of the microstructures and mechanical properties of ti–6al–4v fabricated by selective laser melting and electron beam melting. *Materials & Design*, 95:21 – 31, 2016.
- [35] Sunil Jha and V.K. Jain. Design and development of the magnetorheological abrasive flow finishing (mraff) process. *International Journal of Machine Tools and Manufacture*, 44(10):1019 – 1029, 2004.
- [36] V.K. Jain. Magnetic field assisted abrasive based micro-/nano-finishing. *Journal of Materials Processing Technology*, 209(20):6022 – 6038, 2009. Special Issue: 1st International Conference on Abrasive Processes.

- [37] Dobrzański L. A., Dobrzańska-Danikiewicz A. D., GawęłT. G., and Achtełik-Franczak A. Selective laser sintering and melting of pristine titanium and titanium ti6al4v alloy powders and selection of chemical environment for etching of such materials. *Archives of Metallurgy and Materials*, 60:2039, 2016-03-02T11:23:34.338+01:00 2015.
- [38] Hazman Hasib, Ola L.A. Harrysson, and Harvey A. West. Powder removal from ti-6al-4v cellular structures fabricated via electron beam melting. *JOM*, 67(3):639–646, 2015.
- [39] Bartłomiej Wysocki, Joanna Idaszek, Karol Szlajak, Karolina Strzelczyk, Tomasz Brynk, Krzysztof J. Kurzydłowski, and Wojciech Swieszkowski. Post processing and biological evaluation of the titanium scaffolds for bone tissue engineering. *Materials*, 9(3):197, 2016.
- [40] Grzegorz Pyka, Andrzej Burakowski, Greet Kerckhofs, Maarten Moesen, Simon Van Bael, Jan Schrooten, and Martine Wevers. Surface modification of ti6al4v open porous structures produced by additive manufacturing. *Advanced Engineering Materials*, 14(6):363–370, 2012.
- [41] Guilherme Arthur Longhitano, Maria Aparecida Larosa, Andrea Luiz Jardini Munhoz, Cecilia Amalia de Carvalho Zavaglia, and Maria Clara Filippini Ierardi. Surface Finishes for Ti-6Al-4V Alloy Produced by Direct Metal Laser Sintering. *Materials Research*, 18:838 – 842, 08 2015.
- [42] Anselm Kuhn. The electropolishing of titanium and its alloys. <https://www.researchgate.net/publication>, June 2004.
- [43] Plasotec GmbH. Process of plasma polishing. <http://www.plasotec.de/plasotec-english/process-plasma-polishing.html>, 01 2017.
- [44]
- [45] B van Hooreweder, R Boonen, D Moens, J-P Kruth, and P Sas. On the determination of fatigue properties of ti6al4v produced by selective laser melting. *Structures, structural dynamics and Materials conference*, 2012.
- [46] W Guo, C H Wang, and L R F Rose. The influence of cross-sectional thickness on fatigue crack growth. *Fatigue fracture engineering material structures*, 22:437–4444, 1999.
- [47] T H Becker, M Beck, and C Scheffer. Microstructure and mechanical preproperties of direct metal laser sintered ti-6al-4v. *South African Journal of Industrial Engineering*, 26(1):1–10, 2015.
- [48] Brecht van Hooreweder, David Moens, Rene Boonen, and Paul Sas. Analysis of fracture toughness and crack propagation of ti6al4v produced by selective laser melting. *Wileyonlinelibrary*, 14(1-2), 2015.

Appendix A

A step-by-step guide for chemical treatments

Appendix D: chemical treatments explained for dummies

1 Chemical etching

Equipment - Step 0

The following equipment is necessary for the chemical etching treatment:

- 2 large beakers (1000mL)
- 2 medium beakers (250mL)
- 2 small beakers (100mL)
- Glass pipette
- Acid(s)
- Distilled water
- Heating plate
- Clamps
- Stopwatch
- Protective gear: lab coat, gloves and glasses
- Tweezers

Setting up the equipment - Step 1

Once the protective gear is on, it is possible to place all the listed elements under the fume hood. Subsequently, the 1000 mL beakers should be filled with about 750mL of distilled water. These will serve as waste beaker for the acid once the experiment has been conducted. The acids that are needed for the experiment can be poured from their container to the medium size beaker so as not to take the acid directly from their original bottle. Once the 250 mL beakers contain enough acid for the experiment, it is recommended to stow the acid bottles back in their storage facility to keep the place under the fume hood clear of unnecessary elements.

Preparing the acid solution - Step 2

The desired acid solutions are obtained by diluting the right amount of acid in the right amount of water. When computing the required quantities of acid and distilled water, one should keep in mind that the computations are performed in weight percent and that the density of the acids is not 1. Before creating the acid solution, the beaker should be firmly held with a clamp and placed in the heating plate. Then, the computed amount of distilled water can be placed in the 100 mL beaker using the glass pipette and then the correct amount of acid can be added. It is important to always add the acid last. The second 100mL beaker should be filled only with distilled water.

Performing the treatment - Step 3

Now that the acid solution is in place, it is possible to immerse a witness sample inside the solution. Since the samples are small and easy to place in the solution, one should place them in the beaker with their strong hand and activate the stop watch at the same time.

Rinsing the specimen - Step 4

Once the treatment time has elapsed, the specimen is removed from the acid solution and placed in the other 100mL beaker containing only distilled water. After a few minutes of rinsing, it can be air dried and stored in a sealable bag that indicates what sample it is and what treatment was performed.

Disposing of the acid solution - Step 5

The acid solution contained in the 100mL beaker can be gently poured into one of the 1000mL beakers. Subsequently, it should be rinsed and air dried before it is used for another treatment.

2 Electropolishing

Equipment - step 0

The following equipment is necessary for the electropolishing treatment:

- 2 large beakers (1000mL)
- 2 medium beakers (250mL)
- 2 small beakers (100mL)
- Glass pipette
- Acid(s)
- Distilled water
- Heating plate
- Clamps
- Stopwatch
- Electric cables
- Electric clamps
- 36 V power supply
- Protective gear: lab coat, gloves and glasses
- Tweezers

Setting up the equipment - Step 1

Once the protective gear is on, it is possible to place all the listed elements under the fume hood. Subsequently, the 1000 mL beakers should be filled with about 750mL of distilled water. These will serve as waste beaker for the acid once the experiment has been conducted. In the case of the electropolishing treatment, the heating plate is placed underneath a movable stage that can go up and down. The platinum wire that will serve as the cathode is connected to the electrical supply with the clamp and the wire. The specimen should also be connected to the power supply in the same fashion. The acids that are needed for the experiment can be poured from their container to the medium size beaker so as not to take the acid directly from their original bottle. Once the 250 mL beakers contain enough acid for the experiment, it is recommended to stow the acid bottles back in their storage facility to keep the place under the fume hood clear of unnecessary elements.

Preparing the acid solution - Step 2

The desired acid solutions are obtained by diluting the right amount of acid in the right amount of water. When computing the required quantities of acid and distilled water, one should keep in mind that the computations are performed in weight percent and that the density of the acids is not 1. The computed amount of distilled water can be placed in the 100 mL beaker using the glass pipette and then the correct amount of acid can be added. It is important to always add the acid last. The second 100mL beaker should be filled only with distilled water.

Performing the treatment - Step 3

Now that the acid solution is in place, it is possible to immerse a witness sample inside the solution. This can be done by turning the knob of the motion stage until the specimen is immersed in acid. Once this is done, the power supply can be turned on and the timer set off.

Rinsing the specimen - Step 4

Once the treatment time has elapsed, the supplied power is shut off and the specimen is removed from the acid solution and placed in the other 100mL beaker containing only distilled water. After a few minutes of rinsing, it can be air dried and stored in a sealable bag that indicates what sample it is and what treatment was performed.

Disposing of the acid solution - Step 5

The acid solution contained in the 100mL beaker can be gently poured into one of the 1000mL beakers. Subsequently, it should be rinsed and air dried before it is used for another treatment.

Appendix B

Roughness data

		Roughness parameters						
		R_p	R_v	P_c	R_t	Ra	R_{sk}	R_{ku}
Sample 1	Measurement 1	5,2546	4,5919	21,032	11,6212	1,0448	0,4042	4,7432
	Measurement 2	11,1388	11,378	32,4341	40,4284	2,7604	-0,1397	3,8807
Sample 2	Measurement 1	4,0913	3,7299	31,0601	38,3609	0,5478	0,2537	9,179
	Measurement 2	16,3888	14,8701	43,7566	31,2589	3,2094	0,1833	4,6194
Sample 3	Measurement 1	5,2187	4,2722	24,9788	21,1267	0,9775	0,1974	4,7348
	Measurement 2	4,5933	4,9721	26,2026	17,0188	0,8824	0,1868	5,5098
	Measurement 3	2,3264	0,7466	15,8126	15,0591	1,1589	1,1633	1,4648
Sample 4	Measurement 1	7,8698	4,2011	37,4457	36,622	2,1228	1,4107	2,95
	Measurement 2	10,4608	8,1495	25,2666	45,1773	1,8993	0,3862	5,0878
	Measurement 3	4,4201	3,5293	19,3944	17,6462	0,7263	0,4089	5,9469
Sample 5	Measurement 1	1,8225	4,1851	17,1365	24,8564	0,4137	-1,9762	15,4843
	Measurement 2	3,1481	3,1659	38,5923	33,7672	0,688	0,2588	4,4017
Sample 6	Measurement 1	2,424	2,5623	12,2958	17,9428	0,5629	0,1102	4,0362
	Measurement 2	4,7184	6,8471	21,2383	21,031	1,0547	-0,3256	5,6499
	Measurement 3	4,4725	5,0308	27,3066	19,8204	1,0659	-1,0796	4,7679
Sample 7	Measurement 1	10,8653	11,0045	28,7975	22,8376	3,4907	-0,0927	2,7217
	Measurement 2	5,9647	4,3273	16,2327	27,4595	0,7098	0,4549	9,2172
	Measurement 3	2,9018	3,1752	21,9227	9,1492	0,8646	-0,6057	3,2583
Sample 8	Measurement 1	10,815	14,2357	29,6529	25,0507	2,7706	-0,3334	4,9562
	Measurement 2	10,7431	9,161	31,8696	19,9041	1,9657	-0,3259	5,4414
Sample 9	Measurement 1	6,2396	11,9637	58,192	22,4519	2,8574	-1,405	3,6578
	Measurement 2	13,7391	13,9644	33,2799	36,0799	2,7489	0,0175	5,3005
	Measurement 3	24,9833	32,4873	29,005	57,4705	2,403	-0,7728	19,5415
Sample 10	Measurement 1	8,8365	8,9611	33,412	19,9469	2,1937	-0,3256	3,9345
	Measurement 2	9,1554	12,9966	46,3135	43,5582	2,3807	-1,3498	5,0346
Sample 11	Measurement 1	8,2276	10,3595	34,4047	23,9185	1,4145	-0,6943	7,9087
	Measurement 2	21,5027	21,8963	48,3095	43,399	3,7122	0,0152	6,2428
Sample 12	Measurement 1	7,4688	8,0053	32,7382	29,2296	2,4251	0,0077	2,7347
	Measurement 2	3,5773	4,3814	24,4083	13,4422	0,9729	-1,1363	4,066
Sample 13	Measurement 1	10,3723	10,6362	44,2555	21,0658	1,6336	0,542	7,2113
	Measurement 2	8,8436	8,4834	35,6837	17,8173	1,9809	0,1346	4,3698
Sample 14	Measurement 1	2,3942	3,5035	9,4637	9,2018	0,6117	-0,4043	4,6794
	Measurement 2	10,8644	10,8097	19,0725	21,9284	2,0224	-0,1395	5,9657
	Measurement 3	4,143	3,0027	39,6075	26,7149	0,8977	0,6862	4,3677
Sample 15	Measurement 1	3,9281	3,3221	15,5808	11,8651	0,8788	-0,6732	3,6726
	Measurement 2	26,4147	29,321	29,3409	55,7357	2,9713	-0,2374	14,2476
Sample 16	Measurement 1	17,2278	21,4069	39,701	38,6347	3,4443	-0,3587	6,0976
	Measurement 2	3,6917	6,6056	31,4735	10,2973	1,2378	-1,2845	4,697
Sample 17	Measurement 1	4,4611	2,7102	37,6006	9,1693	1,2439	1,3408	2,7673
	Measurement 2	9,2714	8,8229	28,3753	18,0942	2,4661	-0,1605	3,2029
Sample 18	Measurement 1	16,592	14,1455	19,9172	44,8827	1,3514	-0,4363	16,4254
	Measurement 2	3,9524	3,5244	23,8075	16,7507	0,7907	-0,0346	4,6035
Average as-built values		8,46488	8,93917	29,4374	25,8998	1,7037	-0,14593	5,92334
Standard deviation		5,95117	6,93275	10,2852	12,4273	0,93646	0,70234	3,79112

Table B.1: As-built surface roughness

Sample 8	Water Grinding						
Roughness parameter	R_p	R_v	P_c	R_t	Ra	R_{sk}	R_{ku}
Measurment 1	1,1271	0,9952	3,5795	3,363	0,1567	0,0003	8,6728
Measurement 2	0,1585	0,1659	0,3165	0,3705	0,0408	-0,0335	3,4653
Measurement 3	2,0498	2,7566	2,3475	4,8065	0,3065	-0,2733	9,9649
Measurement 4	0,6683	0,4809	0,7566	1,1492	0,084	0,2365	8,2404
Measurement 5	0,0819	0,0854	0,3545	0,4725	0,024	-0,3236	2,9261
Measurement 6	0,9567	1,7287	5,3882	3,1017	0,3744	-1,4799	4,2001
Average value	0,84038	1,03545	2,1238	2,21057	0,1644	-0,31225	6,24493
Standard deviation	0,66185	0,94963	1,8749	1,65299	0,13279	0,55401	2,78798

Table B.2: Roughness values Sample 8

Sample 13	Chemical etching						
Hydrochloric acid [37wt%]	R_t	10mins					
Roughness parameter	R_p	R_v	P_c	R_t	Ra	R_{sk}	R_{ku}
Measurement 1	2,2551	2,1791	11,8393	9,3671	0,3833	-0,0495	6,5432
Measurement 2	2,8345	3,0915	11,2011	8,9207	0,7437	-0,8401	3,7049
Measurement 3	3,4699	2,9767	7,6779	6,4466	0,9241	1,1183	3,491
Measurement 4	4,0402	3,4297	14,5819	8,1174	0,9658	0,2442	3,3341
Measurement 5	2,7866	2,5718	12,6164	8,3626	0,5816	0,1727	4,3742
Measurement 6	4,6581	3,2161	14,5269	15,9896	0,5563	0,4803	8,234
Average value	3,34073	2,91082	12,0739	9,534	0,69247	0,18765	4,9469
Standard deviation	0,81479	0,41828	2,33607	3,02737	0,20713	0,58704	1,82321

Table B.3: Sample 13 roughness values

Sample 11	Electropolishing						
Perchloric acid in acetic acid	50 C	30.90V	5 mins				
Roughness parameter	R_p	R_v	P_c	R_t	Ra	R_{sk}	R_{ku}
Measurement 1	11,0129	9,3662	25,9747	20,3791	1,683	0,0813	6,1095
Measurement 2	2,5407	2,9583	10,7667	20,1939	0,4554	-0,2954	6,2877
Measurement 3	4,8005	6,0041	18,2013	12,9232	1,6389	-0,1512	3,168
Measurement 4	5,8261	2,7216	21,8032	9,0456	1,3832	1,4697	3,6866
Measurement 5	2,8264	2,3015	21,0937	19,5403	0,725	0,6266	3,1704
Measurement 6	1,8447	4,1405	20,4905	13,4518	1,0142	-1,3746	2,9012
Average value	4,80855	4,58203	19,7217	15,9223	1,14995	0,0594	4,22057
Standard deviation	3,09262	2,4632	4,62619	4,35099	0,45808	0,86965	1,41878

Table B.4: Sample 11 surface roughness

Sample 14	Electropolishing						
Perchloric acid in acetic acid	R_t	30V	15mins				
Roughness parameter	R_p	R_v	P_c	R_t	Ra	R_{sk}	R_{ku}
Measurement 1	0,2587	1,6054	15,2633	3,2056	0,6674	-1,2145	1,6338
Measurement 2	0,6655	1,5118	11,2002	2,7567	0,4863	-1,3272	2,2277
Measurement 3	0,7803	0,8518	8,0274	3,4117	0,2188	-0,6162	3,3219
Measurement 4	2,0471	2,3459	13,8776	4,393	0,5231	-0,2785	4,2246
Measurement 5	1,7739	1,562	7,7713	3,6	0,3709	0,008	4,2181
Measurement 6	1,828	1,2721	7,8363	7,8114	0,2735	0,2973	6,5474
Average value	1,22558	1,52483	10,6627	4,1964	0,42333	-0,52185	3,69558
Standard deviation	0,68133	0,44703	3,02995	1,68981	0,15304	0,59836	1,59327

Table B.5: Sample 14 surface roughness

Sample 15	Electropolishing						
Hydrochloric acid	R_t	10V	5A	5mins			
Roughness parameter	R_p	R_v	P_c	R_t	Ra	R_{sk}	R_{ku}
Measurement 1	0	1,0919	4,6299	6,0669	0,6527	-1,0675	1,1847
Measurement 2	0,7949	1,9551	10,6589	4,9368	0,683	-1,3021	1,9886
Measurement 3	0	0,9773	8,1073	5,5851	0,6268	-1,0729	1,1962
Measurement 4	0,7792	0,7442	1,9986	3,8513	0,1834	-0,1865	3,8264
Measurement 5	3,4102	3,3817	2,53	6,7919	0,4036	0,258	12,1243
Measurement 6	0,8643	0,6578	2,6462	6,0746	0,2078	0,1336	2,9696
Measurement 7	0,4752	0,5196	1,4467	1,6727	0,1502	0,0972	2,744
Average value	0,9034	1,33251	4,57394	4,99704	0,41536	-0,4486	3,71911
Standard deviation	1,07759	0,94363	3,24742	1,61425	0,22039	0,62176	3,5447

Table B.6: Sample 15 surface roughness

Sample 16	Unknown						
Roughness parameter	R_p	R_v	P_c	R_t	Ra	R_{sk}	R_{ku}
Measurement 1	2,631	2,9523	6,9901	5,9524	0,7165	-0,2966	3,5835
Measurement 2	1,8133	1,6629	8,0487	9,3626	0,4067	0,3149	4,2297
Measurement 3	1,8983	2,1357	12,8421	6,3517	0,3575	-0,1	6,3601
Measurement 4	2,6826	1,9787	8,0748	4,6614	0,694	0,6342	3,1083
Measurement 5	1,5023	1,2545	6,7557	4,2951	0,3651	0,9777	3,9781
Measurement 6	0,9359	1,0106	6,3386	5,6441	0,3225	-0,8214	2,9116
Average value	1,91057	1,83245	8,175	6,04455	0,47705	0,11813	4,02855
Standard deviation	0,61119	0,6332	2,18322	1,64552	0,16333	0,59808	1,1381

Table B.7: Sample 16 surface roughness

Sample 17	Chemical etching						
Perchloric acid in acetic acid	25 C	20mins					
Roughness parameter	R_p	R_v	P_c	R_t	Ra	R_{sk}	R_{ku}
Measurement 1	2,3614	2,391	16,04	12,6526	0,4057	-0,1232	6,1235
Measurement 2	2,7404	2,8729	16,2852	8,085	0,732	0,0132	3,4779
Measurement 3	2,7445	2,6727	6,2799	8,2924	0,616	0,0271	4,1607
Measurement 4	3,1959	2,2768	23,931	10,0946	0,5342	0,7364	5,862
Measurement 5	4,316	5,9471	14,345	10,2631	0,7805	-0,3029	8,4068
Measurement 6	3,877	2,5248	10,8519	6,4018	0,7974	1,1109	3,8701
Average value	3,20587	3,11422	14,6222	9,29825	0,6443	0,24358	5,31683
Standard deviation	0,68624	1,28128	5,40548	1,98704	0,14115	0,50468	1,69839

Table B.8: Sample 17 surface roughness

Sample 22	Unknown						
Roughness parameter	R_p	R_v	P_c	R_t	Ra	R_{sk}	R_{ku}
Measurement 1	6,9405	8,6145	21,6917	15,9762	1,8485	-0,1219	3,6183
Measurement 2	5,8849	5,0431	24,1232	13,8099	1,0712	0,0757	5,3703
Measurement 3	5,9255	5,0092	20,4457	21,0187	1,1046	0,1498	4,6844
Measurement 4	2,0246	2,2535	18,3508	7,4593	0,643	-0,5201	2,8431
Measurement 5	1,8185	1,7135	10,7523	6,873	0,4549	0,1041	3,5894
Measurement 6	2,9218	3,5706	25,8053	12,3165	0,7565	-0,5653	3,9843
Average value	4,25263	4,3674	20,1948	12,9089	0,97978	-0,14628	4,01497
Standard deviation	2,05539	2,27497	4,86098	4,87289	0,45044	0,29313	0,81627

Table B.9: Sample 22 surface roughness

Sample 23	Chemical etching						
3,5ml HCl @ 37wt% + 1,2ml H2SO4 @ 95wt%	5mins	R_t					
Roughness parameter	R_p	R_v	P_c	R_t	Ra	R_{sk}	R_{ku}
Measurement 1	3,6856	2,62	16,8399	17,5555	0,5399	0,3534	6,4647
Measurement 2	8,3458	7,5462	37,0767	51,9075	2,1483	0,0929	3,1317
Measurement 3	5,2594	4,2391	20,2992	17,4495	1,6374	0,1198	2,2728
Measurement 4	7,749	6,0835	34,9751	13,8325	2,4571	1,2491	2,7833
Measurement 5	2,0189	4,6266	14,4077	23,3664	1,2365	-1,4527	2,6139
Measurement 6	5,5649	4,3129	32,0954	23,8587	1,2413	1,1182	3,7715
Average value	5,43727	4,90472	25,949	24,6617	1,54342	0,24678	3,50632
Standard deviation	2,18347	1,55229	9,04776	12,6783	0,63273	0,88538	1,40258

Table B.10: Sample 23 surface roughness

Sample 27	Chemical etching						
Perchloric acid in acetic acid	25 C	5 mins					
Roughness parameter	R_p	R_v	P_c	R_t	Ra	R_{sk}	R_{ku}
Measurment 1	3,2734	3,4348	19,2848	33,1448	1,0655	-0,1103	2,8543
Measurement 2	5,6776	4,7142	18,4566	14,1784	1,1952	0,2149	3,8495
Measurement 3	5,2086	4,8446	19,1199	19,1634	0,8863	0,143	5,8654
Measurement 4	4,7825	3,7656	20,9271	14,9157	0,9258	1,1177	4,72
Measurement 5	3,5801	4,288	22,082	13,0783	1,0923	-0,3195	3,1281
Measurement 6	3,2135	3,3498	27,7245	9,5631	0,7577	-0,0794	4,1871
Average value	4,28928	4,06617	21,2658	17,3406	0,98713	0,16107	4,10073
Standard deviation	0,97537	0,5884	3,1336	7,61174	0,14552	0,46202	1,00563

Table B.11: Sample 27 roughness values

Sample 28	Chemical etching						
HCl [37wt%]	R_t	5 mins					
Roughness parameter	R_p	R_v	P_c	R_t	Ra	R_{sk}	R_{ku}
Measurement 1	5,3359	5,2025	11,6562	11,7146	1,1765	0,0507	3,9759
Measurement 2	4,6494	3,7306	9,3379	11,3191	1,1681	0,3425	3,6206
Measurement 3	4,6494	3,7306	9,3379	11,3191	1,1681	0,3425	3,6206
Measurement 4	4,2794	3,0242	8,2424	8,128	1,0759	0,7105	3,0522
Measurement 5	3,7192	2,7318	7,3916	10,5574	0,8036	1,0355	4,4062
Measurement 6	3,3581	3,2628	7,3011	9,3454	0,8654	-0,9873	3,5146
Average value	4,3319	3,61375	8,87785	10,3973	1,04293	0,24907	3,69835
Standard deviation	0,65014	0,79582	1,48556	1,27257	0,15224	0,63467	0,41662

Table B.12: Sample 28 roughness values

Sample 31	Chemical etching						
Perchloric acid in acetic acid	25 C	10 mins					
Roughness parameter	R_p	R_v	P_c	R_t	Ra	R_{sk}	R_{ku}
Measurement 1	2,9262	3,6254	21,6284	10,9718	0,7625	-1,109	4,3971
Measurement 2	1,8121	3,172	12,7146	15,4372	0,6302	-1,1518	4,5063
Measurement 3	4,2989	3,9481	16,1959	8,2469	0,8402	0,7541	5,4826
Measurement 4	5,2373	3,4379	19,0709	14,218	1,0739	0,592	4,1352
Measurement 5	3,3712	4,7105	15,9818	37,5722	0,9143	-0,5846	4,3864
Measurement 6	4,1543	3,7035	11,4364	11,1996	0,6828	0,219	6,3376
Average value	3,63333	3,76623	16,1713	16,2743	0,81732	-0,21338	4,8742
Standard deviation	1,09337	0,48466	3,47832	9,80508	0,14825	0,77375	0,78089

Table B.13: Sample 31 roughness values

Sample 35	Electropolishing						
HCl [37wt%]	R_t	2mins	10V	5A			
Roughness parameter	R_p	R_v	P_c	R_t	Ra	R_{sk}	R_{ku}
Measurement 1	2,2578	2,4923	8,9695	5,0901	0,6571	-0,3019	3,0139
Measurement 2	2,879	2,8114	11,49	11,1352	0,7364	-0,0922	3,2458
Measurement 3	1,8247	1,6415	9,1515	8,4092	0,5176	0,0408	2,8844
Measurement 4	0,9624	1,9198	19,3599	6,1851	0,8183	-1,2771	1,8474
Measurement 5	1,5195	1,7695	10,3623	12,0173	0,3476	-1,1558	4,5449
Measurement 6	1,9865	1,6496	7,9923	5,1276	0,4203	0,7899	4,4158
Average value	1,90498	2,04735	11,2209	7,99408	0,58288	-0,33272	3,32537
Standard deviation	0,59489	0,44687	3,80412	2,77331	0,1686	0,71039	0,92723

Table B.14: Sample 35 surface roughness

Sample 36	Electropolishing						
Perchloric acid in acetic acid	50 C	30.9V	15 mins				
Roughness parameter	R_p	R_v	P_c	R_t	Ra	R_{sk}	R_{ku}
Measurement 1	2,7895	2,6201	13,5522	10,5094	0,4313	-0,5104	7,8921
Measurement 2	4,8144	5,0177	19,2785	9,8321	0,8643	-0,6768	6,3853
Measurement 3	2,1878	1,8716	16,2478	14,679	0,4521	0,4832	4,1698
Measurement 4	8,7343	8,2041	22,8042	19,9795	1,5437	0,0344	4,7007
Measurement 5	3,9764	5,1402	27,0725	14,8838	0,5913	-0,2446	9,8296
Measurement 6	7,8047	8,1169	25,5276	24,5525	1,1119	-0,0288	9,014
Average value	5,05118	5,16177	20,7471	15,7394	0,83243	-0,15717	6,99858
Standard deviation	2,43833	2,42539	4,85219	5,16002	0,39764	0,37984	2,10291

Table B.15: Sample 36 roughness values

Sample 37	Chemical etching						
3,5ml HCl @ 37wt% + 1,2ml H2SO4 @ 95wt%	R_t	10 mins					
Roughness parameter	R_p	R_v	P_c	R_t	Ra	R_{sk}	R_{ku}
Measurement 1	3,9358	3,8939	11,6015	14,9603	0,6936	-0,0175	5,1541
Measurement 2	6,8753	5,2387	11,4707	14,2581	1,4678	0,4239	3,7285
Measurement 3	4,9788	3,9677	20,5143	10,0515	1,1497	0,0457	3,6784
Measurement 4	2,3796	2,1924	8,712	7,1429	0,7517	0,5298	2,3442
Measurement 5	3,6261	3,4274	10,8484	7,0535	1,0095	-0,0716	2,7698
Measurement 6	3,395	2,8942	15,2818	8,3086	0,6806	0,3793	4,7602
Average value	4,19843	3,60238	13,0715	10,2958	0,95882	0,21493	3,7392
Standard deviation	1,42155	0,9501	3,85036	3,21246	0,2854	0,23615	0,99448

Table B.16: Sample 37 Roughness values

Specimen 2 (after)							
Roughness parameters	R_p	R_v	P_c	R_t	Ra	R_{sk}	R_{ku}
measurement 1	0,9051	0,9642	3,9603	11,0617	0,3137	-0,1644	2,5908
measurement 2	4,0728	3,9081	12,0072	7,9809	0,7255	0,103	5,5914
measurement 3	0,8	0,6703	2,4404	3,306	0,2291	-0,0044	2,6304
measurement 4	2,0403	0,8453	5,4511	2,8857	0,4939	1,5171	3,3963
measurement 5	1,8905	0,8045	10,1123	3,5169	0,6256	1,4112	2,4101
measurement 6	0,7011	0,6165	1,8639	1,3176	0,2049	0,0002	2,6755
Average	1,734966667	1,3014833	5,972533	5,011467	0,432117	0,477117	3,21575
Standard deviation	1,170085851	1,1712458	3,812975	3,384493	0,197565	0,702957	1,106831

Table B.17: Specimen 2 surface roughness

Specimen 3 (after)							
Roughness parameters	R_p	R_v	P_c	R_t	Ra	R_{sk}	R_{ku}
measurement 1	0,5033	0,7101	2,0515	1,3652	0,1807	-1,0239	3,0393
measurement 2	1,5221	1,2333	2,5258	2,7554	0,2642	1,0017	5,5625
measurement 3	0,5416	0,6179	2,1594	1,6167	0,203	-0,7335	2,5002
measurement 4	2,2781	2,299	3,8764	4,5771	0,4456	-0,0066	4,9157
measurement 5	0,8076	0,8498	2,1173	2,4528	0,2478	-0,1149	2,6283
measurement 6	0,9738	0,9621	1,9146	2,9652	0,2597	-0,1258	3,0594
Average	1,104416667	1,1120333	2,440833	2,622067	0,266833	-0,16717	3,617567
Standard deviation	0,623866523	0,5657679	0,668388	1,046964	0,08551	0,639166	1,179054

Table B.18: Specimen 3 roughness values

Specimen 4 (after)							
Roughness parameters	R_p	R_v	P_c	R_t	Ra	R_{sk}	R_{ku}
measurement 1	0,8273	0,9113	2,1036	2,2146	0,2814	-0,1998	2,424
measurement 2	0,8386	0,9382	2,4147	3,9261	0,3238	-0,0828	2,2376
measurement 3	0,9971	1,0076	1,9215	2,4128	0,2695	-0,0418	3,3338
measurement 4	0,7326	0,9568	2,2372	1,9989	0,2201	-1,2061	3,6691
measurement 5	0,8455	0,5679	1,9333	1,6792	0,2178	0,7396	2,8879
measurement 6	0,8858	0,8181	2,2582	2,1791	0,183	0,6641	4,3831
Average	0,854483333	0,86665	2,14475	2,401783	0,249267	-0,02113	3,155917
Standard deviation	0,078790554	0,1453247	0,178202	0,717952	0,046956	0,644018	0,736186

Table B.19: Specimen 4 roughness values

Specimen 5 (after)							
Roughness parameters	R_p	R_v	P_c	R_t	Ra	R_{sk}	R_{ku}
measurement 1	1,1611	0,244	5,2496	2,474	0,4878	1,2203	1,6902
measurement 2	0,7942	0,1109	3,2551	2,0138	0,346	1,2418	1,6819
measurement 3	0,5503	0,4442	1,6256	0,9945	0,1563	0,8475	2,7664
measurement 4	0,7889	0,7524	1,5238	1,7863	0,2484	-0,0088	2,651
measurement 5	1,0184	1,1297	2,683	2,4173	0,23	-0,2093	4,7732
measurement 6	0,7315	0,9015	1,804	2,6394	0,2602	-0,1193	2,6608
Average	0,840733333	0,5971167	2,690183	2,054217	0,288117	0,495367	2,703917
Standard deviation	0,19804702	0,3616833	1,300571	0,554812	0,105146	0,623865	1,029776

Table B.20: Specimen 5 roughness values

Specimen 6 (after)							
Roughness parameters	R_p	R_v	P_c	R_t	Ra	R_{sk}	R_{ku}
measurement 1	1,2022	1,2421	2,9	2,9361	0,3049	-0,1168	3,7107
measurement 2	1,0198	1,1187	3,0915	4,2983	0,2871	-0,1453	3,3384
measurement 3	1,4094	1,225	2,9546	4,4186	0,4088	0,0497	2,7472
measurement 4	0,8042	0,6143	2,3064	1,898	0,2351	0,7851	2,7514
measurement 5	0,388	0,9839	4,1233	2,668	0,2309	-1,3292	2,7389
measurement 6	0,8621	0,3763	3,5037	3,5738	0,2553	1,3731	2,4735
Average	0,947616667	0,9267167	3,146583	3,2988	0,287017	0,102767	2,960017
Standard deviation	0,322572785	0,3238132	0,560968	0,896314	0,060555	0,840874	0,424481

Table B.21: Specimen 6 roughness values

Specimen 7 (after)							
Roughness parameters	R_p	R_v	P_c	R_t	Ra	R_{sk}	R_{ku}
measurement 1	0,2915	1,0971	3,4013	1,516	0,4136	-1,3271	1,9661
measurement 2	0,3451	0,911	3,5297	2,3317	0,2805	-1,4583	2,558
measurement 3	1,4489	0,9663	9,5893	2,4152	0,2692	1,0969	4,3964
measurement 4	1,0051	1,2953	3,7968	6,2613	0,4062	-0,2091	2,3773
measurement 5	1,6086	2,0494	2,5294	5,2312	0,4043	-0,4692	4,7259
measurement 6	1,0361	1,0272	5,7804	5,5688	0,3051	-0,3187	2,9532
Average	0,955883333	1,2243833	4,77115	3,887367	0,346483	-0,44758	3,162817
Standard deviation	0,498735563	0,3884971	2,367335	1,847495	0,06252	0,842069	1,03472

Table B.22: Specimen 7 roughness values

Specimen 8 (after)							
Roughness parameters	R_p	R_v	P_c	R_t	Ra	R_{sk}	R_{ku}
measurement 1	3,0844	3,4119	6,7095	6,4964	0,5365	-0,0819	6,1085
measurement 2	2,2846	1,7747	6,9426	4,0593	0,4354	0,091	4,249
measurement 3	0,4159	0,4259	3,3395	1,5015	0,1463	0,1649	2,2688
measurement 4	2,9907	1,5843	19,5304	4,5751	0,7312	1,3984	3,0508
measurement 5	0	1,095	1,6004	3,2202	0,5828	-1,1437	1,391
measurement 6	0,345	0,4796	1,9545	2,26	0,1264	-1,0087	2,7054
Average	1,5201	1,4619	6,679483	3,685417	0,426433	-0,09667	3,295583
Standard deviation	1,297753235	1,0073191	6,116838	1,625356	0,222869	0,843323	1,522687

Table B.23: Specimen 8 roughness values

Specimen 9 (after)							
Roughness parameters	R_p	R_v	P_c	R_t	Ra	R_{sk}	R_{ku}
measurement 1	0,4825	0,7363	2,3552	2,9515	0,2453	-1,2636	2,5894
measurement 2	4,6269	3,4616	7,716	8,0885	0,9258	1,2326	4,9832
measurement 3	0,7409	0,3483	2,6268	2,4243	0,2779	1,3902	2,2753
measurement 4	5,6427	5,4185	4,692	11,0612	0,8845	0,0882	6,3804
measurement 5	1,1839	1,4037	3,1477	4,3395	0,3081	-0,1567	3,619
measurement 6	1,5425	1,5957	2,7359	4,0579	0,3732	0,0258	3,7022
Average	2,3699	2,1606833	3,878933	5,48715	0,502467	0,219417	3,924917
Standard deviation	2,004676838	1,756492	1,875944	3,082409	0,28758	0,893754	1,402224

Table B.24: Specimen 9 roughness values

Specimen 10 (after)							
Roughness parameters	R_p	R_v	P_c	R_t	Ra	R_{sk}	R_{ku}
measurement 1	0,7312	0,9789	2,2534	2,6977	0,2866	-0,3522	2,6194
measurement 2	0,5712	0,6455	2,1603	1,874	0,1836	-0,2098	2,9021
measurement 3	0,9908	1,0375	2,0875	2,3373	0,2913	-0,076	3,0172
measurement 4	0,4701	0,5763	1,7785	1,3595	0,1739	0,2268	2,4895
measurement 5	0,9101	0,6736	1,7785	2,1041	0,2375	1,1249	2,9856
measurement 6	0,7019	0,4635	2,3339	1,5883	0,2353	1,4025	2,6117
Average	0,729216667	0,7292167	2,06535	1,993483	0,2347	0,3527	2,770917
Standard deviation	0,179817254	0,2087546	0,216623	0,44847	0,045117	0,672222	0,204718

Table B.25: Specimen 10 roughness values

Specimen 11 (after)							
Roughness parameters	R_p	R_v	P_c	R_t	Ra	R_{sk}	R_{ku}
measurement 1	0,7216	0,5233	1,6945	1,6254	0,2291	0,981	2,6339
measurement 2	0,9456	0,5647	2,0276	2,154	0,2299	1,1766	3,0754
measurement 3	0,88	0,7411	1,5942	1,6771	0,2165	0,2626	3,2493
measurement 4	0,7428	0,7572	2,3231	2,2449	0,2416	-0,0083	2,6815
measurement 5	0,9286	0,8716	3,9253	2,5858	0,2537	-0,3195	2,8272
measurement 6	1,1282	1,1332	2,0308	3,3269	0,3287	-0,053	2,8187
Average	0,891133333	0,7651833	2,265917	2,269017	0,249917	0,3399	2,881
Standard deviation	0,136283561	0,202528	0,779596	0,577045	0,037061	0,551887	0,216437

Table B.26: Specimen 11 roughness values

Specimen 12 (after)							
Roughness parameters	R_p	R_v	P_c	R_t	Ra	R_{sk}	R_{ku}
measurement 1	1,6485	1,3678	2,2644	3,0163	0,3756	-0,129	3,7244
measurement 2	0,6944	0,8079	1,6081	2,3664	0,256	-0,1588	2,7179
measurement 3	0,6139	0,7216	2,8117	2,9922	0,2174	-0,1538	2,7094
measurement 4	0,7255	0,202	2,9357	1,862	0,2809	1,3901	2,1331
measurement 5	0,7252	0,324	2,745	3,1271	0,2035	1,4452	2,8131
measurement 6	0,7524	0,327	2,9875	3,2305	0,2512	1,3989	2,4742
Average	0,859983333	0,62505	2,558733	2,76575	0,2641	0,6321	2,762017
Standard deviation	0,355330801	0,3985118	0,485621	0,489365	0,055976	0,779542	0,485091

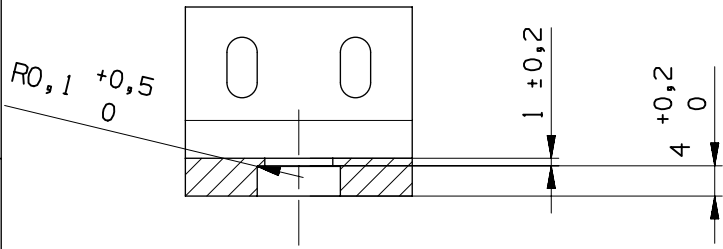
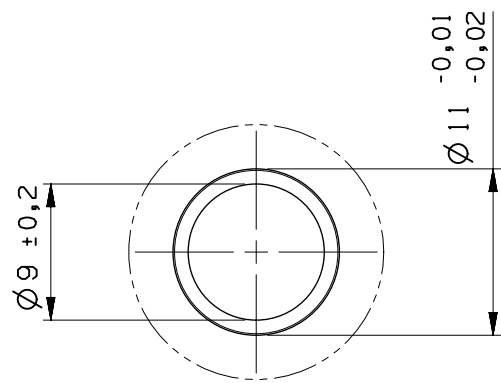
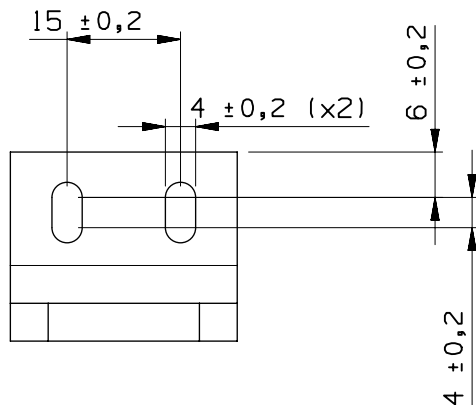
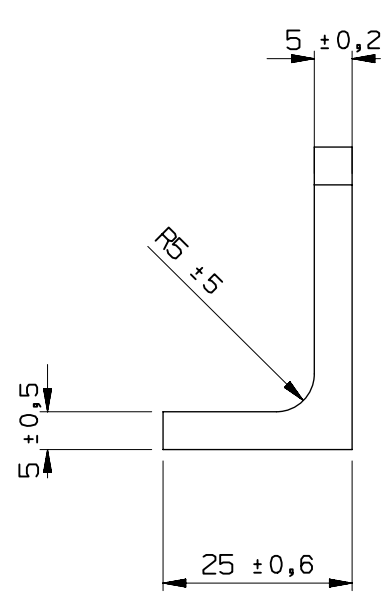
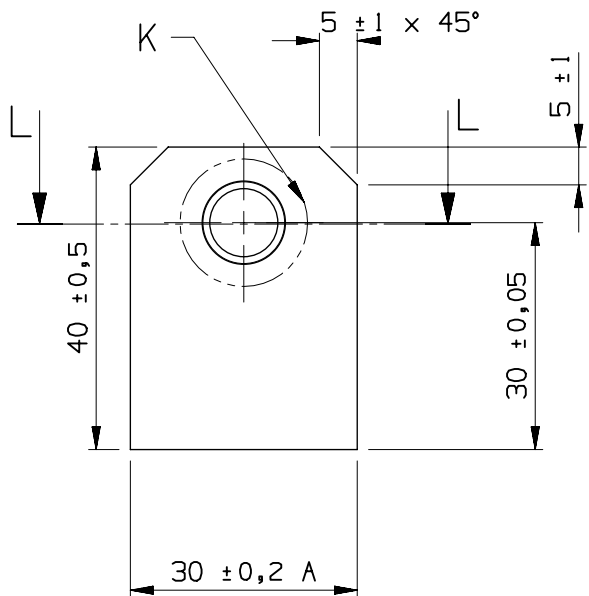
Table B.27: Specimen 12 roughness values

Appendix C

Fatigue data

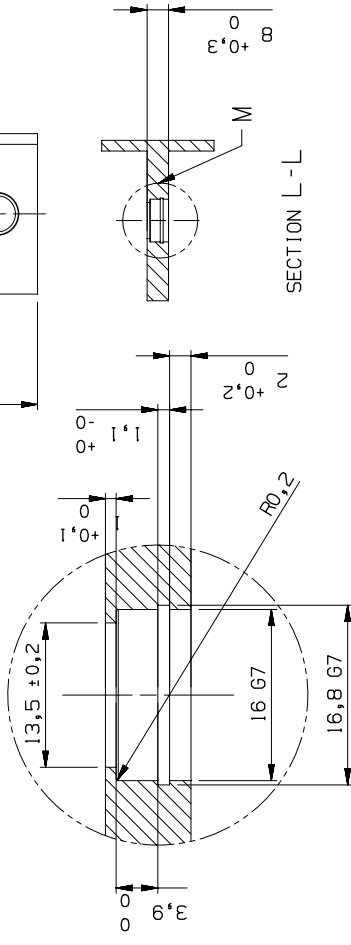


All rights are reserved. Reproduction in whole or in part is prohibited without the written consent of the copyright owner.

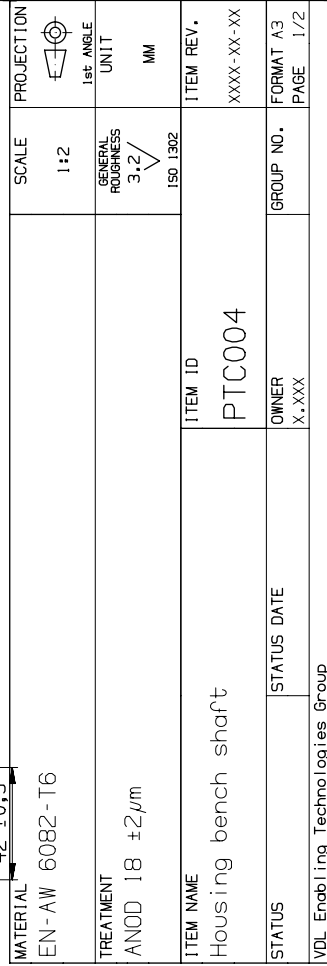


SECTION L - L

MATERIAL EN - AW 6082-T6			SCALE 1:1	PROJECTION 1st ANGLE
TREATMENT			GENERAL ROUGHNESS 3.2 ISO 1302	UNIT MM
ITEM NAME Shaft centering unit		ITEM ID NP_001		ITEM REV. XXXX-XX-XX
STATUS	STATUS DATE	OWNER X	GROUP NO.	FORMAT A4 PAGE 1/2
VDL Enabling Technologies Group				

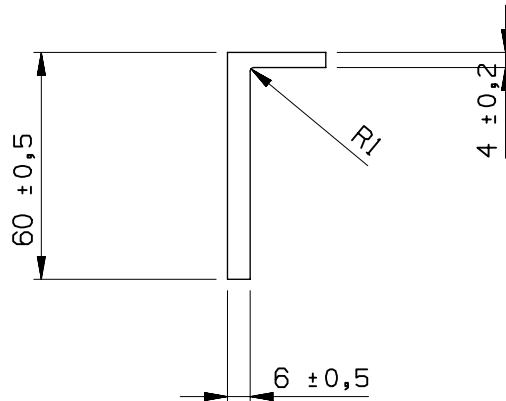
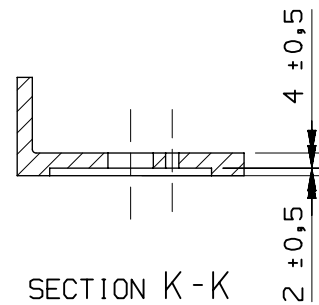
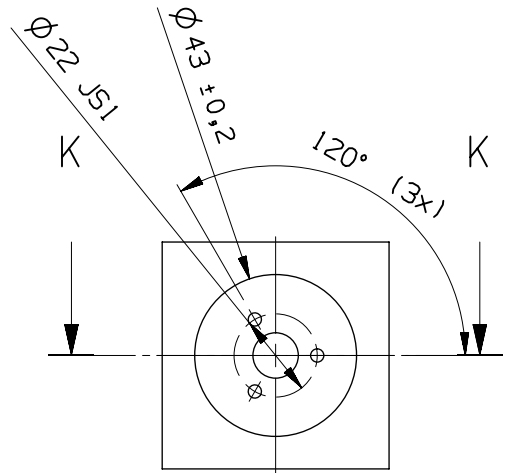
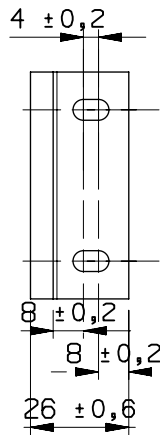
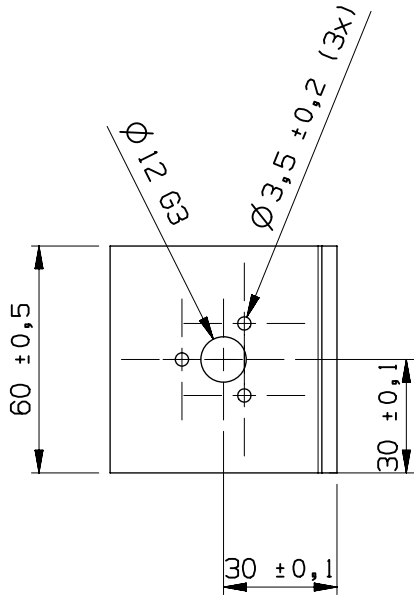


DETAIL M
SCALE 2:1

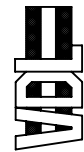




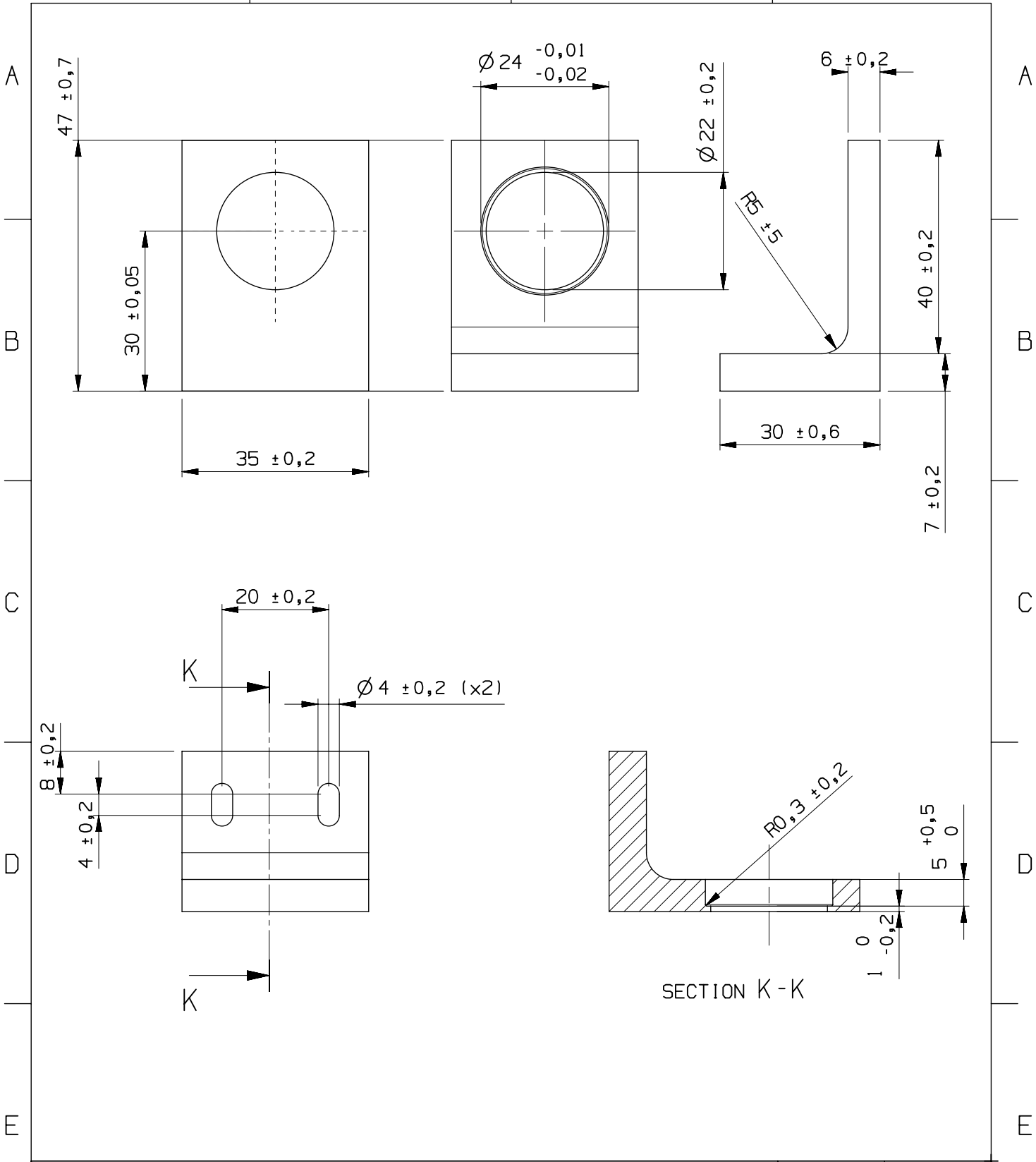
All rights are reserved. Reproduction in whole or in part is prohibited without the written consent of the copyright owner.




MATERIAL EN-AW 6082-T6			SCALE 1:2	PROJECTION 1st ANGLE
TREATMENT ANOD 18 ±2µm			GENERAL ROUGHNESS 3.2 ISO 1302	UNIT MM
ITEM NAME Motor housing		ITEM ID PTC005		ITEM REV. XXXX-XX-XX
STATUS	STATUS DATE	OWNER X.XXX	GROUP NO.	FORMAT A4 PAGE 1/1
VDL Enabling Technologies Group				



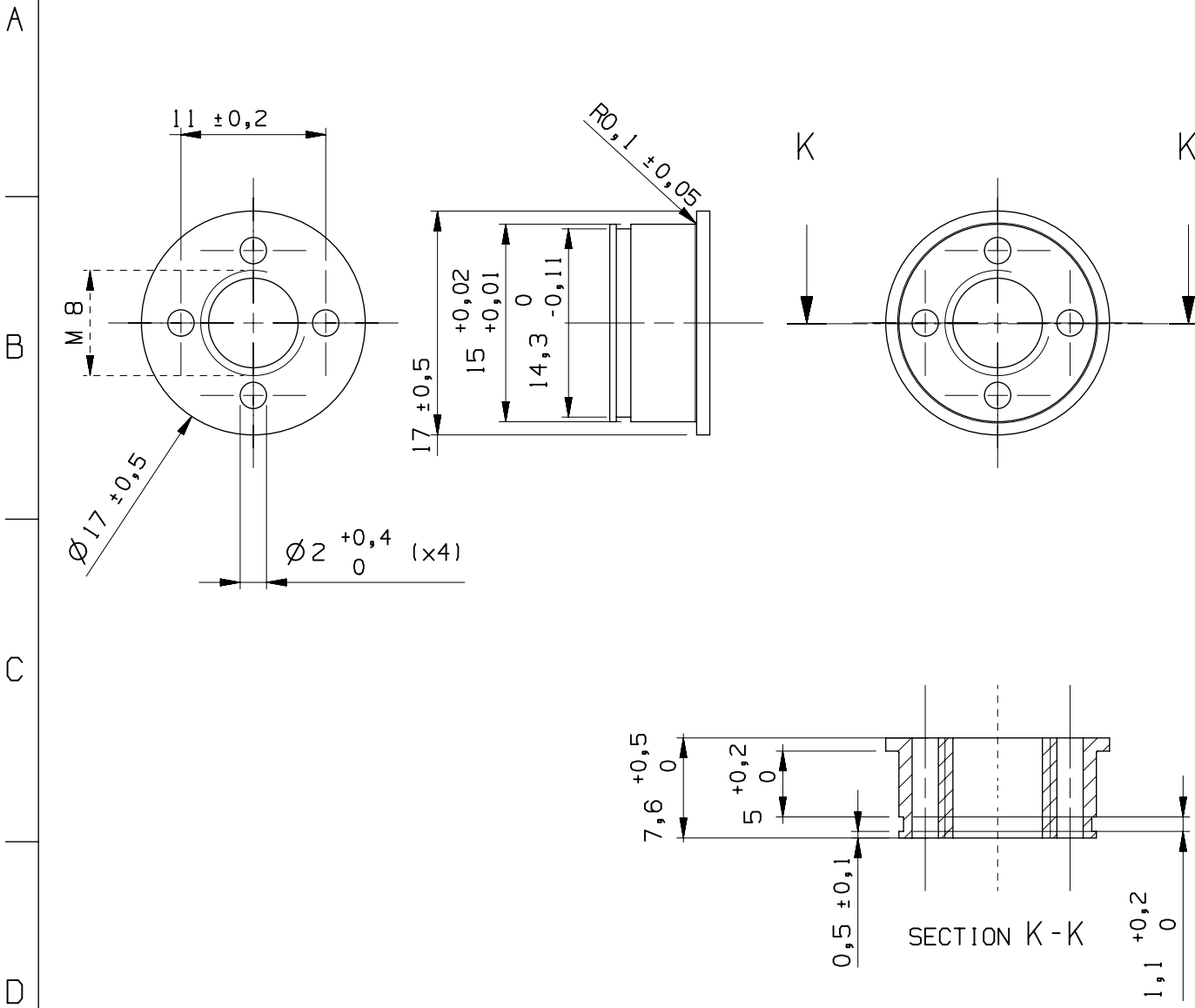
All rights are reserved. Reproduction in whole or in part is prohibited without the written consent of the copyright owner.

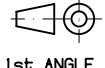


MATERIAL EN - AW 6082 - T6		SCALE 1:1	PROJECTION  1st ANGLE
TREATMENT		GENERAL ROUGHNESS 3.2 ISO 1302	UNIT MM
ITEM NAME Motor centering unite		ITEM ID NP_002	ITEM REV. XXXX-XX-XX
STATUS	STATUS DATE	OWNER X	GROUP NO.
VDL Enabling Technologies Group		FORMAT A4	PAGE 1/1



All rights are reserved. Reproduction in whole or in part is prohibited without the written consent of the copyright owner.



MATERIAL EN - AW 6082 - T6			SCALE 2:1	PROJECTION  1st ANGLE
TREATMENT			GENERAL ROUGHNESS 3.2 ISO 1302	UNIT MM
ITEM NAME Motor Shaft locking ring		ITEM ID NP_003		ITEM REV. XXXX-XX-XX
STATUS	STATUS DATE	OWNER X	GROUP NO.	FORMAT A4 PAGE 1/1
VDL Enabling Technologies Group				



All rights are reserved. Reproduction in whole or in part is prohibited without the written consent of the copyright owner.

A

B

C

D

E

F

A

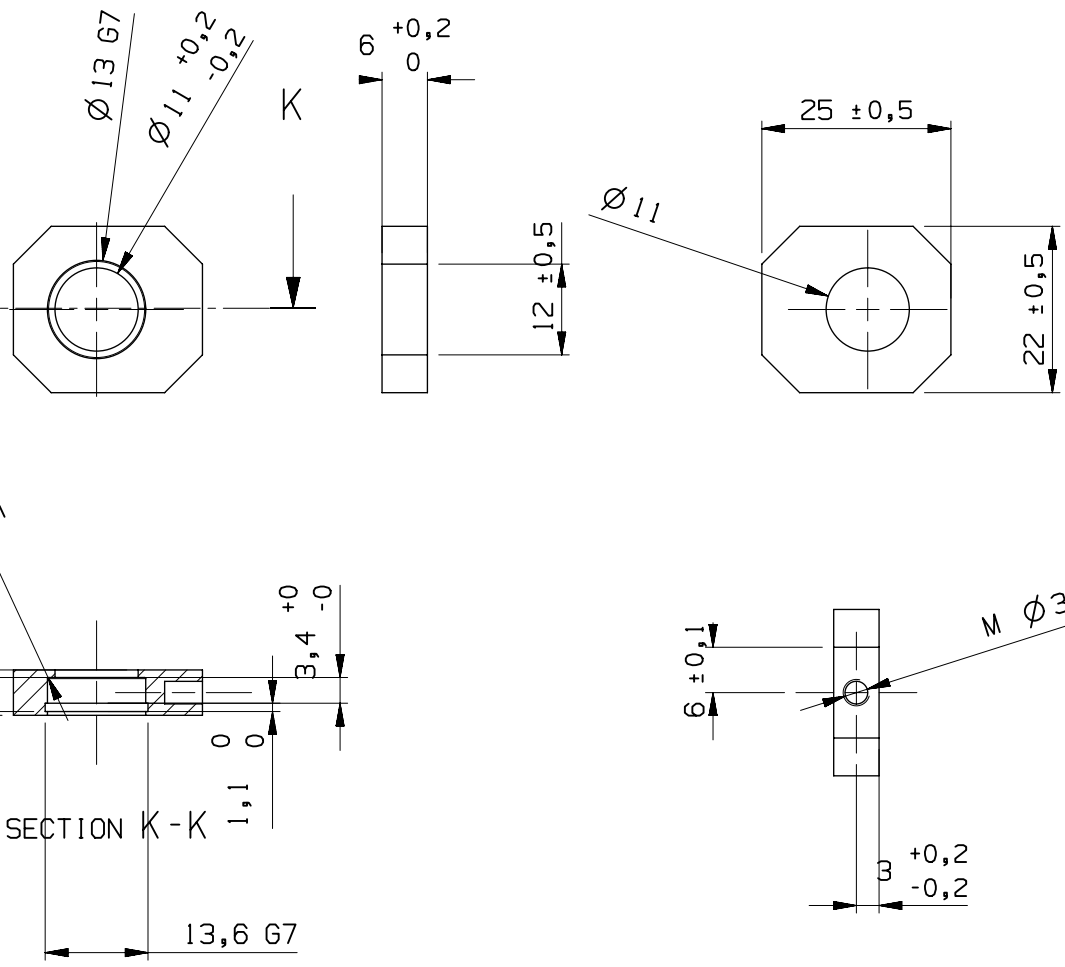
B

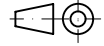
C

D

E

F



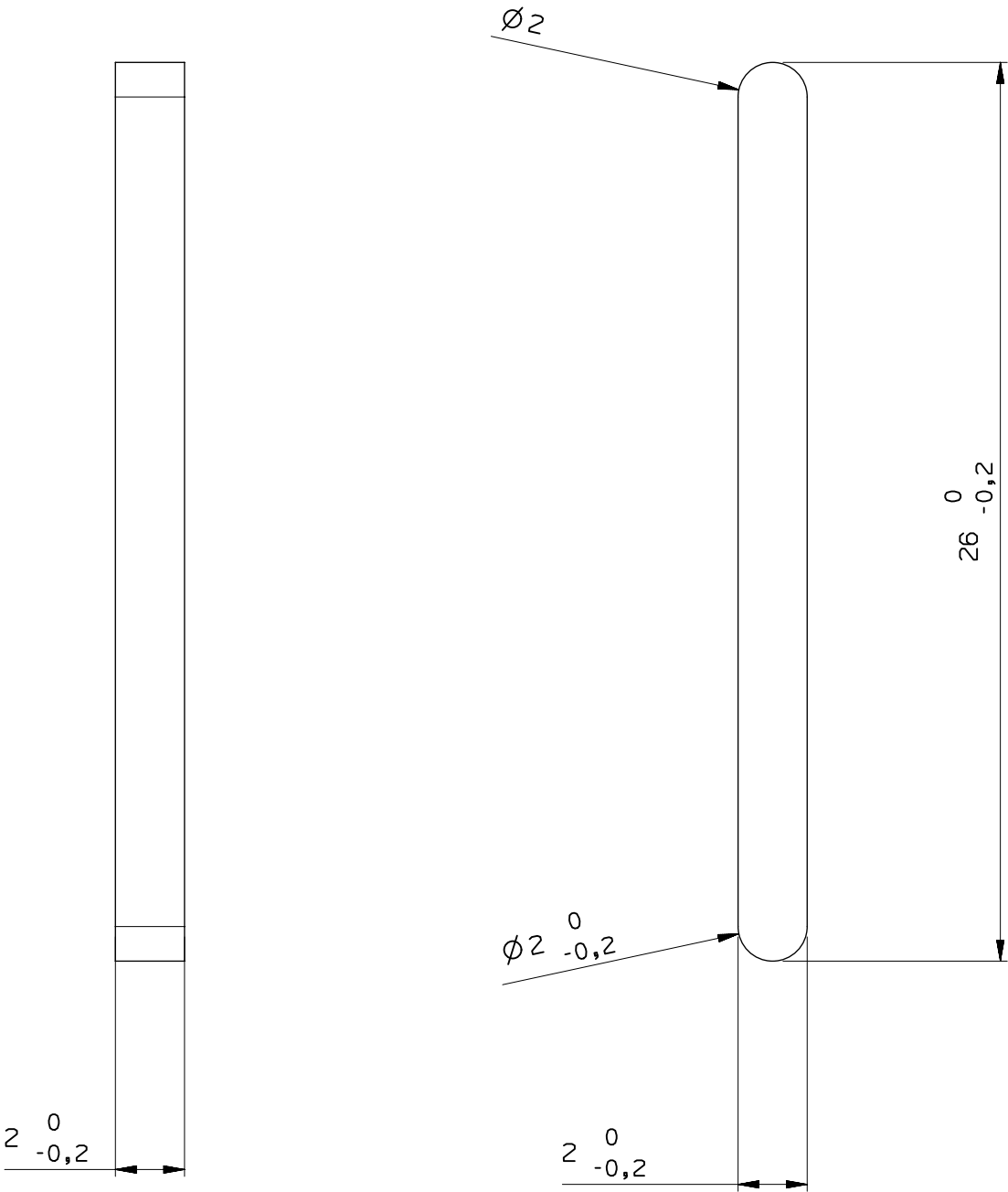
MATERIAL EN-AW 6082-T6		SCALE 1:1	PROJECTION  1st ANGLE
TREATMENT ANOD 18 ±2µm		GENERAL ROUGHNESS 3.2 ISO 1302	UNIT MM
ITEM NAME Outer bearing		ITEM ID PTC006	
ITEM REV. XXXX-XX-XX			
STATUS	STATUS DATE	OWNER X.XXX	GROUP NO.
VDL Enabling Technologies Group		FORMAT A4	PAGE 1/1

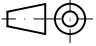
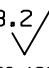


All rights are reserved. Reproduction in whole or in part is prohibited without the written consent of the copyright owner.

A
B
C
D
E
F

A
B
C
D
E
F

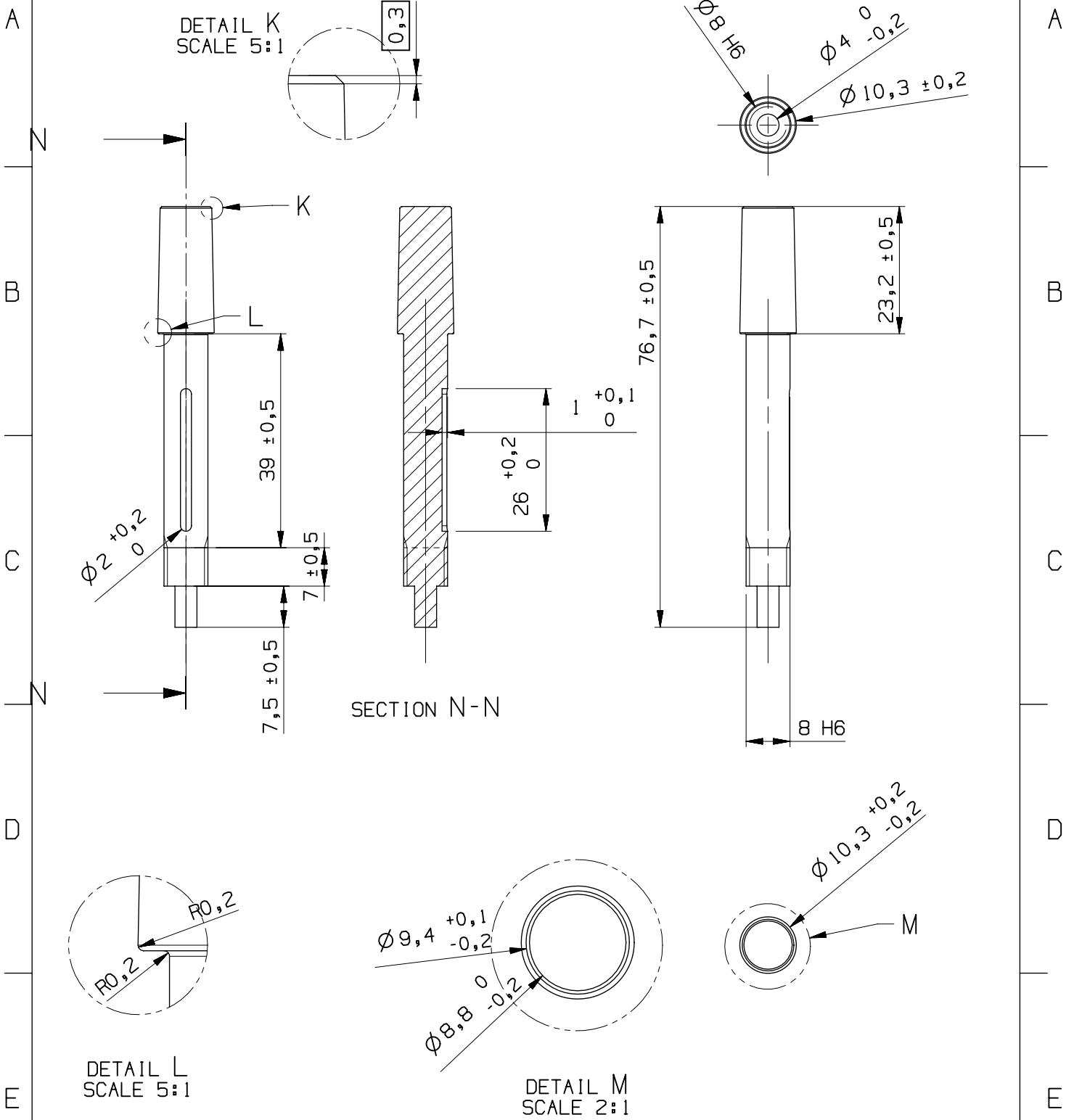



MATERIAL 1.4305; AISI 303			SCALE 5:1	PROJECTION  1st ANGLE
TREATMENT ANOD 18 ±2µm			GENERAL ROUGHNESS 3.2/  ISO 1302	UNIT MM
ITEM NAME Alignment Pin		ITEM ID PTC010		ITEM REV. XXXX-XX-XX
STATUS	STATUS DATE	OWNER X.XXX	GROUP NO.	FORMAT A4 PAGE 1/1
VDL Enabling Technologies Group				

1 2 3 4



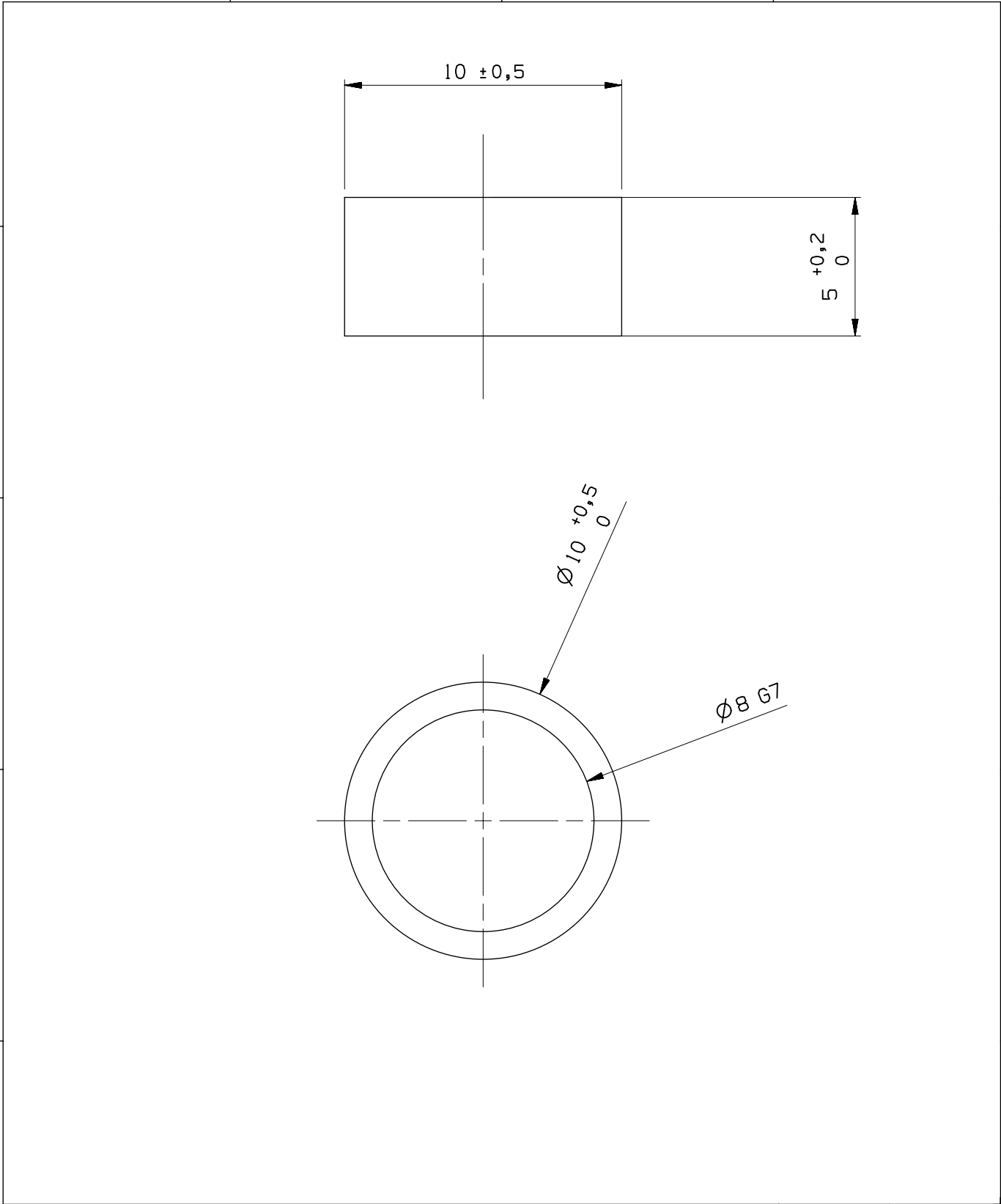
All rights are reserved. Reproduction in whole or in part is prohibited without the written consent of the copyright owner.

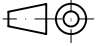


MATERIAL 1.4301; AISI 304			SCALE 1:1	PROJECTION  1st ANGLE
TREATMENT ANOD 18 ±2µm			GENERAL ROUGHNESS 3.2 ISO 1302	UNIT MM
ITEM NAME Shank Shaft		ITEM ID PTC007		ITEM REV. XXXX-XX-XX
STATUS	STATUS DATE	OWNER X.XXX	GROUP NO.	FORMAT A4 PAGE 1/2
VDL Enabling Technologies Group				



All rights are reserved. Reproduction in whole or in part is prohibited without the written consent of the copyright owner.



MATERIAL 1.4305; AISI 304		SCALE 5:1	PROJECTION  1st ANGLE
TREATMENT ANOD 18 ±2µm		GENERAL ROUGHNESS 3.2 ISO 1302	UNIT MM
ITEM NAME Washer shank shaft		ITEM ID PTC008	
ITEM REV. XXXX-XX-XX			
STATUS	STATUS DATE	OWNER X.XXX	GROUP NO.
VDL Enabling Technologies Group		FORMAT A4	PAGE 1/1

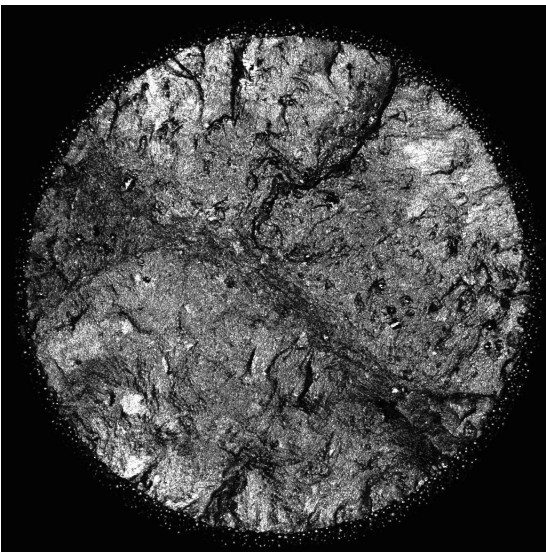
Item	manufacturer	model
Motor	Maxon	brushless EC flat 42W
Controller	Maxon	Maxpos 50/5
Timing belt	Synchroflex	
Bearing (small)	SKF	628/6-2Z
Bearing (big)	SKF	
Circlipse (big)	General manufacturer	16 mm dia
Circlipse (small)	General manufacturer	12 mm dia
Drill chuck	Proxxon	6.5 mm
Weight rod	Praxis	200 mm
Aluminum plate (frame)	Aluminum Op Mat	
L-beams (frame)	Aluminum Op Mat	
Bolts	General manufacturer	3 to 5 mm
Nuts	General manufacturer	3 to 5 mm

Table C.1: Equipment used for the fatigue tool

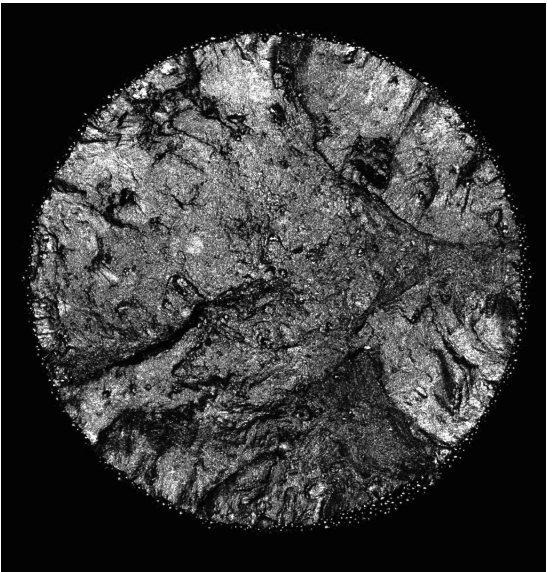
Appendix D

Fatigue data

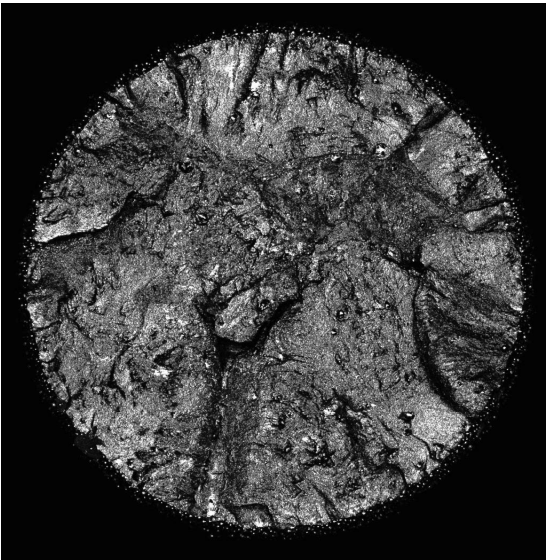
- 1 As-built + HIP
- 2 Electropolished
- 3 Plasmapolishing



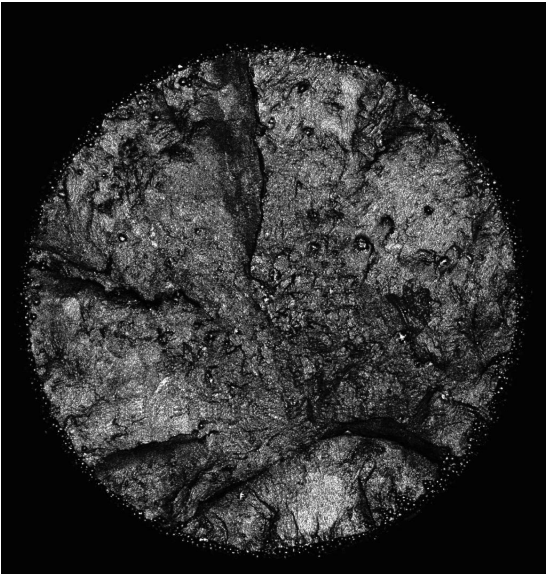
(a)



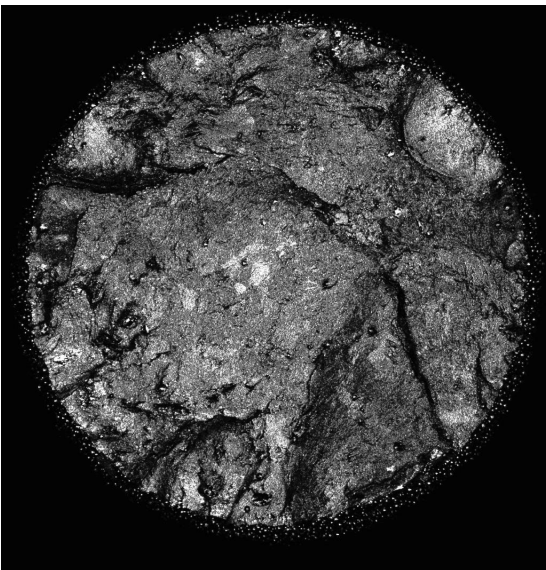
(b)



(c)



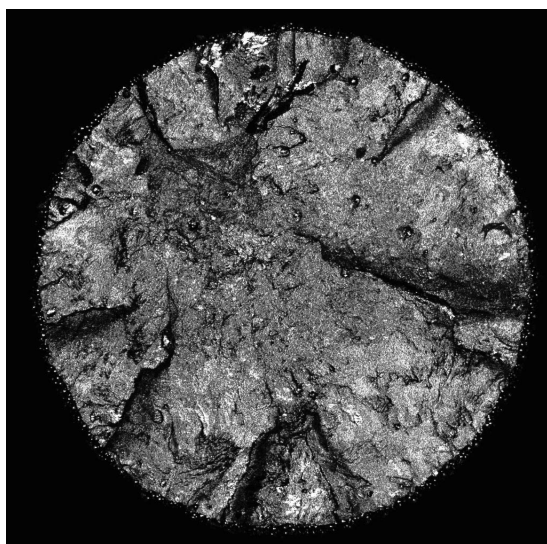
(d)



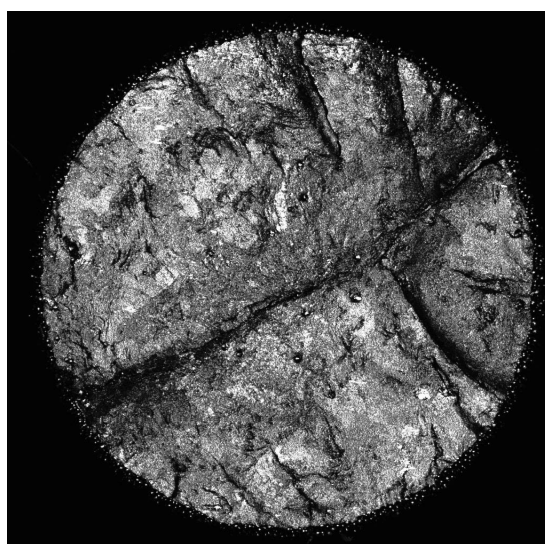
(e)



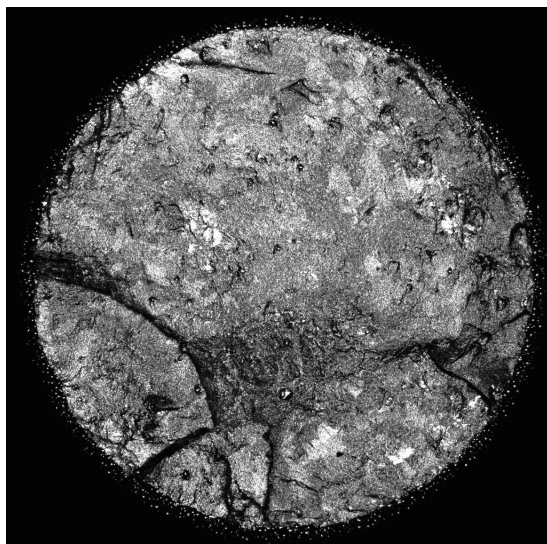
(f)



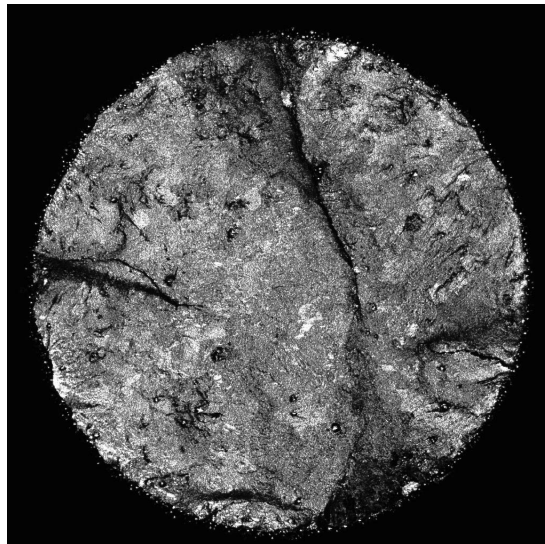
(a)



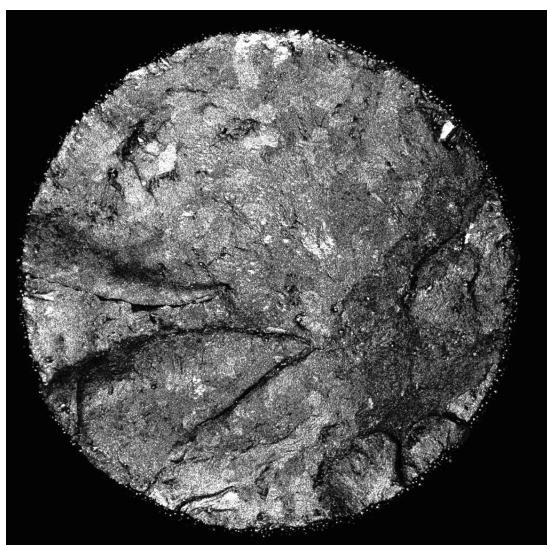
(b)



(c)

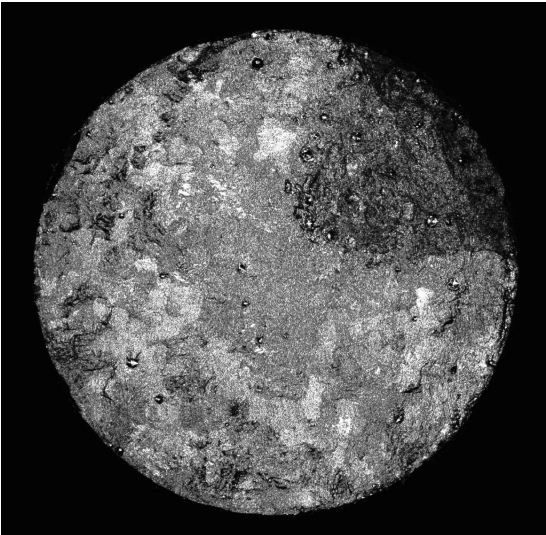


(d)

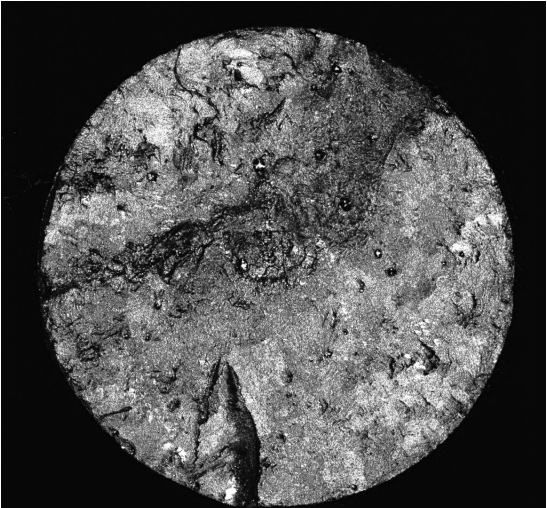


(e)

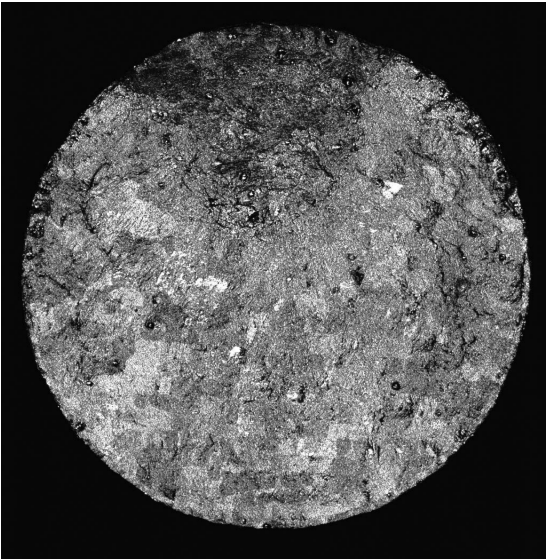
Figure D.2



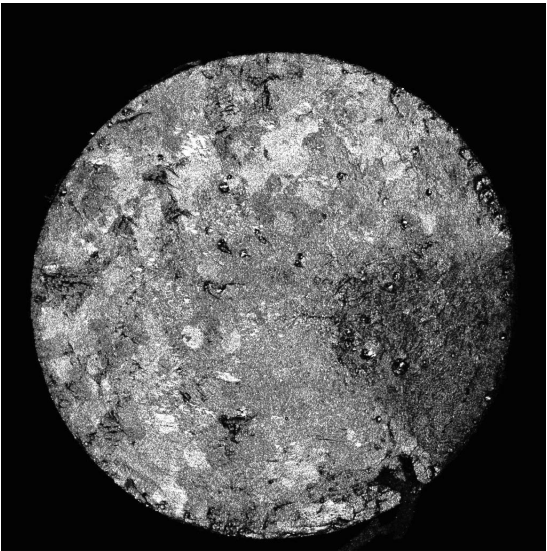
(a)



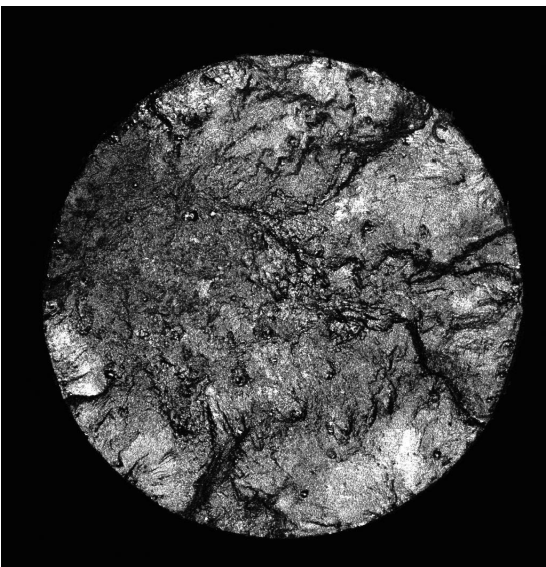
(b)



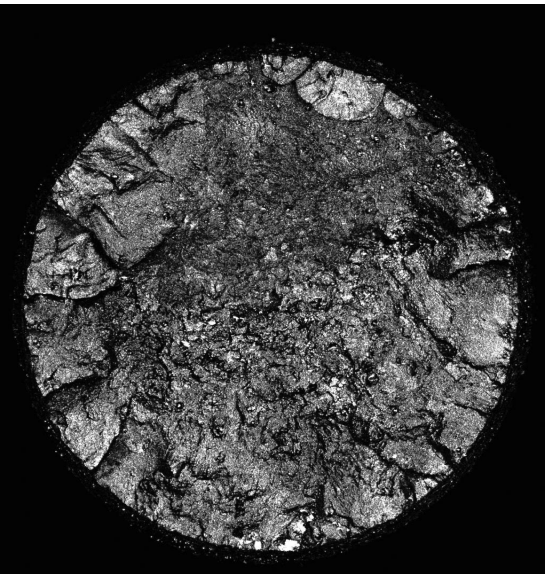
(c)



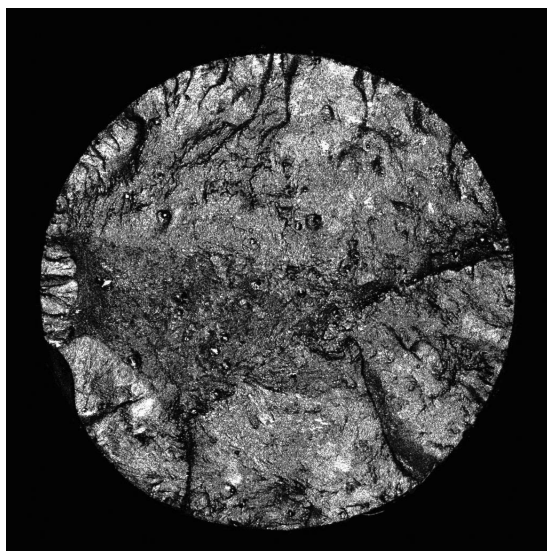
(d)



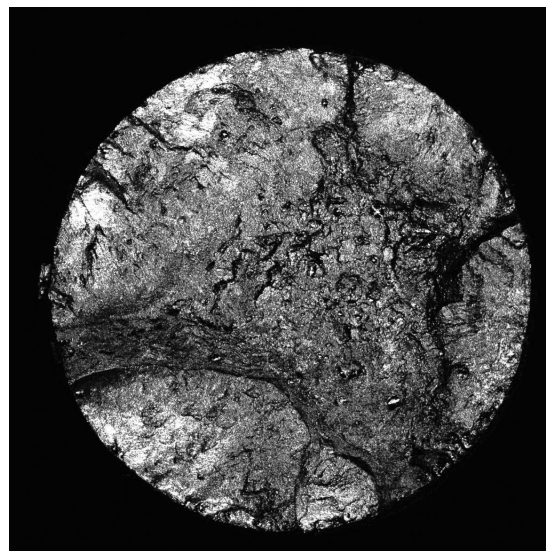
(e)



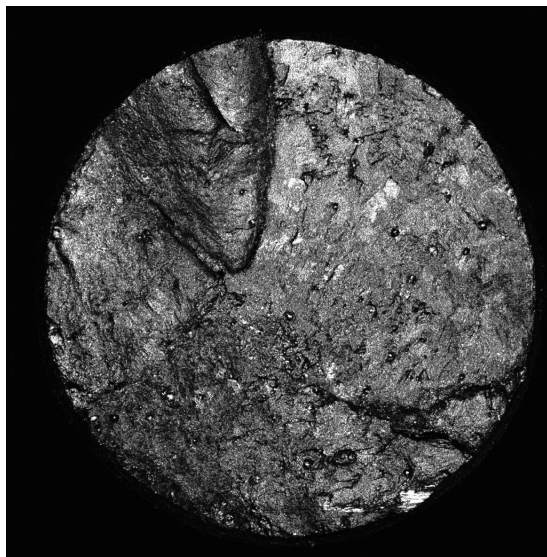
(f)



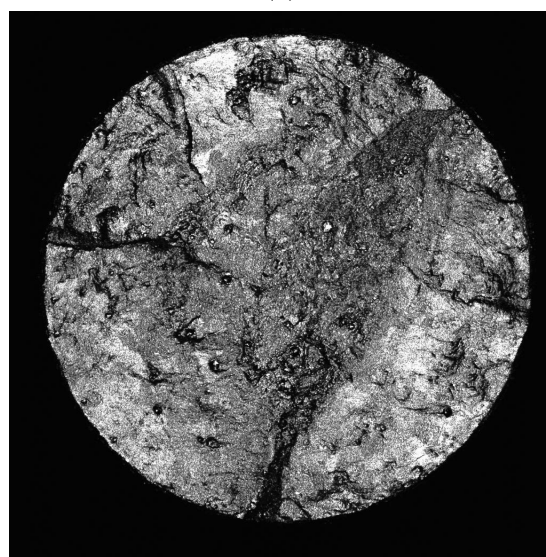
(a)



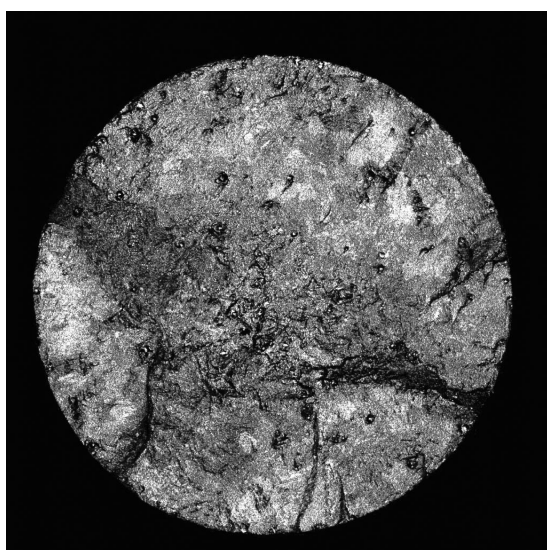
(b)



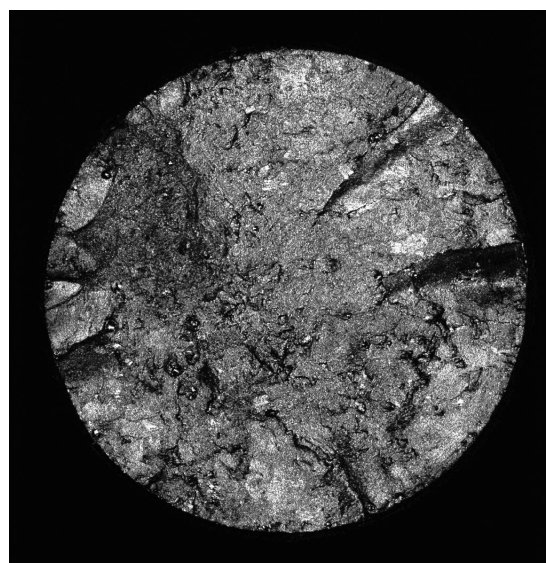
(c)



(d)

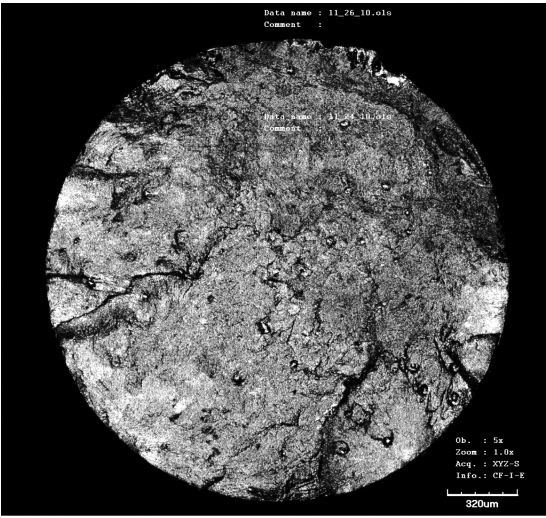


(e)

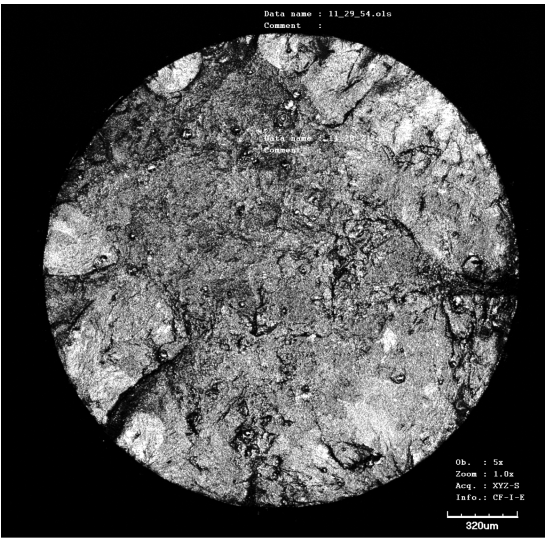


(f)

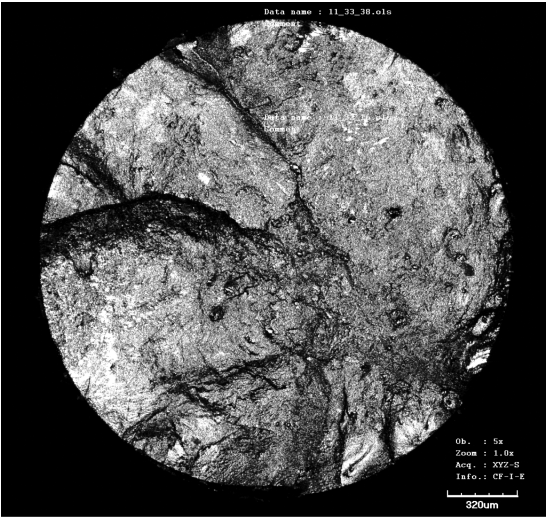
Figure D.4



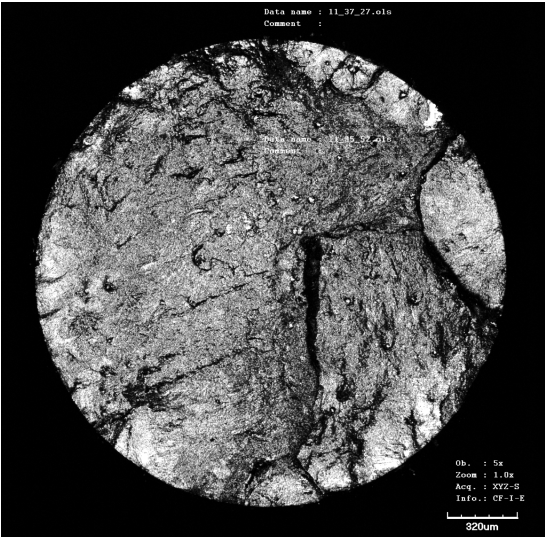
(a)



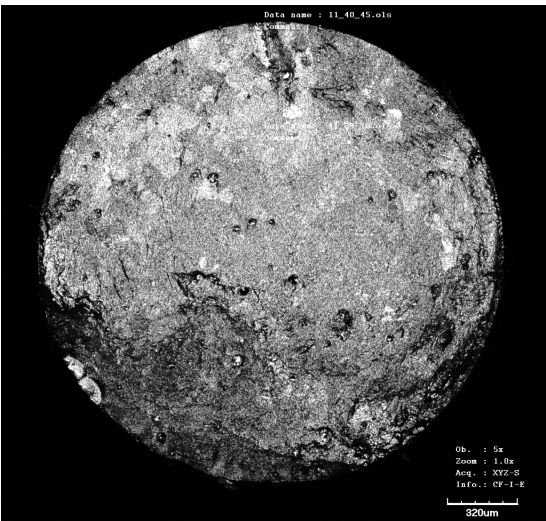
(b)



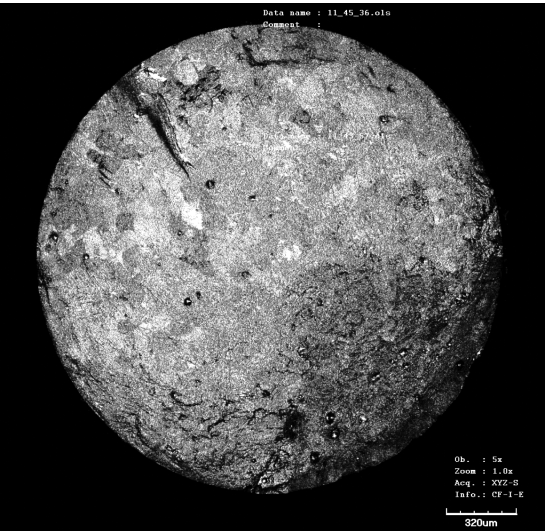
(c)



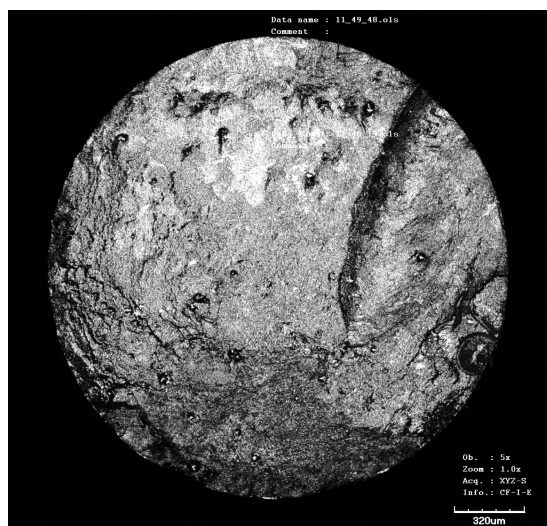
(d)



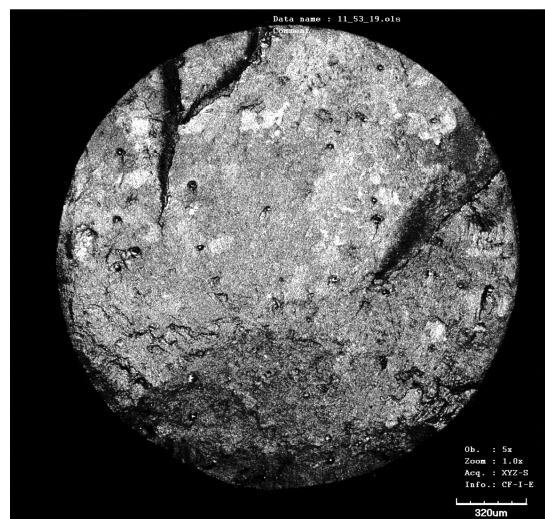
(e)



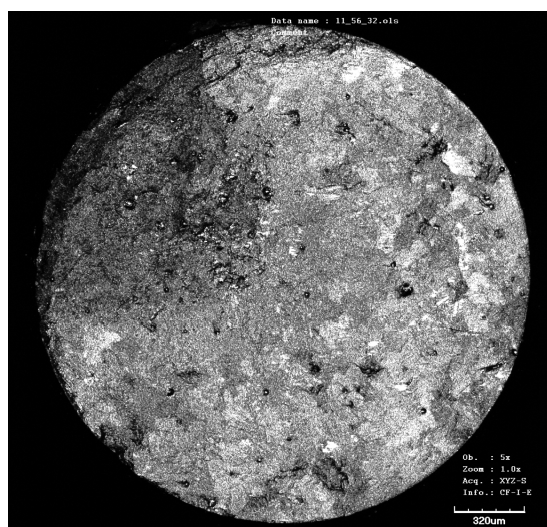
(f)



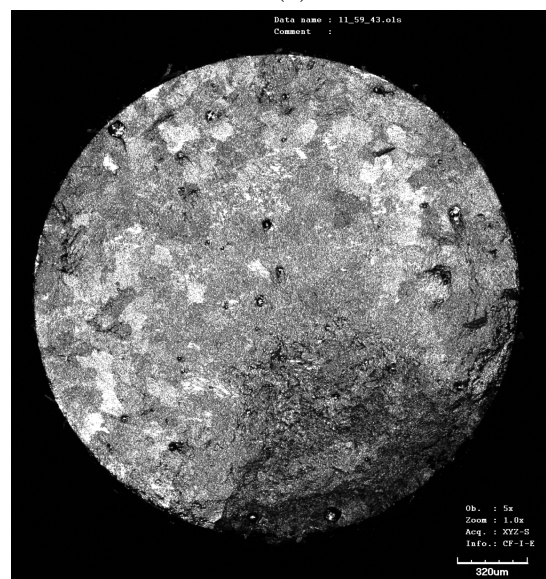
(a)



(b)



(c)



(d)

Figure D.6